Eur. Phys. J. C (2020) 80:942
https://doi.org/10.1140/epjc/s10052-020-8223-0

THE EUROPEAN PHYSICAL JOURNAL C

Regular Article - Experimental Physics

Measurements of the Higgs boson inclusive and differential fiducial cross sections in the 4ℓ decay channel at $\sqrt{s} = 13$ TeV

ATLAS Collaboration[⋆]

CERN, 1211 Geneva 23, Switzerland

Received: 8 April 2020 / Accepted: 8 July 2020 / Published online: 12 October 2020

Abstract Inclusive and differential fiducial cross sections of the Higgs boson are measured in the $H \to ZZ^* \to 4\ell$ ($\ell = e, \mu$) decay channel. The results are based on proton-proton collision data produced at the Large Hadron Collider at a centre-of-mass energy of 13 TeV and recorded by the ATLAS detector from 2015 to 2018, equivalent to an integrated luminosity of 139 fb^{-1}. The inclusive fiducial cross section for the $H \to ZZ^* \to 4\ell$ process is measured to be $\sigma_{\text{fid}} = 3.28 \pm 0.32$ fb, in agreement with the Standard Model prediction of $\sigma_{\text{fid,SM}} = 3.41 \pm 0.18$ fb. Differential fiducial cross sections are measured for a variety of observables which are sensitive to the production and decay of the Higgs boson. All measurements are in agreement with the Standard Model predictions. The results are used to constrain anomalous Higgs boson interactions with Standard Model particles.

Contents

⋆ e-mail: atlas.publications@cern.ch

1 Introduction

The observation of the Higgs boson by the ATLAS and CMS Collaborations [1,2] using data from proton-proton (pp) collisions at the Large Hadron Collider (LHC) recorded in 2011 and 2012 at centre-of-mass energies of $\sqrt{s} = 7$ TeV and 8 TeV, respectively, was a major step forward in the understanding of the electroweak (EW) symmetry breaking mechanism [3–5]. Studies of the spin and parity of the Higgs boson, its coupling structure to other particles, and measurements of fiducial and differential cross sections have been performed [6–28]. These show no significant deviations from the Standard Model (SM) predictions for the Higgs boson with a mass of 125.09 ± 0.24 GeV [15].

This paper presents updated inclusive and differential cross-section measurements of the Higgs boson in the $H \to ZZ^* \to 4\ell$ decay channel (where $\ell = e$ or μ). The full ATLAS Run 2 dataset, consisting of pp collision data at $\sqrt{s} = 13$ TeV taken between 2015 and 2018, is used for this analysis. The total integrated luminosity after imposing data quality requirements is 139 fb^{-1}, with a data-taking efficiency of 91.5%.

All measurements are performed with the assumption that the mass of the Higgs boson is 125 GeV, and are compared with SM predictions. The signal is extracted from a binned likelihood fit to the four-lepton invariant mass, $m_{4\ell}$, distribution. All major background processes are estimated from data. In particular, the normalisation of the dominant non-resonant ZZ^* background is now constrained from dedicated data sidebands rather than from simulation. Signal events are corrected for detector measurement inefficiency and resolu-

tion by unfolding using the detector response matrix in the likelihood fit, in place of a bin-by-bin correction. Compared with the previous published results [11], this paper also benefits from the full LHC Run 2 integrated luminosity, improved event and electron reconstruction [29,30], and improved lepton isolation to mitigate the impact of additional pp interactions in the same or neighbouring bunch crossing (pile-up). The fiducial phase-space definition has also been updated with respect to the previous publication to harmonise the selection of the leptons.

The paper is organised as follows. A brief introduction of the ATLAS detector is given in Sect. 2, while in Sect. 3, the data and simulated signal and background samples are described. The selection of the Higgs boson candidate events is detailed in Sect. 4. Section 5 outlines the fiducial phase-space definition and the observables that are unfolded, while the background modelling is described in Sect. 6. The unfolding strategy is described in Sect. 7. The experimental and theoretical systematic uncertainties, detailed in Sect. 8, are taken into account for the statistical interpretation of the data. The final results are presented in Sect. 9 and their interpretation to constrain possible beyond the SM (BSM) contact interactions or non-SM values of the b- and c-quark Yukawa couplings are shown in Sect. 10. Concluding remarks are given in Sect. 11. More information about general aspects of the analysis is contained in the concurrent Ref. [31], where, in particular, details of the event selection and background estimation can be found.

2 The ATLAS detector

The ATLAS detector [32] is a multipurpose particle detector with a forward–backward symmetric cylindrical geometry[1] and a near 4π coverage in solid angle. It consists of an inner tracking detector (ID) surrounded by a thin superconducting solenoid, which provides a 2 T axial magnetic field, electromagnetic (EM) and hadron calorimeters, and a muon spectrometer. The inner tracking detector covers the pseudorapidity range $|\eta| < 2.5$. It consists of a silicon pixel detector, including the newly installed insertable B-layer [33,34], a silicon microstrip detector, and a straw-tube tracking detector featuring transition radiation to aid in the identification of electrons. Lead/liquid-argon (LAr) sampling calorimeters provide electromagnetic energy measurements with high granularity. A steel/scintillator-tile hadron calorimeter covers the central pseudorapidity range ($|\eta| < 1.7$). The endcap and forward regions are instrumented up to $|\eta| = 4.9$ with LAr calorimeters for both the EM and hadronic energy measurements. The calorimeters are surrounded by the muon spectrometer, which has three large air-core toroidal superconducting magnets with eight coils each. The field integral of the toroid magnets ranges between 2.0 and 6.0 T m across most of the detector. The muon spectrometer includes a system of precision tracking chambers and fast detectors for triggering with a coverage of $|\eta| < 2.7$. Events are selected using a first-level trigger implemented in custom electronics, which reduces the event rate to a maximum of 100 kHz using a subset of detector information. Software algorithms with access to the full detector information are then used in the high-level trigger to yield a recorded event rate of about 1 kHz [35].

3 Theoretical predictions and event simulation

The production of the SM Higgs boson via gluon–gluon fusion (ggF), via vector-boson fusion (VBF), with an associated vector boson (VH, where V is a W or Z boson), and with a top quark pair (ttH) was modelled with the POWHEG-BOX v2 Monte Carlo (MC) event generator [36–43]. Table 1 summarises the predicted SM production cross sections and branching ratios for the $H \to ZZ^* \to 4\ell$ decay for $m_H = 125$ GeV together with their theoretical accuracy.

For ggF, the PDF4LHC next-to-next-to-leading-order (NNLO) set of parton distribution functions (PDF) was used, while for all other production modes, the PDF4LHC next-to-leading-order (NLO) set was used [71]. The simulation of ggF Higgs boson production used the POWHEG method for merging the NLO Higgs + jet cross section with the parton shower and the MINLO method [75] to simultaneously achieve NLO accuracy for the inclusive Higgs boson production. In a second step, a reweighting procedure (NNLOPS) [76], exploiting the Higgs boson rapidity distribution, was applied using the HNNLO program [77,78] to achieve NNLO accuracy in the strong coupling constant α_s.

The matrix elements of the VBF, $q\bar{q} \to VH$ and ttH production mechanisms were calculated to NLO accuracy in QCD. For VH production, the MINLO method was used to merge 0- and 1-jet events [43,75]. The $gg \to ZH$ contribution was modelled at leading order (LO) in QCD.

The production of a Higgs boson in association with a bottom quark pair (bbH) was simulated at NLO with MADGRAPH5_AMC@NLO v2.3.3 [79], using the CT10 NLO PDF [80]. The production in association with a single top quark (tH+X where X is either jb or W, defined in the following as tH) was simulated at NLO with

[1] ATLAS uses a right-handed coordinate system with its origin at the nominal interaction point (IP) in the centre of the detector and the z-axis along the beam pipe. The x-axis points from the IP to the centre of the LHC ring, and the y-axis points upwards. Cylindrical coordinates (r, ϕ) are used in the transverse plane, ϕ being the azimuthal angle around the z-axis. The pseudorapidity is defined in terms of the polar angle θ as $\eta = -\ln\tan(\theta/2)$ and the rapidity is defined as $y = \frac{1}{2}\ln\frac{E+p_z}{E-p_z}$. Angular distance is measured in units of $\Delta R \equiv \sqrt{(\Delta\eta)^2 + (\Delta\phi)^2}$.

Table 1 Predicted SM Higgs boson production cross sections (σ) for ggF, VBF and five associated production modes in pp collisions for $m_H = 125$ GeV at $\sqrt{s} = 13$ TeV [44–74]. For bbH the accuracy of calculations in the 4- and 5-flavour schemes (FS) is reported. The quoted uncertainties correspond to the total theoretical systematic uncertainties calculated by adding in quadrature the uncertainties due to missing higher-order corrections and PDF+α_s. The decay branching ratios ($\mathcal{B}$) with the associated uncertainty for $H \to ZZ^*$ and $H \to ZZ^* \to 4\ell$, with $\ell = e, \mu$, are also given

Production process		Accuracy	σ [pb]
ggF	$(gg \to H)$	N^{3}LO in QCD, NLO in EW	48.6 ± 2.4
VBF	$(qq' \to Hqq')$	(approximate) NNLO in QCD, NLO in EW	3.78 ± 0.08
WH	$(q\bar{q}' \to WH)$	NNLO in QCD, NLO in EW	1.373 ± 0.028
ZH	$(q\bar{q}/gg \to ZH)$	NNLO in QCD, NLO in EW	0.88 ± 0.04
ttH	$(q\bar{q}/gg \to t\bar{t}H)$	NLO in QCD, NLO in EW	0.51 ± 0.05
bbH	$(q\bar{q}/gg \to b\bar{b}H)$	NNLO (NLO) in QCD for 5FS (4FS)	0.49 ± 0.12
tH	$(q\bar{q}/gg \to tH)$	NLO in QCD	0.09 ± 0.01
Decay process		NLO in QCD, NLO in EW	$\mathcal{B}$ [$\cdot 10^{-4}$]
$H \to ZZ^*$			262 ± 6
$H \to ZZ^* \to 4\ell$			1.240 ± 0.027

MadGraph5_aMC@NLO v2.6.0 using the NNPDF30 PDF set [74].

For all production mechanisms the Pythia 8 [81] generator was used for the $H \to ZZ^* \to 4\ell$ decay as well as for the parton shower modelling. The AZNLO set of tuned parameters [82] was used, except for ttH, where, like for the $t\bar{t}$ samples, the A14 tune [83] was employed. The event generator was interfaced to EvtGen v1.2.0 [84] for simulation of the bottom and charm hadron decays. All signal samples were simulated for a Higgs boson mass $m_H = 125$ GeV.

For additional cross-checks, the ggF sample was also generated with MadGraph5_aMC@NLO. This simulation has NLO QCD accuracy for zero, one and two additional partons merged with the FxFx merging scheme [85,86], and top and bottom quark mass effects are taken into account [87–89]. Higgs boson are decayed using MadSpin [90,91]. Some final results are also compared with ggF predictions calculated with RadISH, which provides resummation at N^{3}LL+NNLO accuracy [92–96], and uses MATRIX for the fixed-order calculation [97,98]. Similarly, ggF predictions are also obtained from NNLOJET for distributions of Higgs plus one- or two-jet events [99–101]. Neither of these two predictions are included for the case in which there are zero jets. Additionally, final results for several of the variables that probe the kinematics of the Higgs boson decay products include comparisons with Hto4l and Prophecy4f. These two programs include the full NLO electroweak corrections to the Higgs boson decay into four charged leptons [68–70,102–107].

The samples are normalised to cross sections obtained from the best available predictions as provided in Refs. [44–46,66,67,72–74,108]. The SM branching ratio prediction, taken from Prophecy4f [68,103], includes the full NLO EW corrections, and interference effects which result in a branching ratio that is 10% higher for same-flavour final states (4μ and $4e$) than for different-flavour states ($2e2\mu$ and $2\mu 2e$).

For the BSM interpretation, described in Sect. 10.1, deviations from the SM are studied using a ggF sample generated with MadGraph5_aMC@NLO using the HPOprodMFV UFO model [109] with FeynRules [110] at LO and the NNPDF23 PDF set. The sample was interfaced to Pythia 8 using the A14 parameter set [83]. For studies of the Yukawa couplings described in Sect. 10.2, the gluon-initiated component of the prediction was calculated using RadISH, while MadGraph5_aMC@NLO was used for the quark-initiated component with FxFx merging for 0- and 1-jet final states.

The ZZ^* continuum background from quark–antiquark annihilation was modelled using Sherpa 2.2.2 [111–113], which provides a matrix element calculation accurate to NLO in α_s for 0- and 1-jet final states, and LO accuracy for 2- and 3-jet final states. The merging with the Sherpa parton shower [114] was performed using the ME+PS@NLO prescription [115]. The NLO EW corrections were applied as a function of the invariant mass of the ZZ^* system m_{ZZ^*} [116,117]. This process was also simulated using two additional MC generators. The first is Powheg-Box v2 interfaced to Pythia 8 for parton showering and hadronisation, with EvtGen for the simulation of bottom and charm hadron decays. The second is MadGraph5_aMC@NLO with FxFx merging at NLO for 0- and 1-jet final states and interfaced to Pythia 8 for parton showering.

The gluon-induced ZZ^* production was modelled by Sherpa 2.2.2 [111–113] at LO in QCD for 0- and 1-jet final states. The higher-order QCD effects for the $gg \to ZZ^*$

continuum production have been calculated for massless quark loops [118–120] in the heavy top-quark approximation [121], including the $gg \to H^* \to ZZ$ processes [122,123]. The $gg \to ZZ$ simulation cross section is scaled by a K-factor of 1.7±1.0, defined as the ratio of the higher-order to leading-order cross section predictions. Production of ZZ^* via vector-boson scattering was simulated at LO in QCD with the SHERPA 2.2.2 generator.

The WZ background was modelled using POWHEG-BOX v2 interfaced to PYTHIA 8 and EVTGEN v1.2.0 for the simulation of bottom and charm hadron decays. The triboson backgrounds ZZZ, WZZ, and WWZ with four or more prompt leptons (denoted by VVV hereafter) were modelled using SHERPA 2.2.2. The simulation of $t\bar{t}+Z$ events with both top quarks decaying semileptonically and the Z boson decaying leptonically was performed with MADGRAPH5_AMC@NLO interfaced to PYTHIA 8. The total cross section is normalised to the prediction of Ref. [62], which includes the two dominant terms at both the LO and the NLO in a mixed perturbative expansion in the QCD and EW couplings. For modelling comparisons, SHERPA 2.2.1 was used to simulate $t\bar{t}+Z$ events at LO. The smaller tWZ, $t\bar{t}W^+W^-$, $t\bar{t}t$, $t\bar{t}t\bar{t}$ and tZ background processes were simulated with MADGRAPH5_AMC@NLO interfaced to PYTHIA 8.

The modelling of events containing Z bosons with associated jets (Z + jets) was performed using the SHERPA 2.2.1 generator. Matrix elements were calculated for up to two partons at NLO and four partons at LO using COMIX [112] and OPENLOOPS [113], and merged with the SHERPA parton shower [114] using the ME+PS@NLO prescription [115]. The NNPDF3.0 NNLO PDF set was used in conjunction with a dedicated set of tuned parton shower parameters.

The $t\bar{t}$ background was modelled using POWHEG-BOX v2 interfaced to PYTHIA 8 for parton showering, hadronisation, and the underlying event, and to EVTGEN v1.2.0 for heavy-flavour hadron decays. For this sample, the A14 tune was used [124]. Simulated Z+jets and $t\bar{t}$ background samples are normalised to the data-driven estimates described in Sect. 6.

Generated events were processed through the ATLAS detector simulation [125] within the GEANT4 framework [126] and reconstructed in the same way as collision data. Additional pp interactions in the same and nearby bunch crossings are included in the simulation. The pile-up was modelled by overlaying the original hard-scattering event with simulated inelastic pp events generated with PYTHIA 8 [81] using the NNPDF2.3LO set of PDFs [127] and the A3 tune [128].

4 Event reconstruction and selection

The details of the selection and reconstruction of Higgs boson candidate events are provided in Ref. [31], while a brief description is provided here. Single-lepton, dilepton, and trilepton triggers are employed and ensure a signal selection efficiency above 98%. Data events are subjected to quality requirements and are required to have at least one vertex with two associated ID tracks with transverse momentum $p_{\mathrm{T}} > 500$ MeV. The primary interaction vertex is selected as the one with the largest $\sum p_{\mathrm{T}}^2$ of all associated tracks.

The lepton identification requirements follow the inclusive event selection described in Ref. [31]. All muons are required to satisfy $p_{\mathrm{T}} > 5$ GeV and $|\eta| < 2.7$, except those that are reconstructed with ID tracks matched to energy deposits in the calorimeter (calorimeter-tagged), which must satisfy $p_{\mathrm{T}} > 15$ GeV and $|\eta| < 0.1$. No more than one calorimeter-tagged or stand-alone muon is allowed per event, where stand-alone muons have not been matched to an ID track. Electrons are required to satisfy $E_{\mathrm{T}} > 7$ GeV and $|\eta| < 2.47$. Jets are reconstructed using the anti-k_t algorithm with a radius parameter $R = 0.4$ and applied to Particle Flow objects [129]. Jets are required to have $p_{\mathrm{T}} > 30$ GeV and $|\eta| < 4.5$. Jets within $|\eta| < 2.5$ are identified as containing a b-hadron using the MV2c10 b-tagging algorithm at the 70% efficiency working point [130,131]. If a jet overlaps geometrically with a reconstructed muon (electron) within a cone of radial size $\Delta R = 0.1(0.2)$, the jet is removed.

Same-flavour opposite-charge (SFOC) lepton pairs are selected to form Higgs boson candidates. The SFOC lepton pair with mass m_{12} closest to the Z boson mass is called the leading pair, while the other becomes the subleading pair, with mass m_{34}. If multiple combinations of SFOC pairs exist, the Higgs boson candidate with m_{12} closest to the Z boson mass is chosen. The three leading leptons of each Higgs boson candidate are required to satisfy $p_{\mathrm{T}} > 20, 15, 10$ GeV. Higgs boson candidate events are subjected to further selection requirements on the dilepton masses, lepton separation, J/ψ veto, impact parameter significance ($d_0/\sigma(d_0)$), and vertex quality, as outlined in Table 2. In addition, isolation requirements are imposed on the leptons to suppress the $t\bar{t}$ and Z + jets reducible backgrounds. If an extra prompt lepton with $p_{\mathrm{T}} > 12$ GeV passing all identification and isolation requirements detailed previously is present in the event, the final Higgs boson candidate is chosen using a method based on the matrix element (ME). The matrix element is calculated at LO using MADGRAPH5_AMC@NLO and the quadruplet with the highest ME value is chosen. This increases the probability of selecting the correct Higgs boson candidate in cases where the extra lepton comes from the decay of a vector boson or top quark in VH-leptonic or ttH/tH production. The four-lepton mass resolution is improved by accounting for reconstructed final-state radiation (FSR) photons in the Z boson decay. After selection criteria are applied, events are divided into bins for each variable of interest for the differential cross-section measurements. Finally, all measurements presented in this paper are performed within a four-lepton

Table 2 A summary of event selection requirements for leptons and Higgs boson candidates outlined in Sect. 4. SFOC lepton pairs are same-flavour opposite-charge lepton pairs. For the mass requirement of the subleading lepton pair, $m_{\text{threshold}}$ is 12 GeV for $m_{4\ell} < 140$ GeV, and rises linearly until reaching 50 GeV for $m_{4\ell} = 190$ GeV

Leptons and jets	
Muons	$p_{\text{T}} > 5$ GeV, $\lvert\eta\rvert < 2.7$
Electrons	$E_{\text{T}} > 7$ GeV, $\lvert\eta\rvert < 2.47$
Jets	$p_{\text{T}} > 30$ GeV, $\lvert\eta\rvert < 4.5$
Lepton selection and pairing	
Lepton kinematics	$p_{\text{T}} > 20, 15, 10$ GeV
Leading pair (m_{12})	SFOC lepton pair with smallest $\lvert m_Z - m_{\ell\ell}\rvert$
Subleading pair (m_{34})	Remaining SFOC lepton pair with smallest $\lvert m_Z - m_{\ell\ell}\rvert$
Event selection (at most one Higgs boson candidate per channel)	
Mass requirements	50 GeV$< m_{12} <$ 106 GeV and $m_{\text{threshold}} < m_{34} <$ 115 GeV
Lepton separation:	$\Delta R(\ell_i, \ell_j) > 0.1$
Lepton/Jet separation	$\Delta R(\mu_i(e_i), \text{jet}) > 0.1(0.2)$
J/ψ veto	$m(\ell_i, \ell_j) > 5$ GeV for all SFOC lepton pairs
Impact parameter	$\lvert d_0\rvert/\sigma(d_0) < 5(3)$ for electrons (muons)
Mass window	105 GeV $< m_{4\ell} <$ 160 GeV
Vertex selection:	$\chi^2/N_{\text{dof}} < 6(9)$ for 4μ (other channels)
If extra lepton with $p_{\text{T}} > 12$ GeV	Quadruplet with largest matrix element (ME) value

mass window of $105 < m_{4\ell} < 160$ GeV. The signal selection efficiency is about 31%, 21%, 17%, and 16% for the 4μ, $2e2\mu$, $2\mu2e$, and $4e$ final states, respectively. Here, the first lepton pair refers to the lepton pair with an invariant mass closest to the Z boson mass.

5 Fiducial phase space and unfolded observables

The fiducial cross sections are defined using simulation at particle level and the selection requirements outlined in Table 3. In order to minimise model-dependent acceptance extrapolations, these are chosen to closely match the selection requirements of the detector-level analysis after the event reconstruction.

The fiducial selection is applied to final-state electrons and muons that do not originate from hadrons or τ-lepton decays, after 'dressing' them, i.e., the four-momenta of photons within a cone of size $\Delta R = 0.1$ around the lepton are added to the lepton's four-momentum. The photons which originate from hadron decays are excluded. Particle-level jets are reconstructed from final-state neutral and charged particles using the anti-k_t algorithm with radius parameter $R = 0.4$. Electrons, muons, neutrinos (if they are not from hadron decays) and photons from Higgs decays as well as those used to dress leptons are excluded from the jet clustering. A jet is labelled as a b-jet if there is a b-hadron with $p_{\text{T}} > 5$ GeV within a cone of size $\Delta R = 0.3$ around the jet axis. Jets are removed if they are within a cone of size $\Delta R = 0.1$ around a selected lepton.

Quadruplet selection using the selected dressed leptons follows the same procedure as for reconstructed events. In the case of VH or ttH production, additional leptons not originating from a Higgs boson decay can induce a 'lepton mispairing' when assigning them to the leading and subleading Z bosons. To improve the lepton pairing efficiency, the matrix-element-based pairing method as described in Sect. 4 is employed. The variables used in the differential cross-section measurement are calculated using the dressed leptons of the quadruplets.

The acceptance of the fiducial selection, defined as the ratio of the number of events passing the particle-level selection to the number of events generated in a given bin or final state (with respect to the full phase space of $H \to ZZ^* \to 2\ell2\ell'$, where $\ell, \ell' = e$ or μ), is about 49% for each final state for a SM Higgs boson with $m_H = 125$ GeV. The ratio of the number of events passing the selection after detector simulation and event reconstruction to those passing the particle-level selection is about 45%. About 1.6% of the events which pass the detector-level selection fail the particle-level selection. This is mostly due to resolution effects for muons. For electrons channels, the difference in the reconstructed and

Table 3 List of event selection requirements which define the fiducial phase space for the cross-section measurement. SFOC lepton pairs are same-flavour opposite-charge lepton pairs

Leptons and jets	
Leptons	$p_{\mathrm{T}} > 5$ GeV, $\lvert\eta\rvert < 2.7$
Jets	$p_{\mathrm{T}} > 30$ GeV, $\lvert y\rvert < 4.4$
Lepton selection and pairing	
Lepton kinematics	$p_{\mathrm{T}} > 20, 15, 10$ GeV
Leading pair (m_{12})	SFOC lepton pair with smallest $\lvert m_Z - m_{\ell\ell}\rvert$
Subleading pair (m_{34})	Remaining SFOC lepton pair with smallest $\lvert m_Z - m_{\ell\ell}\rvert$
Event selection (at most one quadruplet per event)	
Mass requirements	50 GeV$< m_{12} <$ 106 GeV and 12 GeV$< m_{34} <$ 115 GeV
Lepton separation	$\Delta R(\ell_i, \ell_j) > 0.1$
Lepton/Jet separation	$\Delta R(\ell_i, \text{jet}) > 0.1$
J/ψ veto	$m(\ell_i, \ell_j) > 5$ GeV for all SFOC lepton pairs
Mass window	105 GeV$< m_{4\ell} <$ 160 GeV
If extra lepton with $p_{\mathrm{T}} > 12$ GeV	Quadruplet with largest matrix element value

fiducial phase space definition, has an additional comparable contribution.

Within the fiducial phase space defined above, differential cross sections are measured for variables which are sensitive to both the production and decay of the Higgs boson. For example, the transverse momentum distribution of the Higgs boson provides a test of perturbative QCD calculations, is sensitive to the structure of the Higgs boson interactions and is sensitive to charm and bottom Yukawa couplings. The rapidity of the Higgs boson is sensitive to the choice of parton distribution functions for the colliding protons, and is also influenced by QCD radiative corrections. The invariant masses of the leading and subleading lepton pair are sensitive to higher-order electroweak corrections to the Higgs boson decay, and are sensitive to BSM contributions. These two variables and the angular variables of the Higgs boson decay are also of interest due to their sensitivity to the spin and parity of the Higgs boson, as well as to same-flavour pair final-state interference and EW corrections. Variables related to jets probe QCD radiation effects and the Higgs boson production. The jet multiplicity is sensitive to different production mechanisms and provides sensitivity to the theoretical modelling of high-p_{T} quark and gluon emission. The transverse momentum of the jets directly probes the quark and gluon radiation. The invariant mass of the two leading jets is also sensitive to the production mechanisms of the Higgs boson, while the signed angle in the transverse plane of the two leading jets is a test of the spin and parity of the Higgs boson. Jet-related variables, in particular double differential variables, also probe the effects of QCD resummation. Additional variables which combine the properties related to the kinematics of the Higgs boson and the jets are also considered. A summary of all the variables and their descriptions is given in Table 4.

6 Background estimation

Non-resonant SM $(Z^{(*)}/\gamma^*)(Z^{(*)}/\gamma^*)$ production via $q\bar{q}$ annihilation and gluon–gluon fusion, referred to as ZZ^*, can result in four prompt leptons in the final state and constitutes the largest background for this analysis. While for previous analyses [11,12] both the shape and the normalisation of this background were exclusively estimated with simulation, in this paper the normalisation is constrained with a data-driven technique. The systematic uncertainty is reduced because both the theoretical and luminosity uncertainties no longer contribute to the normalisation uncertainty. The normalisation of the non-resonant ZZ^* component, which dominates outside the Higgs boson peak region, is obtained from data by extending the mass interval considered from 115–130 GeV to 105–160 GeV. The increased mass interval allows an estimation of this process with minimal impact on the expected sensitivity for the signal process. This contribution is determined as part of the 4ℓ mass fit (discussed in Sect. 7) in the full four-lepton mass region, with the shape of the background taken from simulation.

The ZZ^* normalisation is estimated separately in each bin of each differential observable, where a different ZZ^* scaling factor is used for each observable bin. In phase-space regions

Table 4 Definitions of observables for which differential cross sections are measured. The angular variables are defined as in Ref. [132]. In addition to the single observables listed, the following double differential observables are built using variables defined below: m_{12} vs. m_{34}, $p_{\mathrm{T}}^{4\ell}$ vs. N_{jets}, $p_{\mathrm{T}}^{4\ell}$ vs. $p_{\mathrm{T}}^{\text{lead. jet}}$, $p_{\mathrm{T}}^{4\ell}$ vs. $p_{\mathrm{T}}^{4\ell\mathrm{j}}$, $p_{\mathrm{T}}^{4\ell}$ vs. $|y_{4\ell}|$, $p_{\mathrm{T}}^{4\ell\mathrm{j}}$ vs. $m_{4\ell j}$, $p_{\mathrm{T}}^{\text{lead. jet}}$ vs. $p_{\mathrm{T}}^{\text{sublead. jet}}$, and $p_{\mathrm{T}}^{\text{lead. jet}}$ vs. $|y^{\text{lead. jet}}|$ (where $|y^{\text{lead. jet}}|$ is the rapidity of the leading jet). Jet-related variables are inclusive, while for the jet multiplicity the results are provided in both the inclusive and exclusive jet bins. $\Delta\phi_{jj}$ is defined as $\phi^{\text{lead. jet}} - \phi^{\text{sublead. jet}}$ if $\eta^{\text{lead. jet}} > \eta^{\text{sublead. jet}}$ or as $\phi^{\text{sublead. jet}} - \phi^{\text{lead. jet}}$ if $\eta^{\text{sublead. jet}} > \eta^{\text{lead. jet}}$. If $\Delta\phi_{jj} < 0$, 2π is added to the value

Higgs boson kinematic-related variables	
$p_{\mathrm{T}}^{4\ell}$, $\lvert y_{4\ell}\rvert$	Transverse momentum and rapidity of the four-lepton system
m_{12}, m_{34}	Invariant mass of the leading and subleading lepton pair
$\lvert\cos\theta^*\rvert$	Magnitude of the cosine of the decay angle of the leading lepton pair in the four-lepton rest frame relative to the beam axis
$\cos\theta_1$, $\cos\theta_2$	Production angles of the anti-leptons from the two Z bosons, where the angle is relative to the Z vector.
ϕ, ϕ_1	Two azimuthal angles between the three planes constructed from the Z bosons and leptons in the Higgs boson rest frame.
Jet-related variables	
N_{jets}, $N_{b\text{-jets}}$	Jet and b-jet multiplicity
$p_{\mathrm{T}}^{\text{lead. jet}}$, $p_{\mathrm{T}}^{\text{sublead. jet}}$	Transverse momentum of the leading and subleading jet, for events with at least one and two jets, respectively. Here, the leading jet refers to the jet with the highest p_{T} in the event, while subleading refers to the jet with the second-highest p_{T}.
m_{jj}, $\lvert\Delta\eta_{jj}\rvert$, $\Delta\phi_{jj}$	Invariant mass, difference in pseudorapidity, and signed difference in ϕ of the leading and subleading jets for events with at least two jets
Higgs boson and jet-related variables	
$p_{\mathrm{T}}^{4\ell\mathrm{j}}$, $m_{4\ell j}$	Transverse momentum and invariant mass of the four-lepton system and leading jet, for events with at least one jet
$p_{\mathrm{T}}^{4\ell\mathrm{jj}}$, $m_{4\ell jj}$	Transverse momentum and invariant mass of the four-lepton system and leading and subleading jets, for events with at least two jets

where the ZZ^* component in the $m_{4\ell}$ sidebands is too low to provide a reliable estimate of its contribution, the estimate is evaluated simultaneously for several differential bins.[2]

Other background processes, such as Z+jets, $t\bar{t}$, and WZ, contain at least one jet, photon or lepton from a hadron decay that is misidentified as a prompt lepton. These reducible backgrounds are significantly smaller than the non-resonant ZZ^* background and are estimated using data where possible, following slightly different approaches for the $\ell\ell + \mu\mu$ and $\ell\ell + ee$ final states [11,12,31].

In the $\ell\ell + \mu\mu$ final states, the normalisations for the Z + jets and $t\bar{t}$ backgrounds are determined by performing fits to the invariant mass of the leading lepton pair in dedicated independent control regions which target each background process for each bin of the differential observables. Depending on the background process being targeted, the control regions are formed by relaxing the χ^2 requirement on the four-lepton vertex fit, and by inverting or relaxing isolation and/or impact-parameter requirements on the subleading muon pair. Additional control regions ($e\mu\mu\mu$ and $\ell\ell + \mu^{\pm}\mu^{\pm}$) are used to improve the background estimate by reducing the statistical uncertainty of the fitted normalisation. Transfer factors to extrapolate from the control regions to the signal region are obtained separately for $t\bar{t}$ and Z+jets using simulation. This method is performed in each differential bin. The $m_{4\ell}$ shape for both processes in each bin is obtained from simulation.

The $\ell\ell + ee$ control-region selection requires the electrons in the subleading lepton pair to have the same charge, and relaxes the identification, impact parameter and isolation requirements on the electron candidate with the lowest transverse energy. This electron candidate, denoted by X, can be a light-flavour jet, an electron from photon conversion or an electron from heavy-flavour hadron decay. The heavy-flavour background is completely determined from simulation, whereas the light-flavour and photon conversion background is obtained with the sPlot method [133]. This is based on a fit to the number of hits in the innermost ID layer in the data control region. Transfer factors to extrapolate from the $\ell\ell + ee$ control region to the signal region for

[2] The same normalisation factor is used for neighbouring bins until the increase in uncertainty on the expected cross section in each measured bin is less than 5% of the total uncertainty.

the light-flavour jets and converted photons, obtained from simulated samples, are corrected using a $Z + X$ data control region. The corrected transfer factors are then used to extrapolate the extracted yields to the signal region. Both the extraction of the global yield in the control region and the extrapolation to the signal mass region are performed in bins of the transverse momentum of the electron candidate and the jet multiplicity. In order to extract the shape of the backgrounds from light-flavour jets and photon conversions for each observable, a similar method is used, except that the extraction and extrapolation is performed only as a function of the transverse momentum of the electron candidate, ignoring the binning in jet multiplicity.

Additional contributions from rare processes, such as tXX ($t\bar{t}Z, t\bar{t}W, tWZ$ and other rare top-associated processes) and VVV are estimated from simulation.

7 Signal extraction and unfolding

To extract the number of signal events in each bin of a differential distribution (or for each decay final state for the inclusive fiducial cross section), invariant mass templates for the Higgs boson signal and the background processes are fitted to the $m_{4\ell}$ distribution in data. Compared to the previous analysis [11], the non-resonant ZZ^* background is fitted simultaneously with the signal and constrained by extending the $m_{4\ell}$ fit range from 115–130 GeV to 105–160 GeV.

For the total and fiducial cross sections in different final states, the same normalisation factor is used for the ZZ^* contribution. For the differential cross-section measurements, multiple ZZ^* normalisation factors are introduced in the model, as described in Sect. 6. The reducible background, composed of Z + jets, $t\bar{t}$, and WZ processes, is estimated from dedicated control regions as described in Sect. 6 and its overall normalisation and shape can vary within the associated systematic uncertainties. Finally, for the differential distributions, no splitting into decay final states is performed, and the SM $ZZ^* \to 4\ell$ decay fractions are assumed.

The number of expected events N_i in each observable reconstruction bin i, expressed as a function of $m_{4\ell}$, is given by

$$N_i(m_{4\ell}) = \sum_j r_{ij} \cdot (1 + f_i^{\text{nonfid}}) \cdot \sigma_j^{\text{fid}} \cdot \mathcal{P}_i(m_{4\ell}) \cdot \mathcal{L} + N_i^{\text{bkg}}(m_{4\ell})$$

with

$$\sigma_j^{\text{fid}} = \sigma_j \cdot A_j \cdot \mathcal{B} \quad (1)$$

where A_j is the acceptance in the fiducial phase space and σ_j the total cross section in fiducial bin j, $\mathcal{L}$ is the integrated luminosity, $\mathcal{B}$ is the branching ratio and $N_i^{\text{bkg}}(m_{4\ell})$ is the background contribution. The index j runs over all observable bins in the fiducial phase space. The term $\mathcal{P}_i(m_{4\ell})$ is the $m_{4\ell}$ signal shape containing the fraction of events as a function of $m_{4\ell}$ expected in each reconstruction bin, taken from MC simulation. The term r_{ij} represents the detector response matrix, created with simulated signal samples and averaged across the different production modes using the expected SM cross-sections [108]. These factors correspond to the probability that an event generated within the fiducial volume in the observable bin j is reconstructed in bin i.

The normalisation, f_i^{nonfid}, represents the fraction of events which are outside of the fiducial region but are reconstructed within the signal region. This ranges from 1.1% to 1.7% depending on the bin of the unfolded observable or final state.

The detector response matrix accounts for bin-to-bin migrations in the unfolding of the signal. It was chosen over the bin-by-bin correction factor technique used in the previous analyses [11,12] due to its lower model dependence. Biases introduced via the unfolding method are minimised when using the response matrix; however, matrix unfolding can amplify small fluctuations in data when the response matrix is characterised by a large condition number.[3] The binning choice made for all observables ensures a statistical significance of more than 2σ for the signal process. The binning is also chosen to minimise migrations between bins. In general, the bin width is more than twice the experimental resolution. As a result, the response matrices for all the variables considered are well-conditioned, with a condition number less than 2.5. The fluctuations of the unfolded distribution can be further reduced using regularisation techniques. Unfolding tests done with toy data sets indicate that while regularisation provides a modest reduction of the statistical uncertainty, this reduction is counterbalanced by the bias introduced by this technique. Therefore, no regularisation of the unfolding was applied. Two of the jet-related variables are also provided in Appendix A using a regularised unfolding method, and are compatible with the matrix-unfolded results presented here.

Figure 1 shows the response matrix for the $p_{\text{T}}^{4\ell}$, N_{jets}, $p_{\text{T}}^{\text{lead. jet}}$, and m_{12} vs. m_{34} observables. For $p_{\text{T}}^{4\ell}$, the purity of the bins ranges from 87% at low $p_{\text{T}}^{4\ell}$, where the bins are narrow, to 97% at high $p_{\text{T}}^{4\ell}$, where wider bins are defined. The purity is defined as the percentage of reconstructed events which match the particle-level events in that bin. For the N_{jets} observable, the migrations are more relevant due to the relatively worse jet energy resolution and the presence of pile-up

[3] The condition number is defined as the ratio of the maximum and minimum singular values of the matrix. Values close to 1 signify a well-conditioned matrix with low sensitivity to statistical fluctuations on the input.

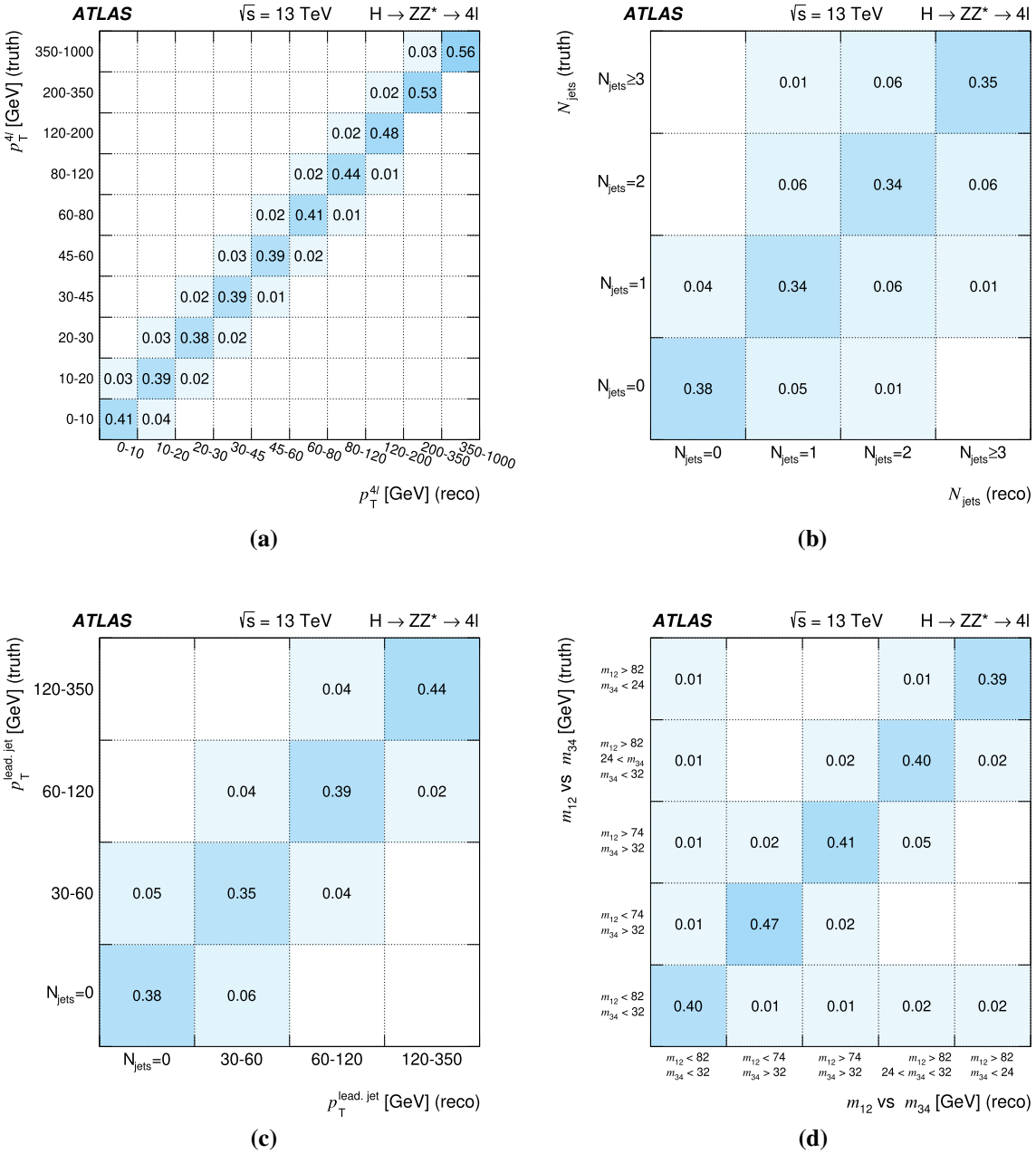

Fig. 1 Response matrices, derived using simulation, for **a** the transverse momentum of the four-lepton system $p_{\mathrm{T}}^{4\ell}$, **b** the number of jets N_{jets}, **c** the transverse momentum of the leading jet $p_{\mathrm{T}}^{\text{lead. jet}}$, and **d** the mass of the leading versus subleading lepton pair m_{12} vs. m_{34}. Only reconstructed events that were matched to generator-level ('truth') events are included. Bins below 0.005 are omitted for clarity

jets in the reconstructed events. This brings the purity for the for $N_{\mathrm{jets}} \geq 3$ bin down to 68%. The $p_{\mathrm{T}}^{\text{lead. jet}}$ migrations are similarly larger, with the lowest purity value of 67% occurring in the lowest $p_{\mathrm{T}}^{\text{lead. jet}}$ bin. The m_{12} vs. m_{34} observable, like $p_{\mathrm{T}}^{4\ell}$, has a higher purity. All bins have a purity of around 90% except the first bin, which has a purity of 78%.

8 Systematic uncertainties

The systematic uncertainties include experimental uncertainties, such as those in object reconstruction, identification, isolation, resolution, and trigger efficiencies, as well as theoretical uncertainties related to the modelling of the signal and background processes. More detail is provided in Ref. [31], while a brief overview of the dominant sources of uncertainty is provided here. The impacts of the experimental and theo-

Table 5 Fractional uncertainties for the inclusive fiducial and total cross sections, and ranges of systematic uncertainties for the differential measurements. The columns 'e/μ' and 'Jets' represent the experimental uncertainties in lepton and jet reconstruction and identification, respectively. The $Z+$jets, $t\bar{t}$, tXX (Other Bkg.) column includes uncertainties related to the estimation of these background sources. The ZZ^* theory (ZZ^* th.) uncertainties include the PDF and scale variations. Signal theory (Sig th.) uncertainties include PDF choice, QCD scale, and shower modelling of the signal. Finally, the column labelled 'Comp.' contains uncertainties related to production mode composition and unfolding bias which affect the response matrices. The uncertainties have been rounded to the nearest 0.5%, except for the luminosity uncertainty, which has been measured to be 1.7%

Observable	Stat.	Syst.	Dominant systematic components (%)						
	unc. (%)	unc. (%)	Lumi.	e/μ	Jets	Other Bkg.	ZZ^* Th.	Sig. Th.	Comp.
σ_{comb}	9	3	1.7	2	< 0.5	< 0.5	1	1.5	< 0.5
$\sigma_{4\mu}$	15	4	1.7	3	< 0.5	< 0.5	1.5	1	< 0.5
$\sigma_{4\text{e}}$	26	8	1.7	7	< 0.5	< 0.5	1.5	1.5	< 0.5
$\sigma_{2\mu 2\text{e}}$	20	7	1.7	5	< 0.5	< 0.5	2	1.5	< 0.5
$\sigma_{2\text{e}2\mu}$	15	3	1.7	2	< 0.5	< 0.5	1	1.5	< 0.5
$\mathrm{d}\sigma / \mathrm{d}p_{\mathrm{T}}^{4\ell}$	20–46	2–8	1.7	1–3	1–2	< 0.5	1–6	1–2	< 1
$\mathrm{d}\sigma / \mathrm{d}m_{12}$	12–42	3–6	1.7	2–3	< 1	< 0.5	1–2	1–2	< 1
$\mathrm{d}\sigma / \mathrm{d}m_{34}$	20–82	3–12	1.7	2–3	< 1	1–2	1–8	1–3	< 1
$\mathrm{d}\sigma / \mathrm{d}\lvert y_{4\ell}\rvert$	22–81	3–6	1.7	2–3	< 1	< 0.5	1–5	1–3	< 1
$\mathrm{d}\sigma / \mathrm{d}\lvert\cos\theta^*\rvert$	23–113	3–6	1.7	2–3	< 1	1–2	1–7	1–3	< 0.5
$\mathrm{d}\sigma / \mathrm{d}\cos\theta_1$	23–44	3–6	1.7	2–3	< 1	< 0.5	1–3	1–2	< 1
$\mathrm{d}\sigma / \mathrm{d}\cos\theta_2$	22–39	3–6	1.7	2–3	< 1	< 0.5	1–3	1–3	< 1
$\mathrm{d}\sigma / \mathrm{d}\phi$	20–29	2–5	1.7	2–3	< 1	< 0.5	1–3	1–2	< 0.5
$\mathrm{d}\sigma / \mathrm{d}\phi_1$	22–33	3–6	1.7	2–3	< 1	< 0.5	1–2	1–3	< 0.5
$\mathrm{d}\sigma / \mathrm{d}N_{\text{jets}}$	15–37	6–14	1.7	1–3	4–10	< 0.5	1–4	3–7	1–4
$\mathrm{d}\sigma / \mathrm{d}N_{b\text{-jets}}$	15–67	6–15	1.7	1–3	4–5	1–3	1–2	3–9	1–4
$\mathrm{d}\sigma / \mathrm{d}p_{\mathrm{T}}^{\text{lead. jet}}$	15–34	3–13	1.7	1–3	4–10	< 0.5	1–2	1–5	< 0.5
$\mathrm{d}\sigma / \mathrm{d}p_{\mathrm{T}}^{\text{sublead. jet}}$	11–67	5–22	1.7	1–3	2–12	< 1	1–3	2–15	1–5
$\mathrm{d}\sigma / \mathrm{d}m_{\text{jj}}$	11–50	5–18	1.7	1–3	1–11	< 0.5	1–3	2–15	1–2
$\mathrm{d}\sigma / \mathrm{d}\eta_{jj}$	11–57	5–17	1.7	1–3	2–10	< 0.5	1–2	2–14	1–4
$\mathrm{d}\sigma / \mathrm{d}\phi_{jj}$	11–50	4–18	1.7	1–3	2–9	< 0.5	1–3	2–14	1–6
$\mathrm{d}\sigma / \mathrm{d}m_{4\ell\text{j}}$	15–66	4–19	1.7	1–3	3–9	< 0.5	1–6	3–14	1–8
$\mathrm{d}\sigma / \mathrm{d}m_{4\ell\text{jj}}$	11–182	5–67	1.7	1–3	4–24	< 0.5	1–5	2–35	1–9
$\mathrm{d}\sigma / \mathrm{d}p_{\mathrm{T}}^{4\ell\text{j}}$	15–76	6–13	1.7	1–3	2–8	< 1	1–5	3–9	1–3
$\mathrm{d}\sigma / \mathrm{d}p_{\mathrm{T}}^{4\ell\text{jj}}$	11–76	5–27	1.7	2–3	2–9	1–2	1–4	3–17	1–12
$\mathrm{d}^2\sigma / \mathrm{d}m_{12}\mathrm{d}m_{34}$	16–65	3–11	1.7	2–3	< 1	1–2	1–9	1–3	1–2
$\mathrm{d}^2\sigma / \mathrm{d}p_{\mathrm{T}}^{4\ell}\mathrm{d}\lvert y_{4\ell}\rvert$	23–63	2–13	1.7	1–3	1–2	< 1	1–6	1–5	1–2
$\mathrm{d}^2\sigma / \mathrm{d}p_{\mathrm{T}}^{4\ell}\mathrm{d}N_{\text{jets}}$	23–93	4–193	1.7	2–14	2–25	1–3	1–7	1–12	1–92
$\mathrm{d}^2\sigma / \mathrm{d}p_{\mathrm{T}}^{4\ell\text{j}}\mathrm{d}m_{4\ell\text{j}}$	15–41	4–12	1.7	1–3	2–8	< 0.5	1–5	2–9	< 1
$\mathrm{d}^2\sigma / \mathrm{d}p_{\mathrm{T}}^{4\ell}\mathrm{d}p_{\mathrm{T}}^{4\ell\text{j}}$	15–53	3–10	1.7	1–3	2–8	< 1	1–2	2–6	1–2
$\mathrm{d}^2\sigma / \mathrm{d}p_{\mathrm{T}}^{4\ell}\mathrm{d}p_{\mathrm{T}}^{\text{lead. jet}}$	15–84	3–21	1.7	1–3	2–18	1–10	1–3	2–9	1–3
$\mathrm{d}^2\sigma / \mathrm{d}p_{\mathrm{T}}^{\text{lead. jet}}\mathrm{d}\lvert y^{\text{lead. jet}}\rvert$	15–38	3–11	1.7	1–3	2–9	< 0.5	1–2	1–4	1–2
$\mathrm{d}^2\sigma / \mathrm{d}p_{\mathrm{T}}^{\text{lead. jet}}\mathrm{d}p_{\mathrm{T}}^{\text{sublead. jet}}$	15–63	5–22	1.7	1–3	4–15	< 0.5	1–4	3–11	1–7

retical uncertainties on the measurements are summarised in Table 5.

8.1 Experimental uncertainties

The uncertainty in the predicted yields due to pile-up modelling ranges between 1% and 2%. The uncertainty in the integrated luminosity is 1.7% and affects the signal yields

and simulated background estimates when not constrained by the sidebands.

The electron (muon) reconstruction and identification efficiency uncertainties are approximately 1.0–2.0% (< 1.0%). The uncertainty in the expected yields due to the muon and electron isolation efficiencies is also considered, and is approximately 1%. Lepton energy momentum scale and resolution uncertainties have negligible impacts on the presented results.

The impact of uncertainties in the jet energy scale and resolution (of between 1 and 3%) is only relevant for the jet-related differential cross-section measurements, where their impact is typically between 3 and 5%, and is negligible in the other measurements. The uncertainty in the performance of the b-tagging algorithm is at the level of a few percent over most of the jet p_{T} range [131].

The impact of the precision of the Higgs boson mass measurement, $m_H = 125.09 \pm 0.24\,\mathrm{GeV}$ [15], on the signal acceptance due to the signal region mass-window requirement is negligible.

For the data-driven measurement of the reducible background, three sources of uncertainty are considered: statistical uncertainty, overall systematic uncertainty for each of $\ell\ell + \mu\mu$ and $\ell\ell + ee$, and a shape systematic uncertainty which varies with the differential variable. Impacts from these sources of uncertainty range from less than 1% to a maximum of around 3%. The inclusive reducible background estimate has a relatively small (3%) statistical uncertainty, which has minimal impact on the cross section.

8.2 Theoretical uncertainties

Sources of theoretical uncertainty include missing higher-order corrections, parton shower and underlying event modelling, and PDF+α_{s} uncertainties, and these all affect modelling of the signal and background processes. For measurements of the cross section, the impact of these theory systematic uncertainties on the signal comes from their effects on the response matrix.

The prediction of the ggF process in different N_{jets} categories and migration effects on the N_{jets} ggF cross sections are large sources of theoretical uncertainty, which are accounted for using the approach detailed in Ref. [108]. The QCD scale uncertainty from the factorisation and renormalisation scales, resummation scales, and migrations between N-jet phase-space bins are considered [52,134–137]. The impact of QCD scale variations on the Higgs boson p_{T} distribution as well as the uncertainty of the p_{T} distribution in the 0-jet bins are also taken into account. Higher-order impacts on the p_{T} distribution predictions due to treating the top quark mass as infinite in the heavy-quark loop are accounted for by comparing these predictions with finite-mass calculations. For the VBF production mode, the uncertainty due to missing higher orders in QCD are considered, including migration effects in number of jets, transverse momentum of the Higgs boson, transverse momentum of the Higgs boson and leading dijet system, and the invariant mass of the two leading jets as outlined in the scheme presented in Ref. [138].

For production modes other than ggF and VBF, the effects of QCD scale uncertainties are estimated by considering all configurations of renormalisation and factorisation scales varied by a factor of two. In each experimental bin, the largest difference between all the variations and the nominal configuration is assigned as uncertainty.

The effects of parton shower and multiple-parton interaction modelling uncertainties on the acceptance are estimated using tune eigenvector variations as well as comparisons between acceptances calculated with Pythia 8 and Herwig 7 parton showering algorithms.

PDF uncertainty impacts are estimated using the eigenvector variations of the PDF4LHC_NLO_30 Hessian PDF set, following the PDF4LHC recommendations [71].

For the cross sections extrapolated to the full phase space, an additional uncertainty (2.2%) related to the $H \to ZZ^*$ branching ratio [68,69] is included in the measurement.

Since the ZZ^* process normalisation is constrained by performing a simultaneous fit of sideband regions enriched in this contribution together with the signal region, most of the theoretical uncertainty in the normalisation for this background vanishes.[4] The uncertainties due to missing higher-order effects in QCD are estimated by varying the factorisation and renormalisation QCD scales by a factor of two; the impact of the PDF uncertainty is estimated using the MC replicas of the NNPDF 3.0 PDF set. Uncertainties due to the parton shower modelling for the ZZ^* process are considered as well. The impact of these uncertainties is below 2% for all the fiducial differential cross sections. In addition, the $m_{4\ell}$ shape obtained from Sherpa is compared with that obtained from Powheg and MadGraph5_aMC@NLO and the difference is taken as an additional source of systematic uncertainty. In each $m_{4\ell}$ bin, the largest difference between Sherpa and Powheg or MadGraph5_aMC@NLO is used, and the systematic uncertainty is determined by interpolating between these shapes. Typically, Sherpa and Powheg have the largest difference in the predicted $m_{4\ell}$ shape, with the impact linearly varying from approximately $\pm 10\%$ at low $m_{4\ell}$ to $\mp 2\%$ at high $m_{4\ell}$.

The uncertainty in the gluon-induced ZZ^* process is taken into account as well by changing the relative composition between the quark-initiated and gluon-initiated ZZ^* components according to the theoretical uncertainty in the predicted cross sections.

[4] Except in cases where the cross-section bins are merged into a single ZZ^* bin, where the relative normalisation uncertainties are included.

Table 6 Expected (pre-fit) and observed numbers of events in the four decay final states after the event selection, in the mass range 115 GeV$< m_{4\ell} <$ 130 GeV. The sum of the expected number of SM Higgs boson events and the estimated background yields is compared with the data. Combined statistical and systematic uncertainties are included for the predictions (see Sect. 8)

Final state	Signal	ZZ^* background	Other backgrounds	Total expected	Observed
4μ	78 ± 5	38.0 ± 2.1	2.85 ± 0.18	119 ± 5	115
$2e2\mu$	53.0 ± 3.1	26.1 ± 1.4	2.98 ± 0.19	82.0 ± 3.4	96
$2\mu 2e$	40.1 ± 2.9	17.3 ± 1.3	3.6 ± 0.5	61.0 ± 3.2	57
$4e$	35.3 ± 2.6	15.0 ± 1.5	2.91 ± 0.33	53.2 ± 3.1	42
Total	206 ± 13	96 ± 6	12.2 ± 1.0	315 ± 14	310

Finally, unfolding-related uncertainties arise from uncertainties in the production mode composition that affect the response matrices, as well as from uncertainties in the bias introduced by the unfolding method. For the former, an uncertainty is assessed by varying the production cross sections within their measured uncertainties taken from Ref. [12], and has an impact of less than 1%. In the latter case, the uncertainty in the bias is obtained independently per bin by comparing the unfolded cross section from simulation with that expected when varying the underlying true cross sections of the simulated data sample within the expected statistical error. The impact of this uncertainty is typically negligible in distributions such as $p_{\mathrm{T}}^{4\ell}$, where the response matrix is largely diagonal, but can be of the order of 10% in distributions with larger bin migrations, such as N_{jets}.

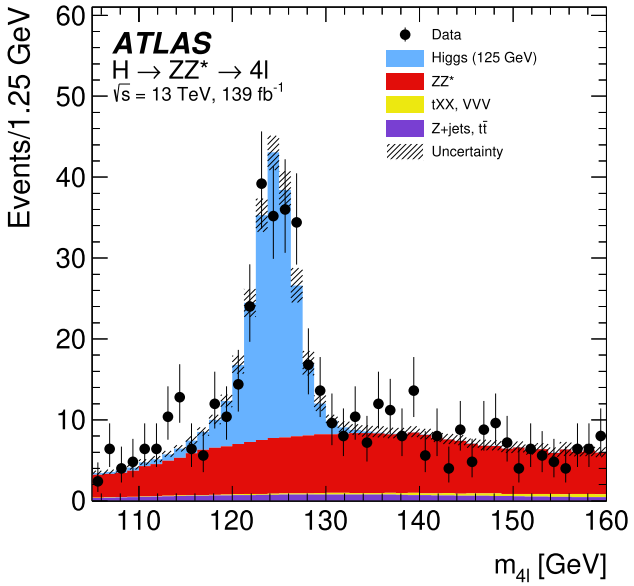

Fig. 2 The observed and expected (pre-fit) inclusive four-lepton invariant mass distributions for the selected Higgs boson candidates, shown for an integrated luminosity of 139 fb^{-1} and at $\sqrt{s} = 13$ TeV. The uncertainty in the prediction is shown by the hatched band, which includes the theoretical uncertainties of the SM cross section for the signal and the ZZ^* background

9 Results

Results are presented for the full set of inclusive and differential variables outlined in Sect. 5. Section 9.1 presents the data yields from the full Run 2 data set. Section 9.2 provides details of the statistical procedure used for the extraction of the measurements. Cross-section results, and comparisons with SM predictions, are provided in Sects. 9.3 and 9.4.

9.1 Measured data yields

The observed number of events in each of the four decay final states, and the expected signal and background yields before fitting to data (pre-fit), are presented in Table 6. These events have passed the event selection and fall in a narrow window around the Higgs boson mass peak ($115 < m_{4\ell} < 130$ GeV).

Figures 2 and 3 show the expected and observed four-lepton invariant mass distributions, inclusively and per final state respectively. The $m_{4\ell}$ distribution shows two clear peaks corresponding to $Z \to 4\ell$ production and the Higgs boson signal with a mass near 125 GeV.

The observed and expected distributions of one-dimensional observables are shown in Figs. 4, 5, 6, 7, 8 and 9. In addition, the observed and expected distributions for the two-dimensional observables are shown in Figs. 10, 11, 12, 13, 14, 15, 16 and 17. All these figures show events selected within an $m_{4\ell}$ mass range of 115–130 GeV. Further details of the compatibility with the SM are reported in Sect. 9.4.

9.2 Statistical analysis

The inclusive fiducial and differential cross sections are measured using a binned profile-likelihood-ratio fit [139], taking into account all bins of a given distribution. The likelihood function includes the shape and normalisation uncertainties of the signal and background predictions as nuisance parameters, as outlined in Sect. 8. The cross sections are extracted by minimising two times the negative logarithm of the profile likelihood ratio, $-2 \ln \Lambda$. In the asymptotic approximation,

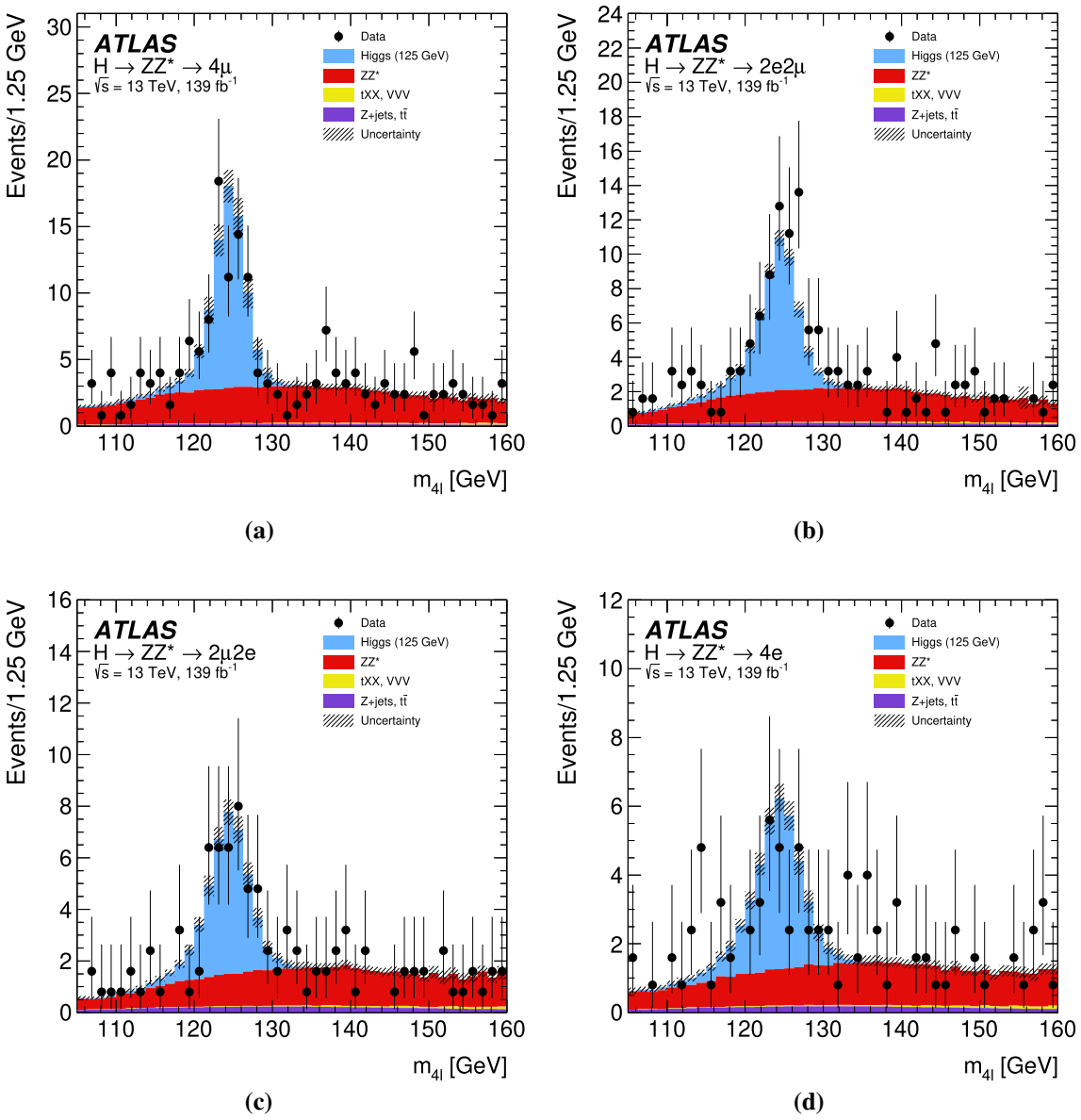

Fig. 3 The observed and expected (pre-fit) four-lepton invariant mass distribution for the selected Higgs boson candidates, for the different decay final states **a** 4μ, **b** $2e2\mu$, **c** $2\mu2e$, **d** $4e$. The uncertainty in the prediction is shown by the hatched band, which includes the theoretical uncertainties of the SM cross section for the signal and the ZZ^* background

i.e. the large sample limit, $-2\ln\Lambda$ behaves as a χ^2 distribution with one degree of freedom. The compatibility of a measured cross section and its theoretical prediction is tested by computing a p-value based on the difference between the value of $-2\ln\Lambda$ at the best-fit value and the value obtained by fixing the cross section in each bin to that predicted by theory. These p-values do not include the uncertainties in the theoretical predictions. For all measured observables the asymptotic approximation is validated with pseudo-experiments, and where the number of observed events is less than three, the uncertainties are corrected to the values obtained with the pseudo-experiments.

For the fiducial and differential cross-section measurements, the fitted $m_{4\ell}$ distribution in each final state or differential bin is used to extract the measured cross section following Eq. (1). The fiducial cross sections of the four final states can either be summed to obtain an inclusive fiducial cross section, or they can be combined assuming the SM $ZZ^* \to 4\ell$ relative branching ratios. The latter combination is more model dependent, but benefits from a smaller statistical uncertainty.

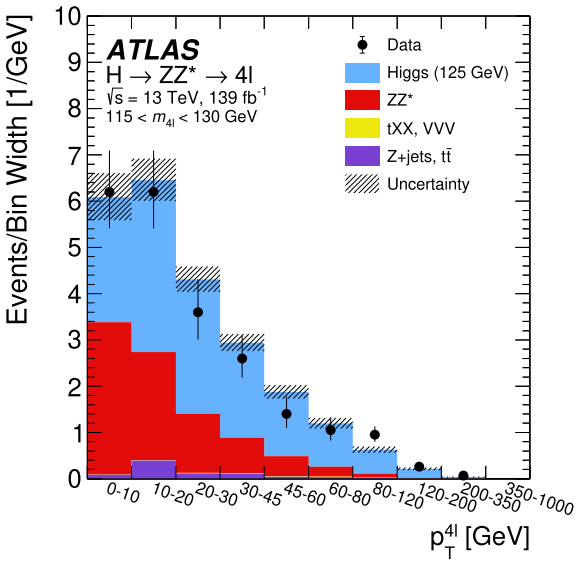

(a)

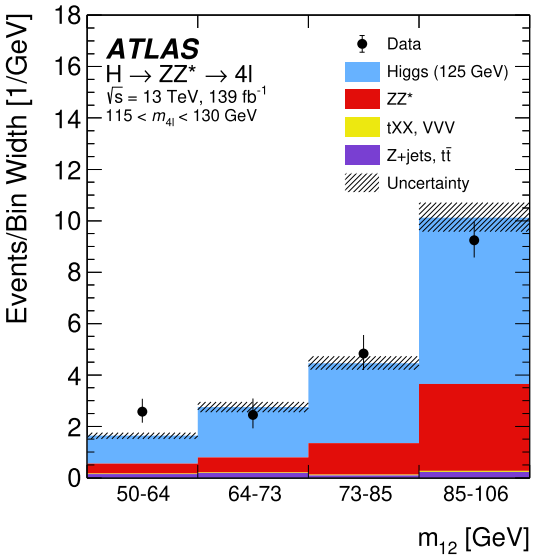

(b)

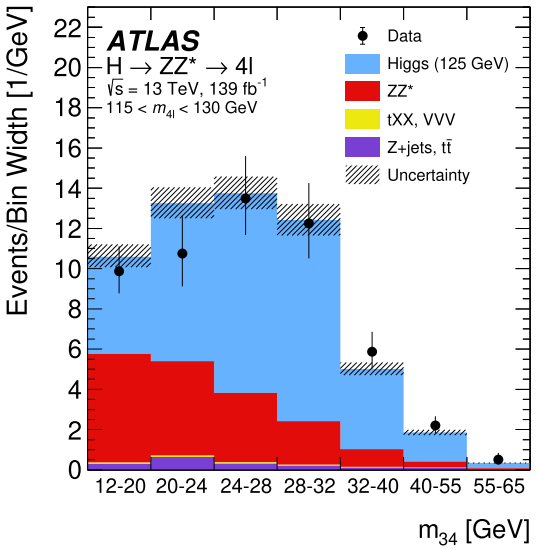

(c)

Fig. 4 The observed and expected (pre-fit) distributions of **a** $p_{\mathrm{T}}^{4\ell}$, **b** m_{12}, and **c** m_{34} in the mass region $115 < m_{4\ell} < 130$ GeV, for an integrated luminosity of 139 fb^{-1} collected at $\sqrt{s} = 13$ TeV. A SM Higgs boson signal with a mass $m_H = 125$ GeV is assumed. The uncertainty in the prediction is shown by the hatched band, which includes the theoretical uncertainties of the SM cross section for the signal and the ZZ^* background

9.3 Inclusive fiducial cross-section measurements

The fiducial production cross sections of the $H \to ZZ^* \to 4\ell$ process are presented in Table 7 and Fig. 18. The left panel in Fig. 18a shows the fiducial cross sections for the four individual decay final states: 4μ, $4e$ decays (hereafter referred to as same flavour), and $2\mu 2e$, $2e2\mu$ decays (hereafter referred to as different flavour). The middle panel shows the cross sections for same- and different-flavour decays, which can provide a probe of same-flavour interference effects, as well as the inclusive fiducial cross sections obtained by either summing all 4ℓ decay final states or combining them assuming relative SM branching ratios.

The data are compared with the SM prediction after accounting for the fiducial acceptance as determined from the SM Higgs boson simulated samples (see Sect. 3).

The combined inclusive fiducial cross section is extrapolated to the full phase space, as shown in the right panel of Fig. 18, using the fiducial acceptance as well as the branching ratios, with the uncertainties described in Sect. 8. The

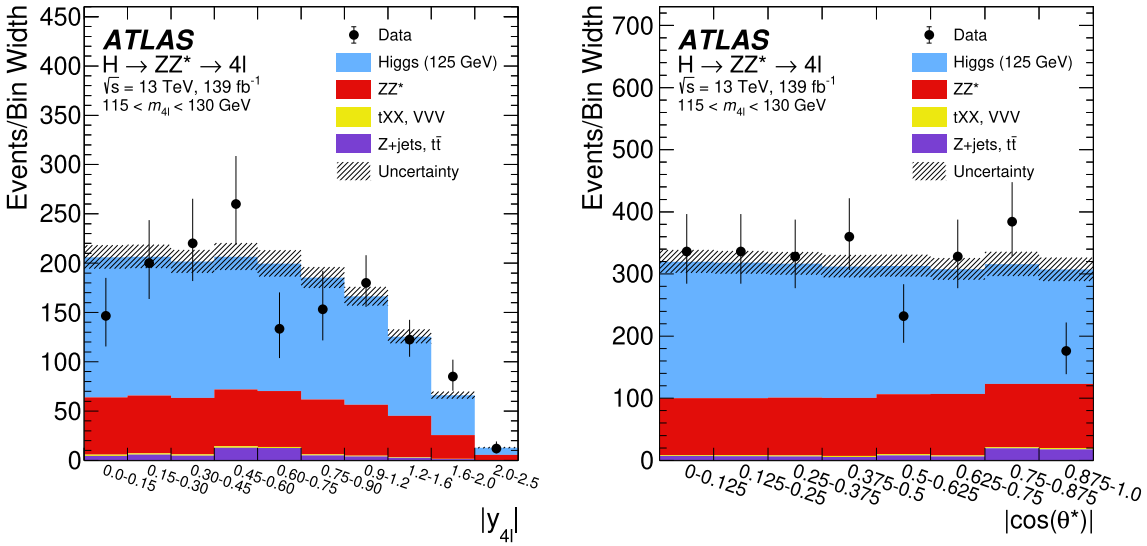

Fig. 5 The observed and expected (pre-fit) distributions of **a** $|y_{4\ell}|$ and **b** $|\cos\theta^*|$ in the mass region $115 < m_{4\ell} < 130$ GeV, for an integrated luminosity of 139 fb^{-1} collected at $\sqrt{s} = 13$ TeV. A SM Higgs boson signal with a mass $m_H = 125$ GeV is assumed. The uncertainty in the prediction is shown by the hatched band, which includes the theoretical uncertainties of the SM cross section for the signal and the ZZ^* background

total cross section is also compared with the cross sections predicted by NNLOPS, MadGraph5_aMC@NLO-FxFx (MG5-FxFx) and Hres 2.3 [51,140] for ggF, while for all other production modes the predictions described in Sect. 3 are used. For ggF, all generators predict cross sections that are lower than the N^{3}LO calculation. The p-values, calculated as described in Sect. 9.2, are shown in Table 7. The probability of compatibility of the measured fiducial cross section (σ_{comb}) and the Standard Model expectation is at the level of 67%.

9.4 Differential cross-section measurements

The measured differential production cross sections for the transverse momentum $p_{\text{T}}^{4\ell}$ of the Higgs boson are shown in Fig. 19, while the measured differential cross sections with respect to the masses of the leading and subleading Z bosons resulting from the Higgs boson decay, m_{12} and m_{34}, are provided in Fig. 20. Figures 21, 22, and 23 show the measured differential production cross sections with respect to angular variables, $|y_{4\ell}|$, $|\cos\theta^*|$, $\cos\theta_1$, $\cos\theta_2$, ϕ, and ϕ_1, that probe the kinematics of the Higgs boson decay products.

Differential production cross-section measurements with respect to variables that probe the jet activity in reconstructed Higgs boson events follow in Figs. 24, 25, 26, 27 and 28. These include the exclusive and inclusive jet multiplicities, N_{jets}, the b-jet multiplicity, $N_{b\text{-jets}}$, variables measuring the transverse momentum of the jets, $p_{\text{T}}^{\text{lead. jet}}$ and $p_{\text{T}}^{\text{sublead. jet}}$, as well as variables that probe the kinematics of pairs of jets in events with at least two jets, m_{jj}, $\Delta\eta_{\text{jj}}$, and $\Delta\phi_{\text{jj}}$.

In addition, differential cross-section measurements are provided for observables aimed at studying the relationship between the reconstructed Higgs boson and accompanying jets. These are presented in Figs. 29 and 30.

Finally, the double differential measurements in bins of m_{12} vs. m_{34}, $p_{\text{T}}^{4\ell}$ vs. $|y_{4\ell}|$, $p_{\text{T}}^{4\ell}$ vs. N_{jets}, $p_{\text{T}}^{4\ell}$ vs. $p_{\text{T}}^{4\ell\text{j}}$, $p_{\text{T}}^{4\ell\text{j}}$ vs. $m_{4\ell\text{j}}$, $p_{\text{T}}^{\text{lead. jet}}$ vs. $p_{\text{T}}^{\text{sublead. jet}}$, and $p_{\text{T}}^{\text{lead. jet}}$ vs. $|y^{\text{lead. jet}}|$ are provided in Figs. 31, 32, 33, 34, 35, 36, 37 and 38.

The data are compared with SM expectations constructed from the ggF predictions provided by NNLOPS and MadGraph5_aMC@NLO-FxFx. Certain distributions related to the production of the Higgs boson also include a comparison with the predictions from NNLOJET and Radish and some of the measurements related to the Higgs boson decay are compared also with predictions from Hto4l and Prophecy4f. The ggF predictions from MadGraph5_aMC@NLO-FxFx and NNLOPS are normalised to the N^{3}LO prediction while the normalisations for NNLOJET and Radish are to their respective predicted cross sections. All the other Higgs boson production modes are normalised to the most accurate SM predictions, as discussed in Sect. 3. The shaded bands on the expected cross sections indicate the PDF and scale uncertainties.[5] The figures include

[5] Given the accuracy of some predictions, this procedure may underestimate the associated uncertainties. In particular, NNLOPS predictions

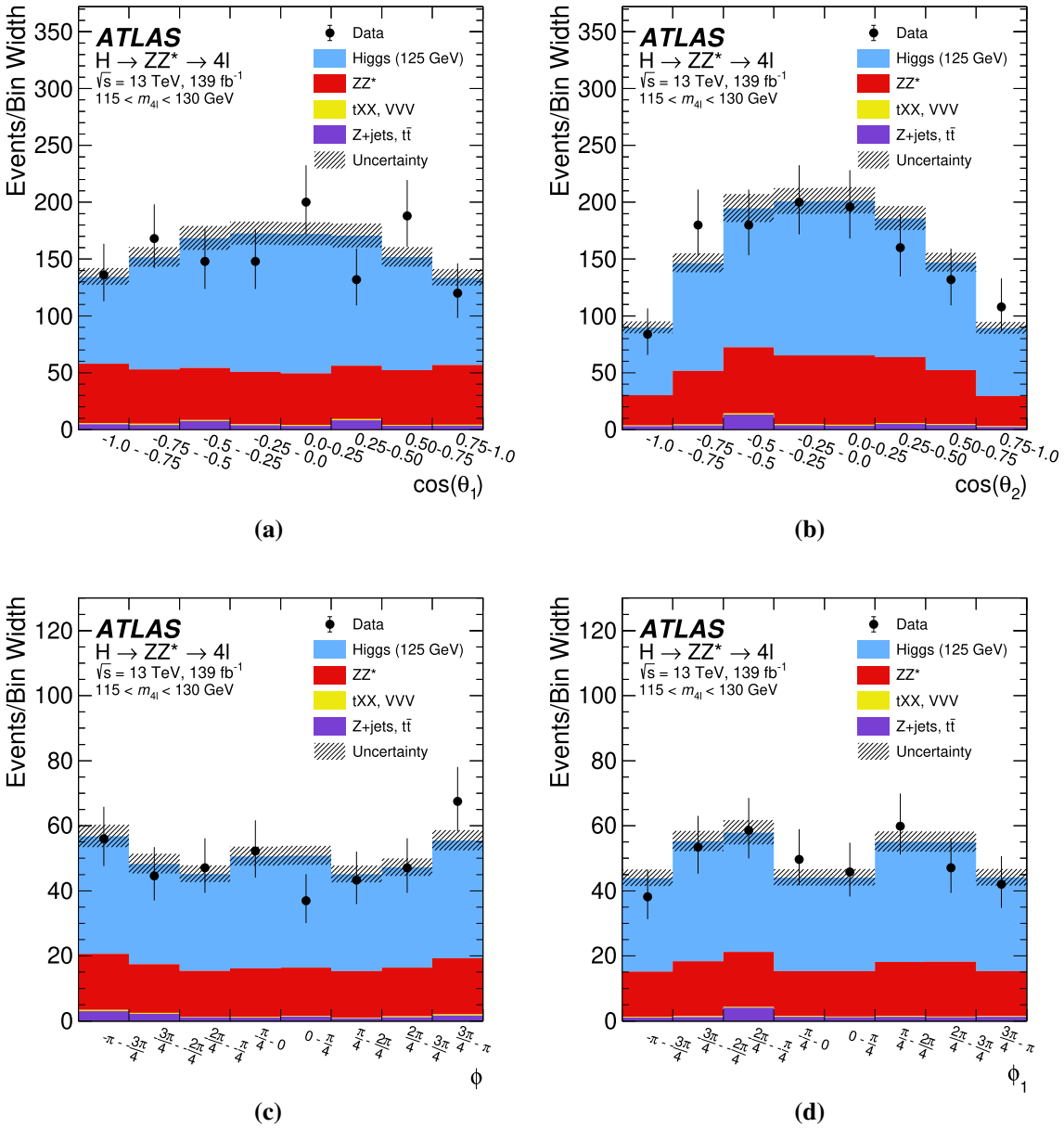

Fig. 6 The observed and expected (pre-fit) distributions of **a** $\cos\theta_1$, **b** $\cos\theta_2$, **c** ϕ, and **d** ϕ_1 in the mass region $115 < m_{4\ell} < 130$ GeV, for an integrated luminosity of 139 fb^{-1} collected at $\sqrt{s} = 13$ TeV. A SM Higgs boson signal with a mass $m_H = 125$ GeV is assumed. The uncertainty in the prediction is shown by the hatched band, which includes the theoretical uncertainties of the SM cross section for the signal and the ZZ^* background

the p-values quantifying the probability of compatibility of the measurements and the SM predictions and show in addition fitted values of the ZZ^* normalisation factors. Finally, the correlation matrices between the measured cross sections and the ZZ^* background normalisation factors are shown in all figures along with the cross-section measurements.

Overall, there is good agreement between measured cross sections and predictions. Small differences between measurement and prediction occur in several of the angular observables, as well as in bins of $m_{4\ell jj}$, and several of the double differential measurements. For example, the p-value for the double differential distribution $p_{\mathrm{T}}^{\text{lead. jet}}$ vs. $|y^{\text{lead. jet}}|$ in Fig. 38 is particularly low due to the downward fluctuation in bin 2. However, when considering the size of the uncertainties these differences are not significant. Since no events are observed in the highest bin for $p_{\mathrm{T}}^{4\ell}$ in Fig. 19, an upper

for ≥ 3 jets, which are affected in part by additional uncertainties which are not accounted by the procedure described in Sect. 8.2.

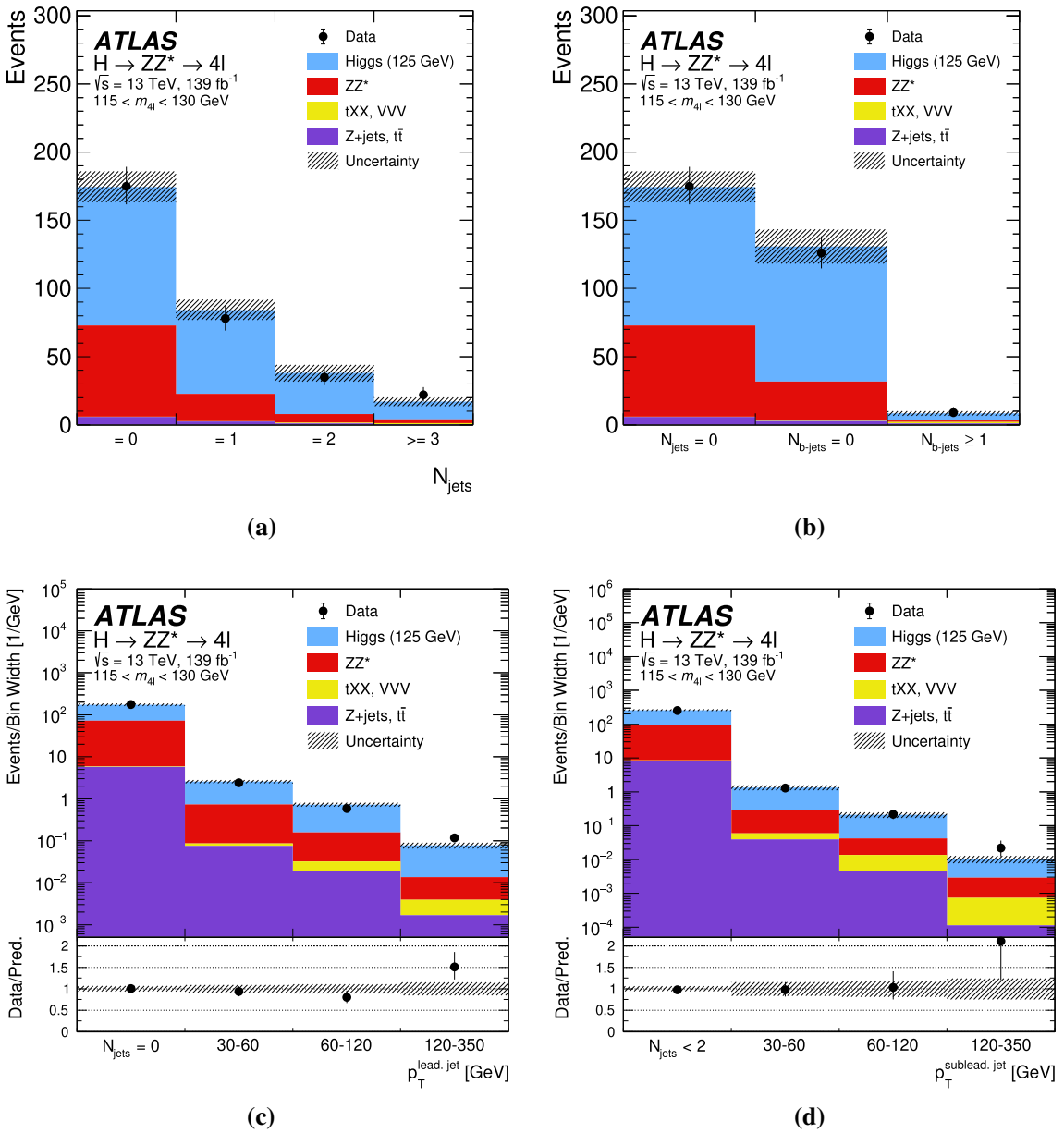

Fig. 7 The observed and expected (pre-fit) distributions of **a** N_{jets}, **b** $N_{b\text{-jets}}$, **c** $p_{\text{T}}^{\text{lead. jet}}$, and **d** $p_{\text{T}}^{\text{sublead. jet}}$ in the mass region $115 < m_{4\ell} < 130$ GeV, for an integrated luminosity of 139 fb^{-1} collected at $\sqrt{s} = 13$ TeV. A SM Higgs boson signal with a mass $m_H = 125$ GeV is assumed. In distribution **c**, the first bin contains events with zero jets, while in distribution **d**, the first bin contains events with fewer than two jets. In both **c** and **d**, all bins except the first are divided by the bin width. The uncertainty in the prediction is shown by the hatched band, which includes the theoretical uncertainties of the SM cross section for the signal and the ZZ^* background

limit of 27 ab at 95% confidence level (CL) is set on the cross section using CLs [141]. Similarly, a limit of $\sigma < 38$ ab at 95% CL is also set in the last bin of $p_{\text{T}}^{4\ell\text{jj}}$ in Fig. 29.

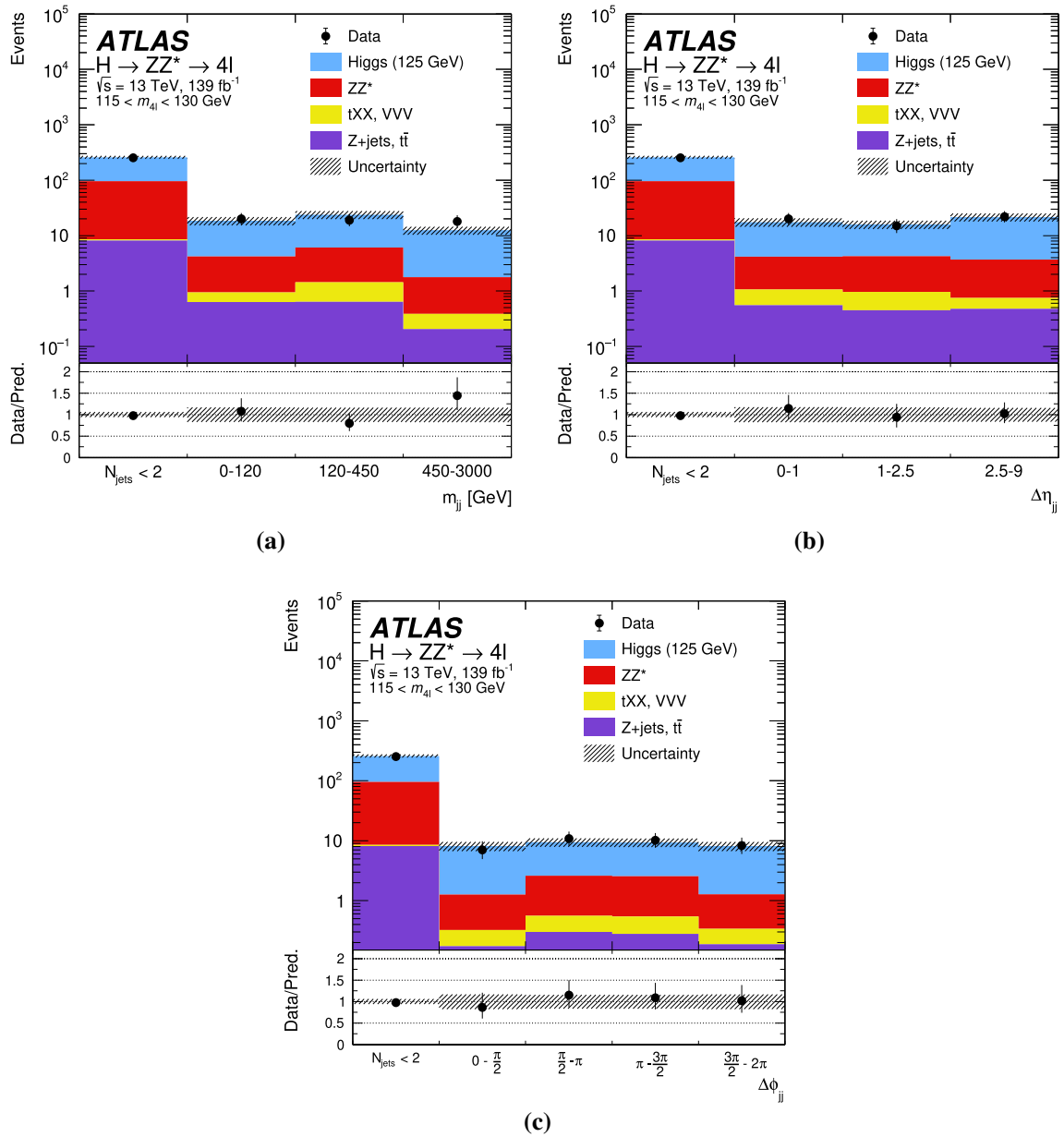

Fig. 8 The observed and expected (pre-fit) distributions of **a** m_{jj}, **b** $\Delta\eta_{\mathrm{jj}}$, and **c** $\Delta\phi_{\mathrm{jj}}$ in the mass region $115 < m_{4\ell} < 130$ GeV, for an integrated luminosity of 139 fb^{-1} collected at $\sqrt{s} = 13$ TeV. A SM Higgs boson signal with a mass $m_H = 125$ GeV is assumed. In all distributions, the first bin contains events with fewer than two jets. The uncertainty in the prediction is shown by the hatched band, which includes the theoretical uncertainties of the SM cross section for the signal and the ZZ^* background

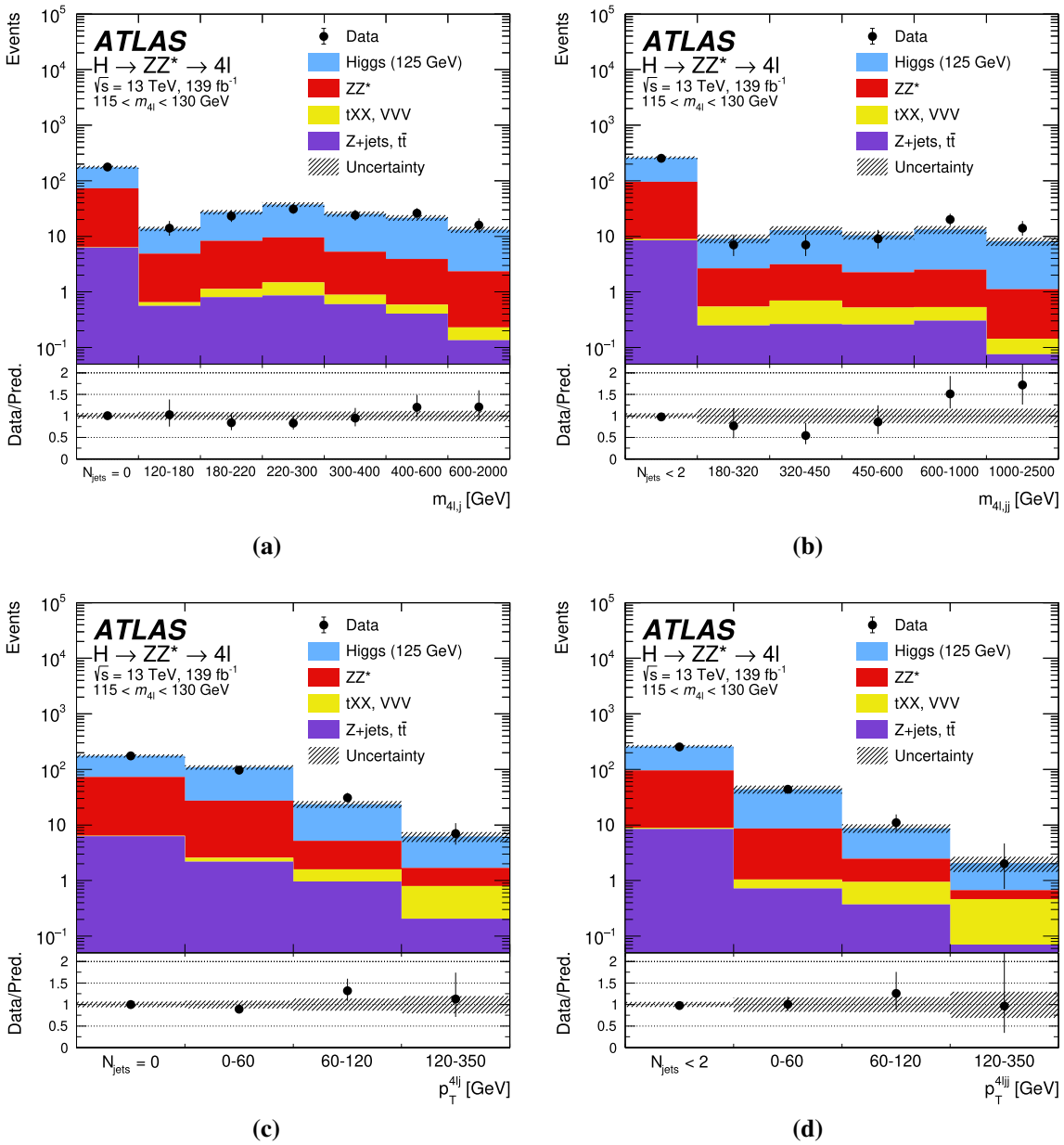

Fig. 9 The observed and expected (pre-fit) distributions of **a** $m_{4\ell j}$, **b** $m_{4\ell jj}$, **c** $p_{\mathrm{T}}^{4\ell j}$, and **d** $p_{\mathrm{T}}^{4\ell jj}$ in the mass region $115 < m_{4\ell} < 130$ GeV, for an integrated luminosity of 139 fb^{-1} collected at $\sqrt{s} = 13$ TeV. A SM Higgs boson signal with a mass $m_H = 125$ GeV is assumed. The first bin in **a** and **c** contains events with no jets, while the first bin in **b** and (**d**) contains events with fewer than two jets. The uncertainty in the prediction is shown by the hatched band, which includes the theoretical uncertainties of the SM cross section for the signal and the ZZ^* background

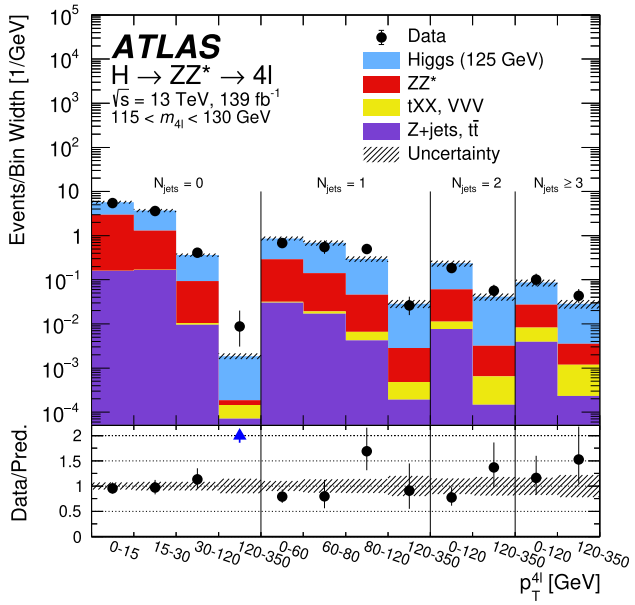

Fig. 10 The observed and expected (pre-fit) distributions of $p_{\mathrm{T}}^{4\ell}$ in N_{jets} bins in the mass region $115 < m_{4\ell} < 130$ GeV, for an integrated luminosity of 139 fb^{-1} collected at $\sqrt{s} = 13$ TeV. A SM Higgs boson signal with a mass $m_H = 125$ GeV is assumed. The uncertainty in the prediction is shown by the hatched band, which includes the theoretical uncertainties of the SM cross section for the signal and the ZZ^* background

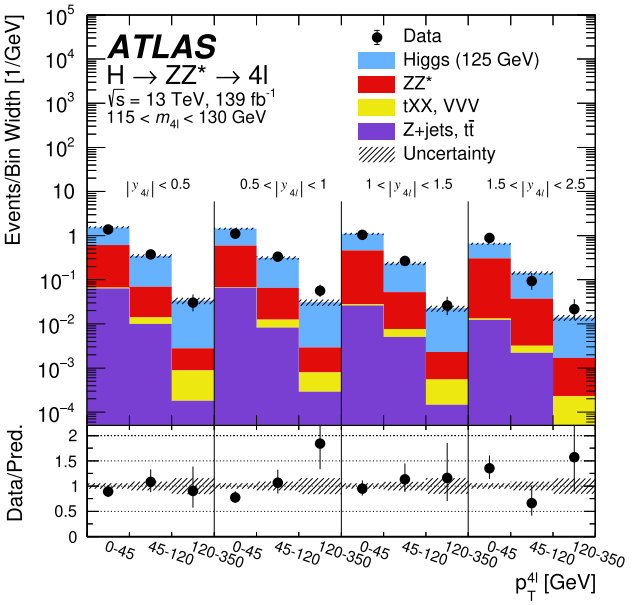

Fig. 11 The observed and expected (pre-fit) distributions of $p_{\mathrm{T}}^{4\ell}$ in $|y_{4\ell}|$ bins in the mass region $115 < m_{4\ell} < 130$ GeV, for an integrated luminosity of 139 fb^{-1} collected at $\sqrt{s} = 13$ TeV. A SM Higgs boson signal with a mass $m_H = 125$ GeV is assumed. The uncertainty in the prediction is shown by the hatched band, which includes the theoretical uncertainties of the SM cross section for the signal and the ZZ^* background

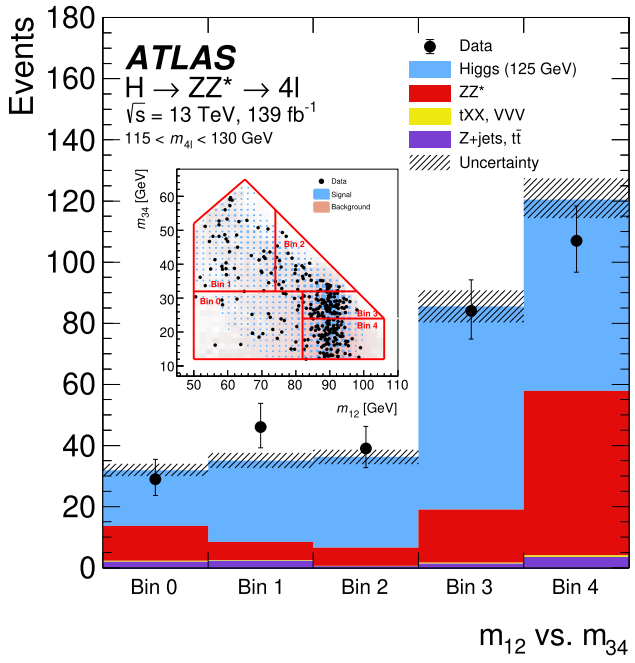

Fig. 12 The observed and expected (pre-fit) distribution in bins of the leading vs. subleading Z boson mass, m_{12} vs. m_{34}. The same distribution in the 2D plane is provided in the inset plot, where the black dots depict data and the blue and pink shaded areas represent simulated signal and background, respectively. The red lines depict the bin boundaries, chosen as described in Sect. 7. These distributions correspond to the mass region $115 < m_{4\ell} < 130$ GeV for an integrated luminosity of 139 fb^{-1} collected at $\sqrt{s} = 13$ TeV. A SM Higgs boson signal with a mass $m_H = 125$ GeV is assumed. The uncertainty in the prediction is shown by the hatched band, which includes the theoretical uncertainties of the SM cross section for the signal and the ZZ^* background

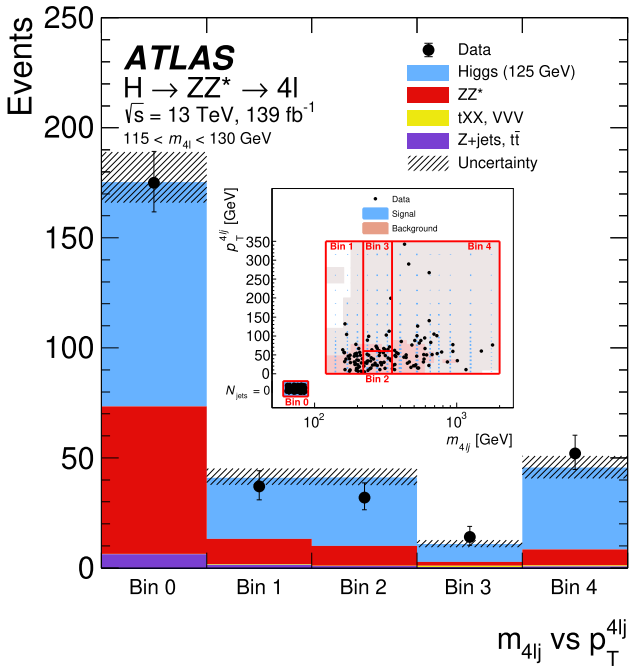

Fig. 13 The observed and expected (pre-fit) distribution in bins of the transverse momentum of the four-lepton plus leading-jet system vs. the invariant mass of the four-lepton plus leading-jet system, $p_{\mathrm{T}}^{4\ell j}$ vs. $m_{4\ell \mathrm{j}}$. The same distribution in the 2D plane is provided in the inset plot, where the black dots depict data and the blue and pink shaded areas represent simulated signal and background, respectively. The red lines depict the bin boundaries, chosen as described in Sect. 7. These distributions correspond to the mass region $115 < m_{4\ell} < 130$ GeV for an integrated luminosity of 139 fb^{-1} collected at $\sqrt{s} = 13$ TeV. A SM Higgs boson signal with a mass $m_H = 125$ GeV is assumed. The uncertainty in the prediction is shown by the hatched band, which includes the theoretical uncertainties of the SM cross section for the signal and the ZZ^* background

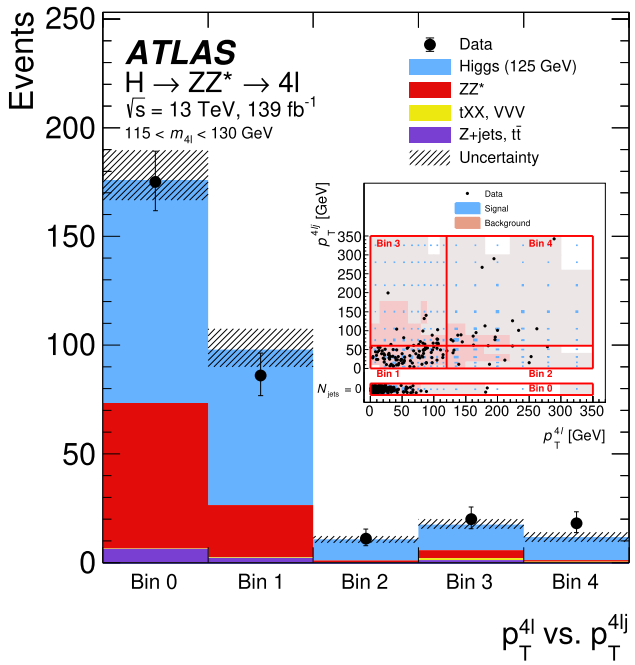

Fig. 14 The observed and expected (pre-fit) distribution in bins of the transverse momentum of the four-lepton system vs. the transverse momentum of the four-lepton plus leading-jet system, $p_{\mathrm{T}}^{4\ell}$ vs. $p_{\mathrm{T}}^{4\ell\mathrm{j}}$. The same distribution in the 2D plane is shown in the inset plot, where the black dots depict data and the blue and pink shaded areas represent simulated signal and background, respectively. The red lines depict the bin boundaries, chosen as described in Sect. 7. These distributions correspond to the mass region $115 < m_{4\ell} < 130$ GeV for an integrated luminosity of 139 fb^{-1} collected at $\sqrt{s} = 13$ TeV. A SM Higgs boson signal with a mass $m_H = 125$ GeV is assumed. The uncertainty in the prediction is shown by the hatched band, which includes the theoretical uncertainties of the SM cross section for the signal and the ZZ^* background

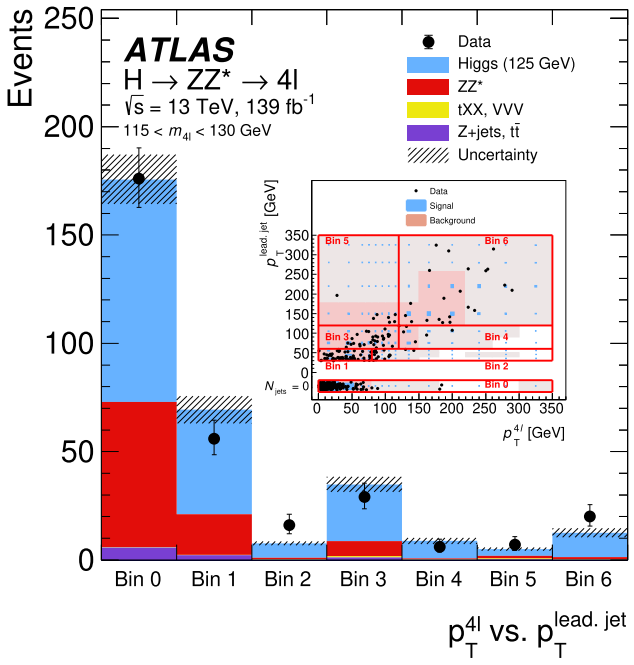

Fig. 15 The observed and expected (pre-fit) distribution in bins of the transverse momentum of the four-lepton system vs. the transverse momentum of the leading jet, $p_{\mathrm{T}}^{4\ell}$ vs. $p_{\mathrm{T}}^{\text{lead. jet}}$. The same distribution in the 2D plane is provided in the inset plot, where the black dots depict data and the blue and pink shaded areas represent simulated signal and background, respectively. The red lines depict the bin boundaries, chosen as described in Sect. 7. These distributions correspond to the mass region $115 < m_{4\ell} < 130$ GeV for an integrated luminosity of 139 fb^{-1} collected at $\sqrt{s} = 13$ TeV. A SM Higgs boson signal with a mass $m_H = 125$ GeV is assumed. The uncertainty in the prediction is shown by the hatched band, which includes the theoretical uncertainties of the SM cross section for the signal and the ZZ^* background

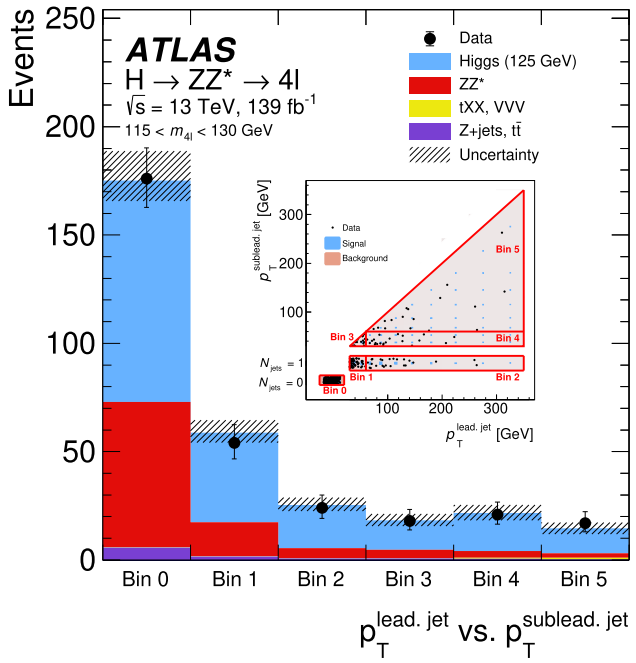

Fig. 16 The observed and expected (pre-fit) distribution in bins of the transverse momentum of the leading vs. subleading jet, $p_{\mathrm{T}}^{\text{lead. jet}}$ vs. $p_{\mathrm{T}}^{\text{sublead. jet}}$. The same distribution in the 2D plane is provided in the inset plot, where the black dots depict data and the blue and pink shaded areas represent simulated signal and background, respectively. The red lines depict the bin boundaries, chosen as described in Sect. 7. These distributions correspond to the mass region $115 < m_{4\ell} < 130$ GeV for an integrated luminosity of 139 fb^{-1} collected at $\sqrt{s} = 13$ TeV. A SM Higgs boson signal with a mass $m_H = 125$ GeV is assumed. The uncertainty in the prediction is shown by the hatched band, which includes the theoretical uncertainties of the SM cross section for the signal and the ZZ^* background. $p_{\mathrm{T}}^{\text{lead. jet}}$ and $p_{\mathrm{T}}^{\text{sublead. jet}}$ are required to have p_{T} greater than 30 GeV

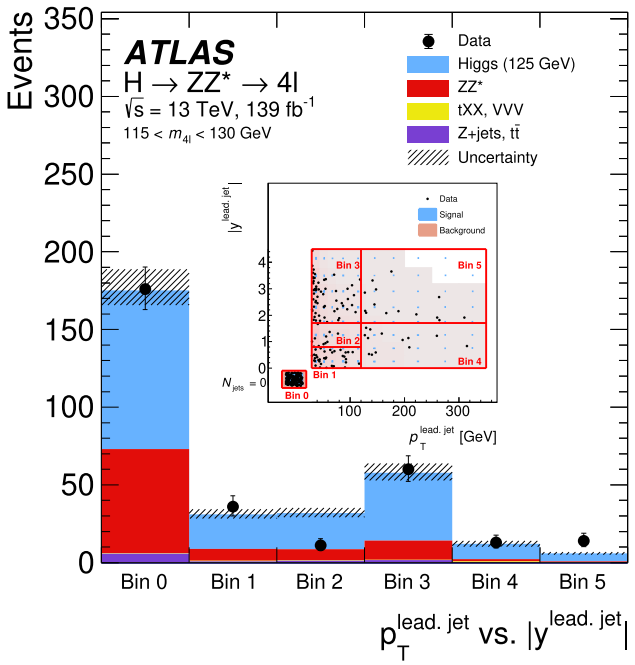

Fig. 17 The observed and expected (pre-fit) distribution in bins of the transverse momentum vs. the rapidity of the leading jet, $p_{\mathrm{T}}^{\text{lead. jet}}$ vs. $|y^{\text{lead. jet}}|$. The same distribution in the 2D plane is provided in the inset plot, where the black dots depict data and the blue and pink shaded areas represent simulated signal and background, respectively. The red lines depict the bin boundaries, chosen as described in Sect. 7. These distributions correspond to the mass region $115 < m_{4\ell} < 130$ GeV for an integrated luminosity of 139 fb^{-1} collected at $\sqrt{s} = 13$ TeV. A SM Higgs boson signal with a mass $m_H = 125$ GeV is assumed. The uncertainty in the prediction is shown by the hatched band, which includes the theoretical uncertainties of the SM cross section for the signal and the ZZ^* background

Table 7 The fiducial and total cross sections of Higgs boson production measured in the 4ℓ final state. The fiducial cross sections are given separately for each decay final state, and for same- and different-flavour decays. The inclusive fiducial cross section is measured as the sum of all final states (σ_{sum}), as well as by combining the per-final-state measurements assuming SM $ZZ^* \to 4\ell$ relative branching ratios (σ_{comb}). For the total cross section (σ_{tot}), the Higgs boson branching ratio at $m_H = 125$ GeV is assumed. The total SM prediction is accurate to N^{3}LO in QCD and NLO EW for the ggF process. For the fiducial cross-section predictions, the SM cross sections are multiplied by the acceptances determined using the NNLOPS sample for ggF. For all the other production modes, the cross sections from the samples discussed in Sect. 3 are added. The p-values indicating the probability of compatibility of the measurement and the SM prediction are shown as well. They do not include the systematic uncertainty in the theoretical predictions

Cross section [fb]	Data	($\pm$ (stat.)	$\pm$ (syst.))	Standard Model prediction	p-value (%)
$\sigma_{4\mu}$	0.81	± 0.12	± 0.03	0.90 ± 0.05	46
σ_{4e}	0.62	± 0.17	± 0.05	0.90 ± 0.05	14
$\sigma_{2\mu 2e}$	0.74	± 0.15	± 0.05	0.80 ± 0.04	67
$\sigma_{2e2\mu}$	1.01	± 0.15	± 0.03	0.80 ± 0.04	15
$\sigma_{4\mu+4e}$	1.43	± 0.21	± 0.05	1.81 ± 0.10	10
$\sigma_{2\mu 2e+2e2\mu}$	1.75	± 0.21	± 0.06	1.61 ± 0.09	51
σ_{sum}	3.18	± 0.31	± 0.11	3.41 ± 0.18	49
σ_{comb}	3.28	± 0.30	± 0.11	3.41 ± 0.18	67
σ_{tot} [pb]	53.5	± 4.9	± 2.1	55.7 ± 2.8	66

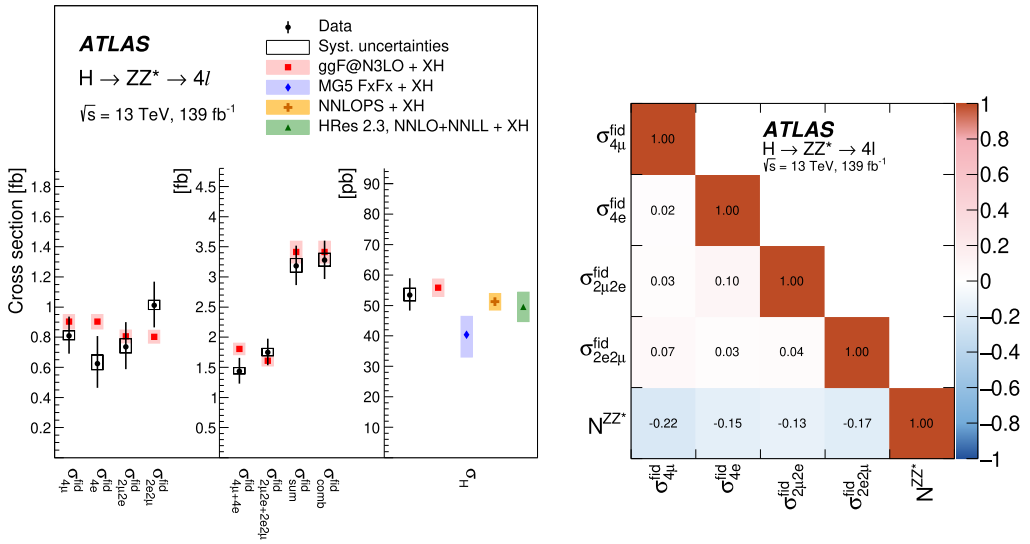

(a) (b)

Fig. 18 **a** The fiducial cross sections (left two panels) and total cross section (right panel) of Higgs boson production measured in the 4ℓ final state. The fiducial cross sections are shown separately for each decay final state, and for same- and different-flavour decays. The inclusive fiducial cross section is measured as the sum of all final states, as well as by combining the per-final-state measurements assuming SM $ZZ^* \to 4\ell$ relative branching ratios. The total SM prediction is accurate to N^{3}LO in QCD for the ggF process. The cross sections for all other Higgs boson production modes XH are added. For the fiducial cross-section predictions, the SM cross sections are multiplied by the acceptances determined using the NNLOPS sample for ggF and the samples discussed in Sect. 3 for the other production modes. For the total cross section, the predictions by the generators NNLOPS, HRES, and MADGRAPH5_AMC@NLO-FxFx are also shown. The error bars on the data points show the total uncertainties, while the systematic uncertainties are indicated by the boxes. The shaded bands around the theoretical predictions indicate the PDF and scale uncertainties, calculated as described in Sect. 8.2. **b** The correlation between the fiducial cross sections for the four individual decay final states and the ZZ^* normalisation factor

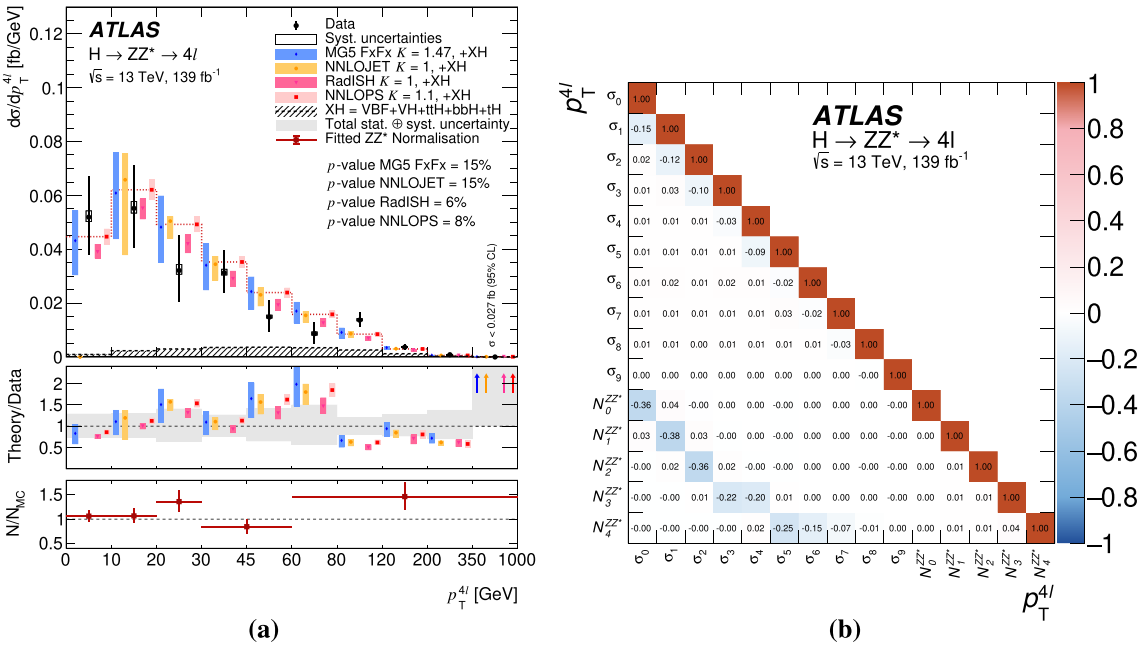

Fig. 19 **a** Differential fiducial cross section for the transverse momentum $p_{\mathrm{T}}^{4\ell}$ of the Higgs boson, along with **b** the corresponding correlation matrix between the measured cross sections and the ZZ^* background normalisation factors. The measured cross sections are compared with ggF predictions by MadGraph5_aMC@NLO-FxFx, NNLOJET, RadISH, and NNLOPS, where MadGraph5_aMC@NLO-FxFx and NNLOPS are normalised to the N^{3}LO total cross section with the listed K-factors while the normalisations for NNLOJET and RadISH are to their respective predicted cross sections. MC-based predictions for all other Higgs boson production modes XH are normalised to the SM predictions. The error bars on the data points show the total uncertainties, while the systematic uncertainties are indicated by the boxes. The shaded bands on the expected cross sections indicate the PDF and scale systematic uncertainties, calculated as described in Sect. 8.2. This includes the uncertainties related to the XH production modes. The p-values indicating the probability of compatibility of the measurement and the SM prediction are shown as well. They do not include the systematic uncertainty in the theoretical predictions. The central panel of **a** shows the ratio of different predictions to the data, and the grey area represents the total uncertainty of the measurement. The bottom panel of **a** shows the ratios of the fitted values of the ZZ^* normalisation factors to the predictions from MC simulation discussed in Sect. 3. As indicated by the horizontal error bars, the ZZ^* normalisation is estimated in each of the first three $p_{\mathrm{T}}^{4\ell}$ bins separately, while the next two bins share a common estimation factor, as do the last five bins

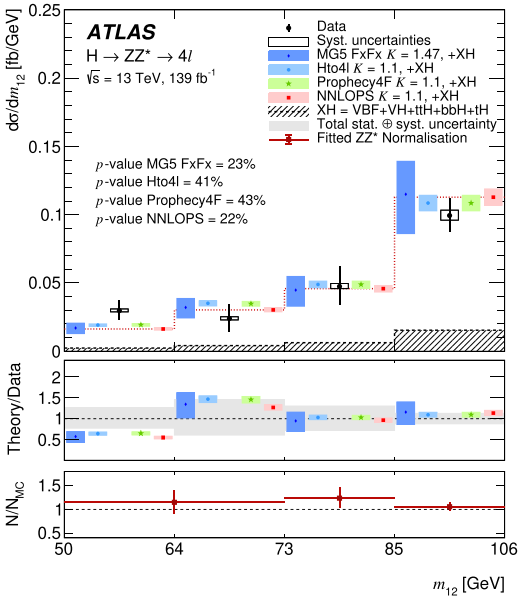

(a)

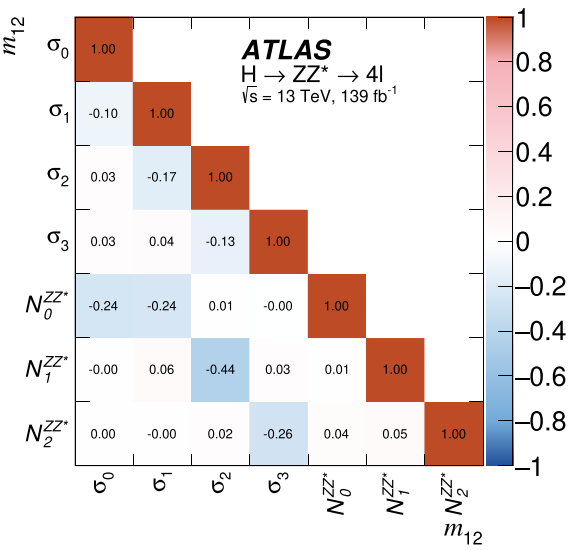

(b)

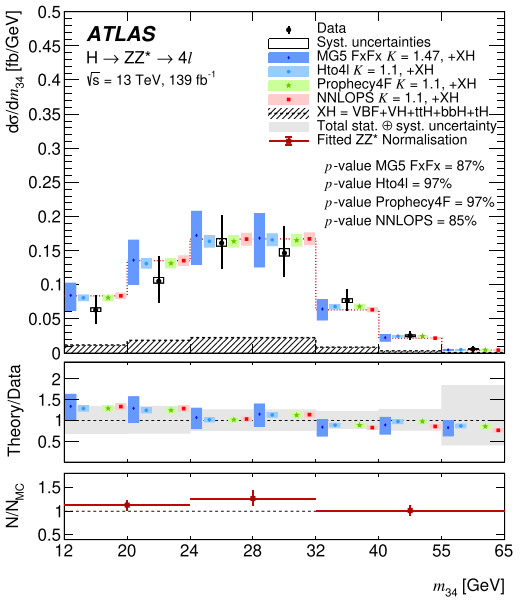

(c)

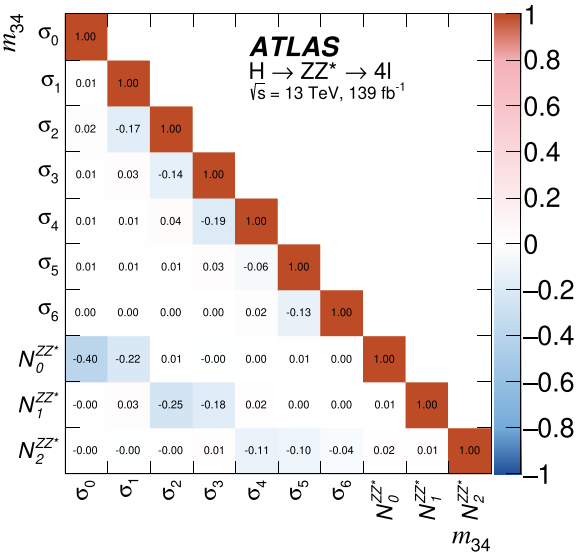

(d)

Fig. 20 Differential fiducial cross sections for **a** the invariant mass m_{12} of the leading Z boson and **c** the invariant mass m_{34} of the subleading Z boson, along with the corresponding correlation matrices between the measured cross sections and the ZZ^* background normalisation factors (**b** and **d**)

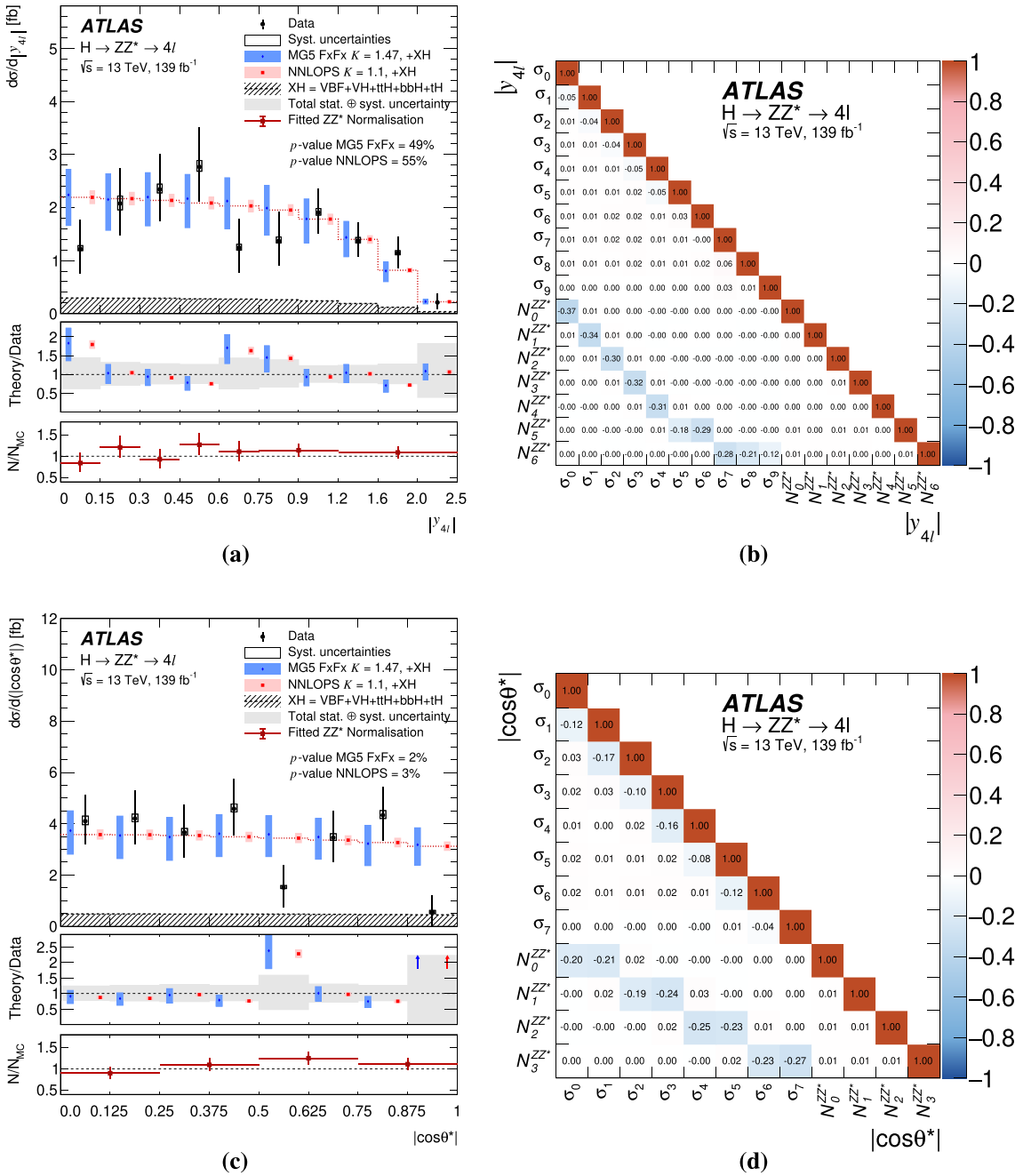

Fig. 21 Differential fiducial cross sections for **a** the rapidity, $|y_{4\ell}|$, of the Higgs boson and **c** the production angle, $|\cos\theta^*|$, of the leading Z boson. The corresponding correlation matrices between the measured cross sections and the ZZ^* background normalisation factors are also shown (**b** and **d**)

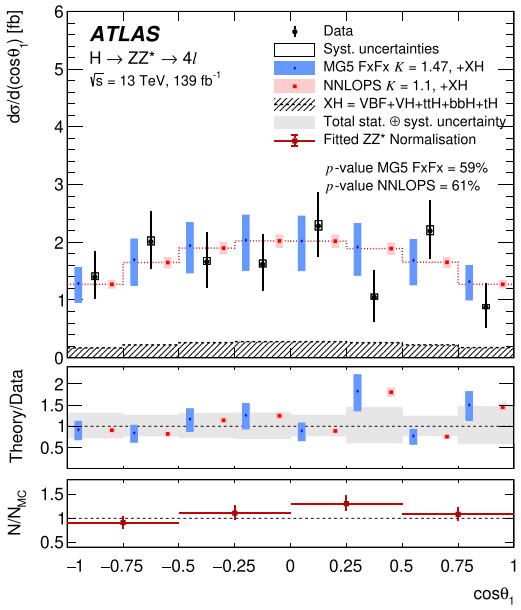

(a)

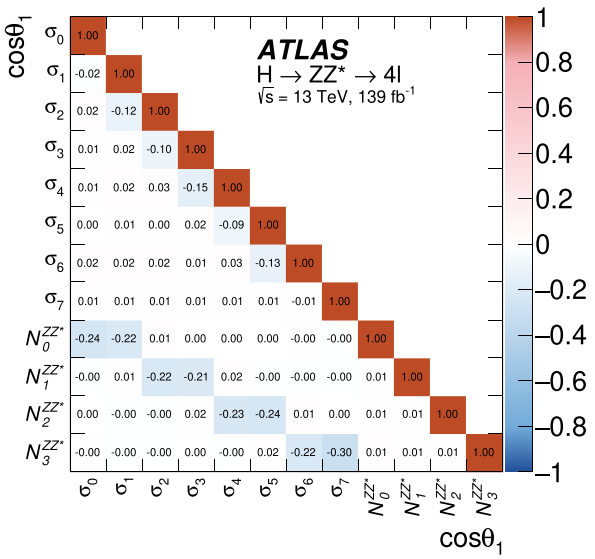

(b)

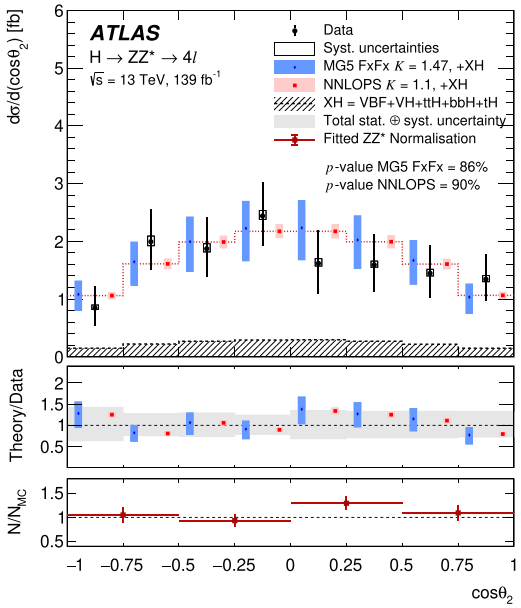

(c)

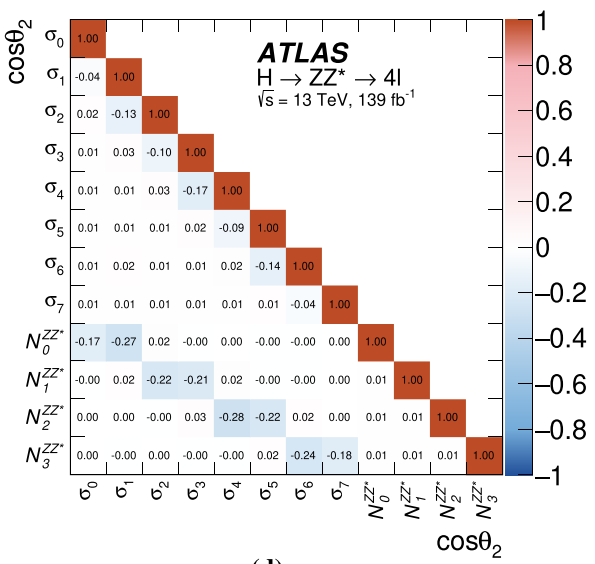

(d)

Fig. 22 Differential fiducial cross sections for **a** production angle, $\cos\theta_1$, of the anti-lepton from the leading Z boson and **c** the production angle, $\cos\theta_2$, of the anti-lepton from the subleading Z boson. The corresponding correlation matrices between the measured cross sections and the ZZ^* background normalisation factors are also shown (**b** and **d**)

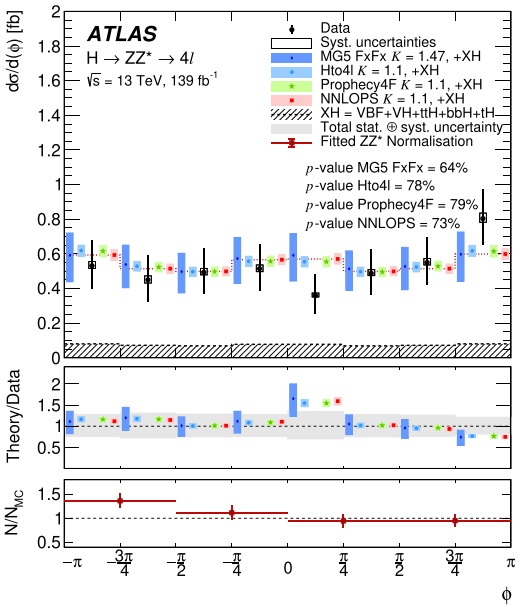

(a)

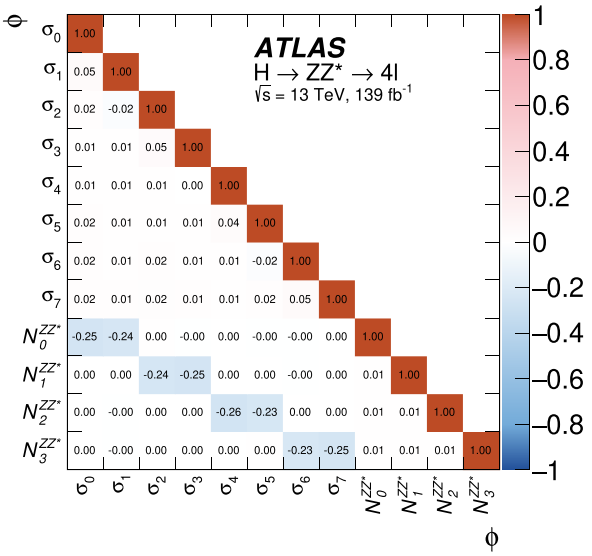

(b)

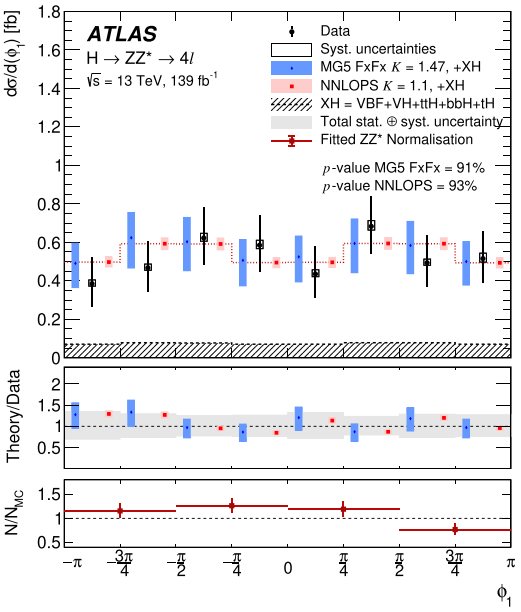

(c)

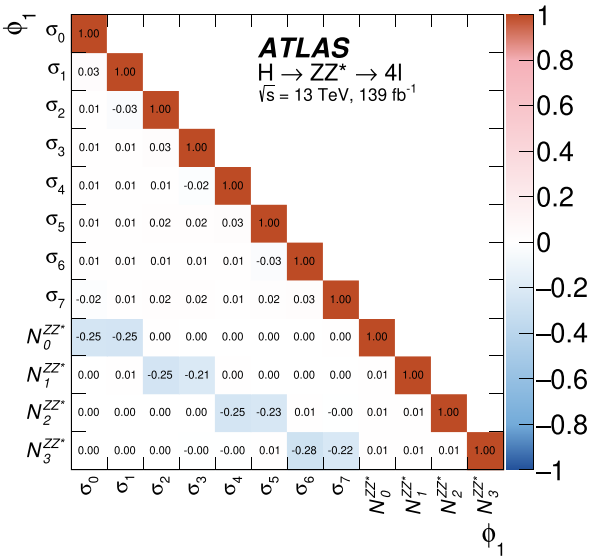

(d)

Fig. 23 Differential fiducial cross sections for **a** the azimuthal angle, ϕ, between the decay planes of the two reconstructed Z bosons and **c** the azimuthal angle, ϕ_1, between the decay plane of the leading Z boson and the plane formed by its four-momentum and the z-axis. The corresponding correlation matrices between the measured cross sections and the ZZ^* background normalisation factors are also shown (**b** and **d**)

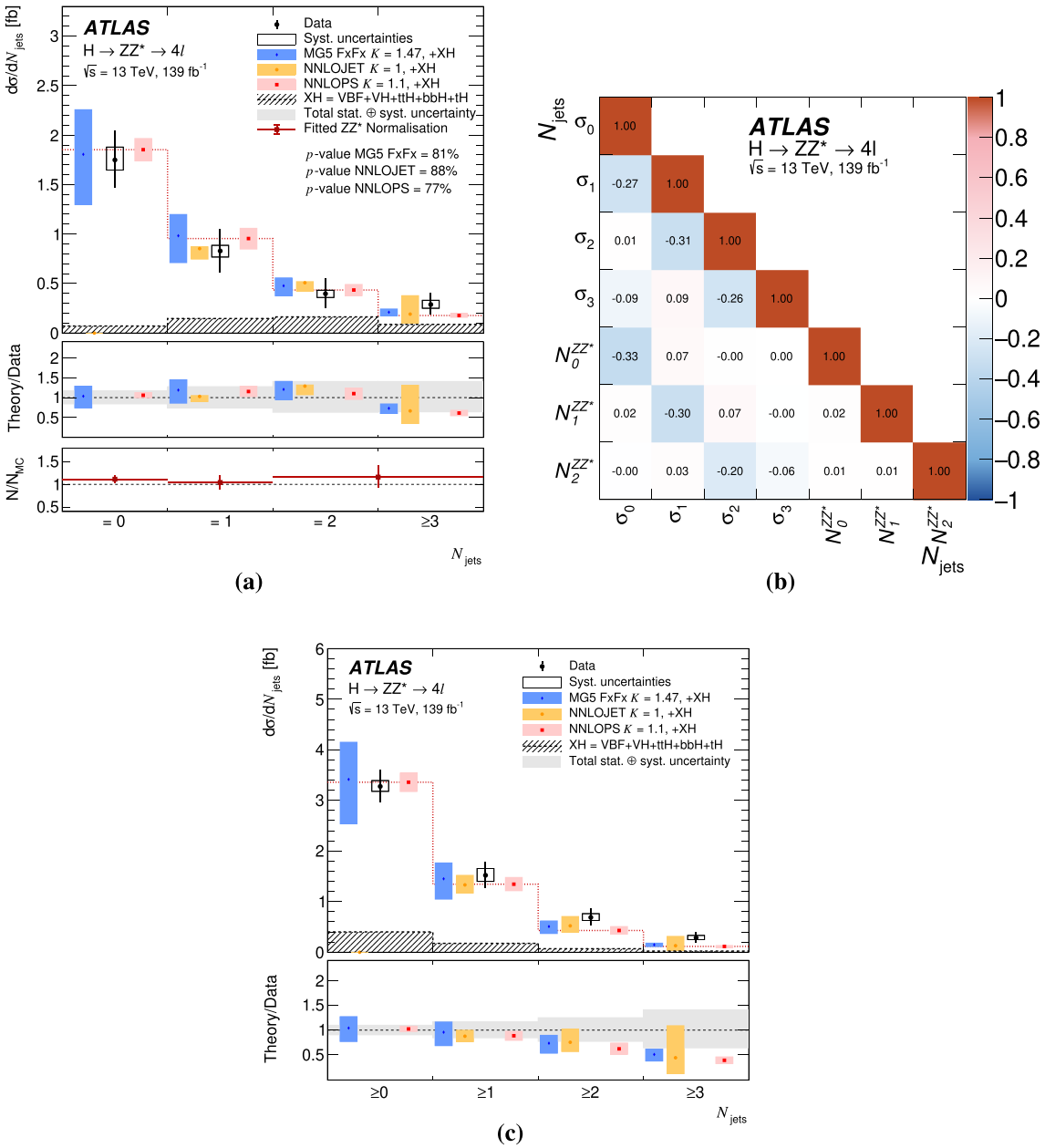

Fig. 24 Differential fiducial cross sections for **a** the jet multiplicity, N_{jets}, in the selected events, and **c**, the inclusive jet multiplicity. In the N_{jets} distribution in **a**, the first three bins are exclusive in number of jets, while the fourth is inclusive. The corresponding correlation matrix between the measured cross sections and the ZZ^* background normalisation factors is also shown in **b**. In the N_{jets} distribution in **c**, all bins are inclusive, with the first bin including all events, the second including all events with at least one jet, and so on

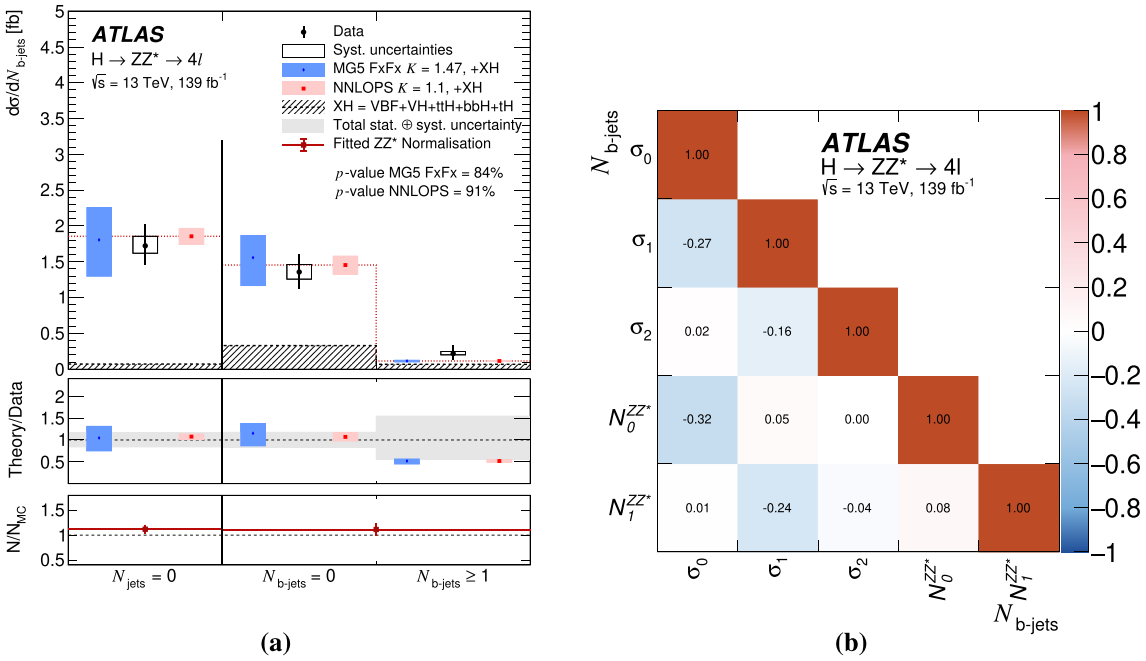

Fig. 25 **a** Differential fiducial cross section as function of the b-jet multiplicity, $N_{b\text{-jets}}$. Three bins are considered. The first bin is filled with events which do not have any jets, the second is filled with events with at least one jet but no b-tagged jets, while the third includes all events with at least one b-tagged jet. The corresponding correlation matrices between the measured cross sections and the ZZ^* background normalisation factors are also shown in (**b**)

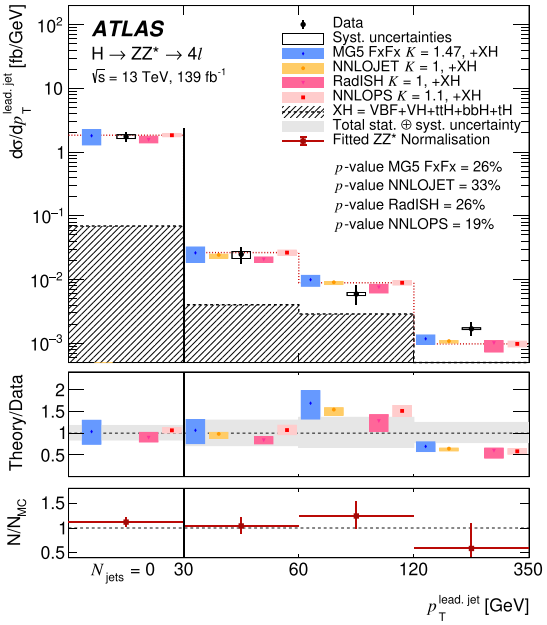

(a)

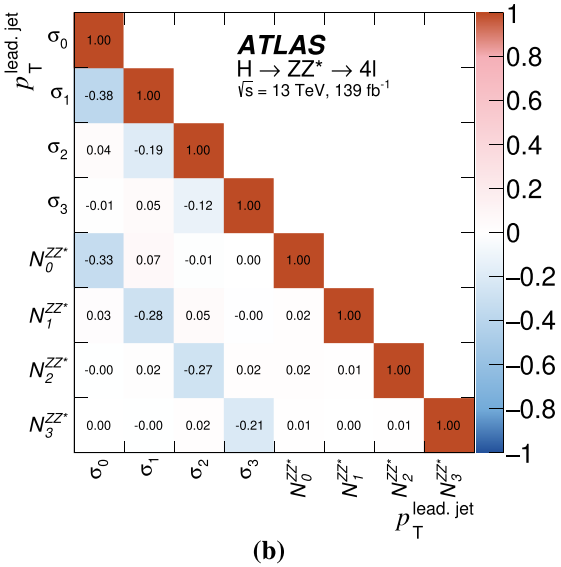

(b)

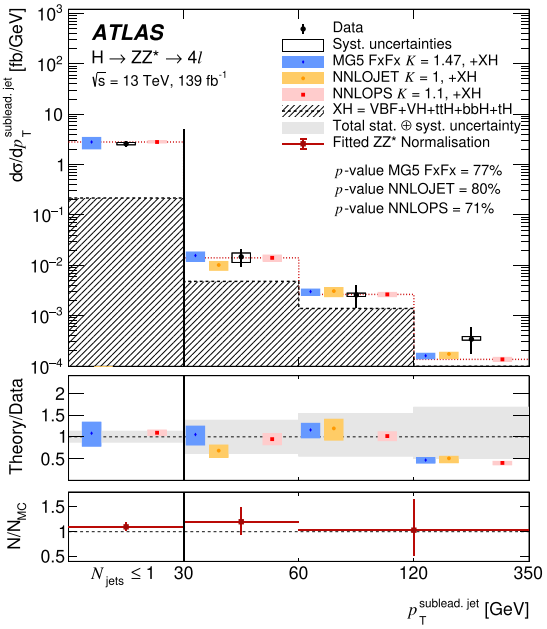

(c)

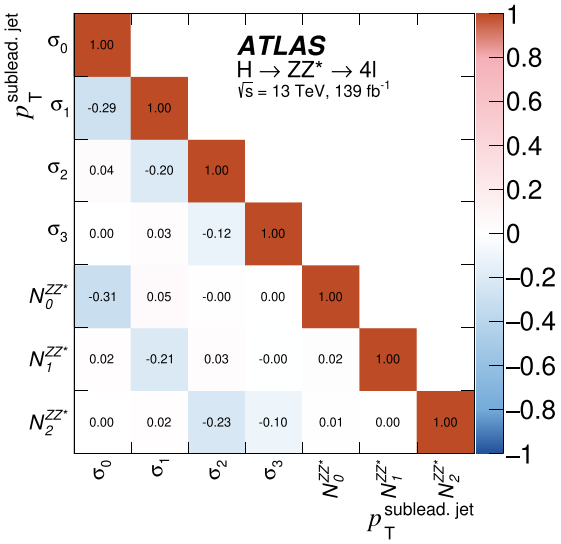

(d)

Fig. 26 Differential fiducial cross sections for **a** the transverse momentum of the leading jet, $p_{\mathrm{T}}^{\text{lead. jet}}$, in events with at least one jet, and **c** the transverse momentum of the subleading jet, $p_{\mathrm{T}}^{\text{sublead. jet}}$, in events with at least two jets. Leading and subleading jets refer to the jets with the highest and second-highest transverse momenta. The first bin contains events which do not pass the jet requirements. The corresponding correlation matrices between the measured cross sections and the ZZ^* background normalisation factors are also shown (**b** and **d**)

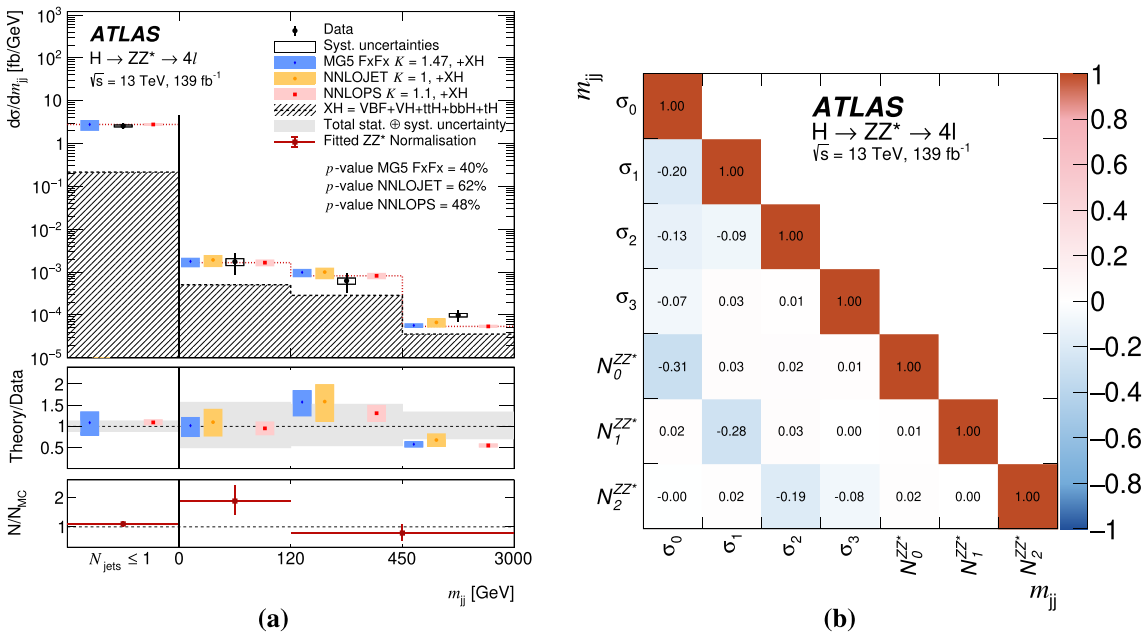

Fig. 27 Differential fiducial cross sections for **a** the invariant mass of the two highest-p_{T} jets, m_{jj}, in events with at least two jets. The corresponding correlation matrix between the measured cross sections and the ZZ^* background normalisation factors is also provided (**b**)

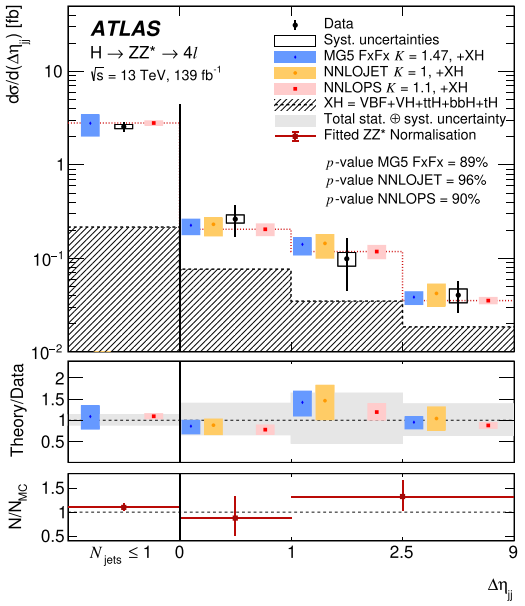

(a)

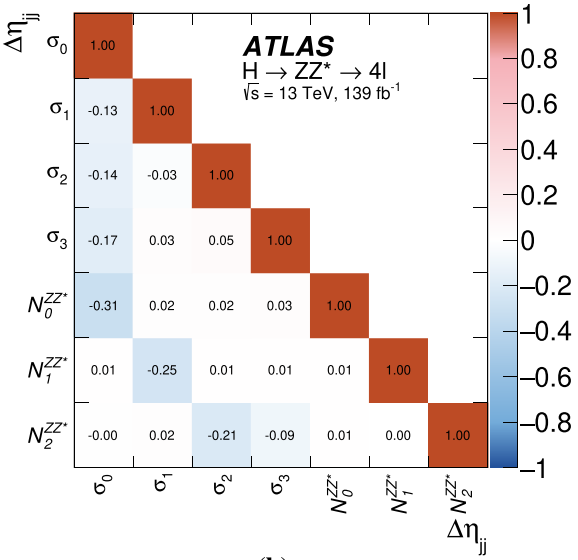

(b)

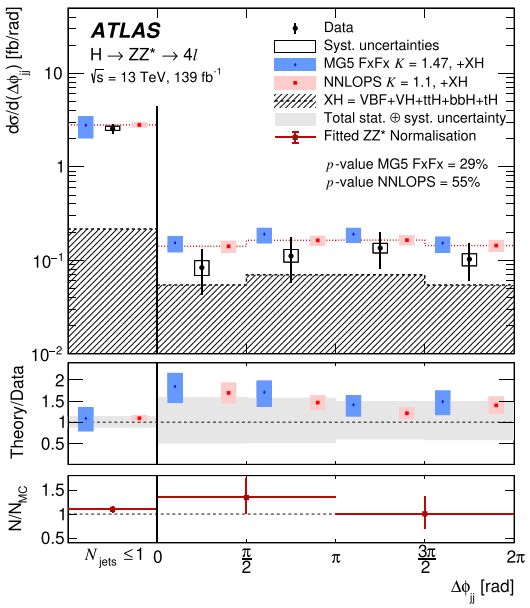

(c)

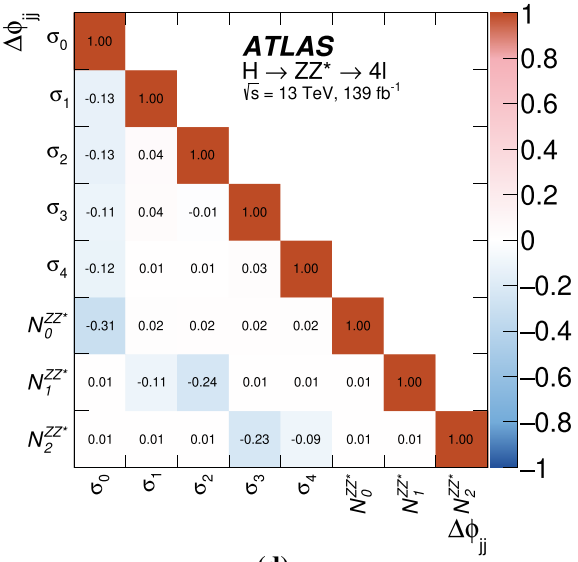

(d)

Fig. 28 Differential fiducial cross sections for **a** the distance between these two jets in pseudorapidity, $\Delta\eta_{jj}$, and **c** the distance between the two jets in ϕ, $\Delta\phi_{jj}$. The first bin contains events with fewer than two jets that pass the jet selection requirements. Finally, the corresponding correlation matrices between the measured cross sections and the ZZ^* background normalisation factors are provided (**b** and **d**)

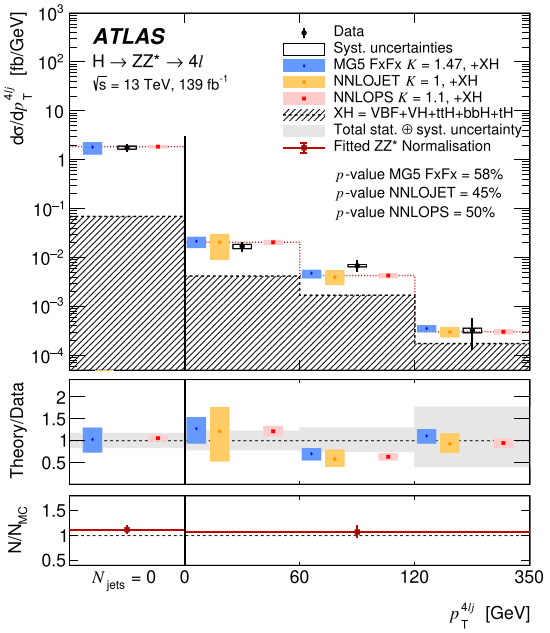

(a)

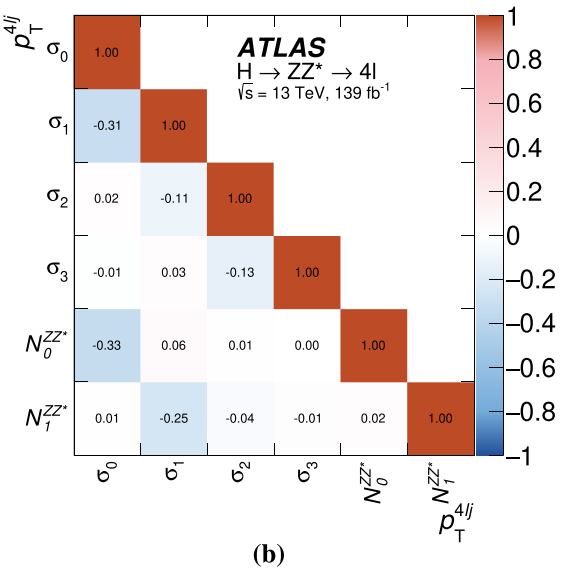

(b)

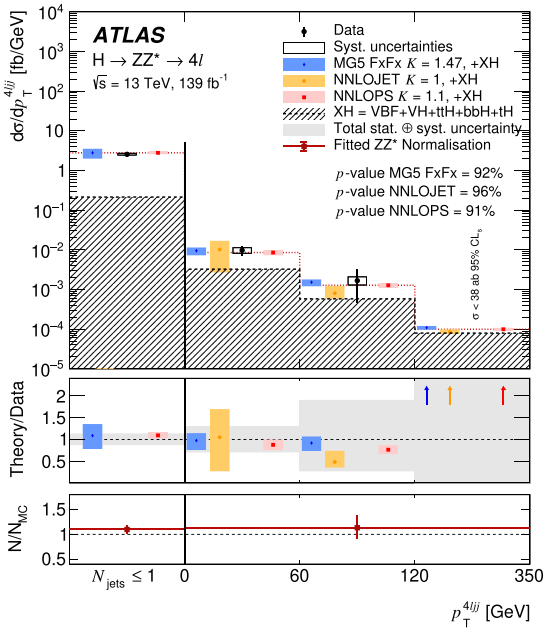

(c)

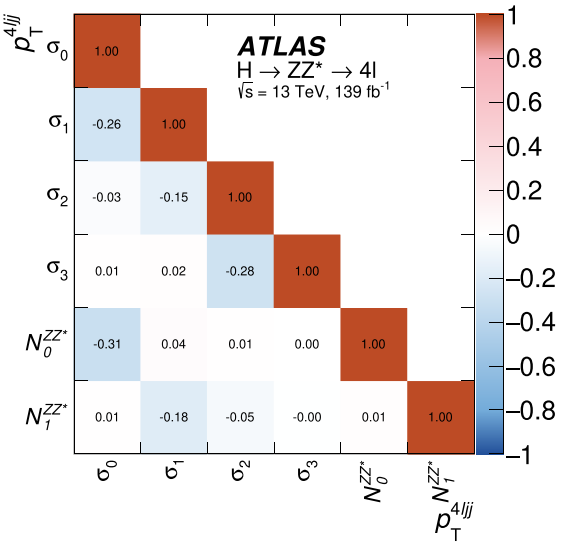

(d)

Fig. 29 Differential fiducial cross sections for **a** the transverse momentum of the four-lepton plus jet system, in events with at least one jet, and **c** the transverse momentum of the four-lepton plus dijet system, in events with at least two jets. The corresponding correlation matrices between the measured cross sections and the ZZ^* background normalisation factors are also shown (**b** and **d**)

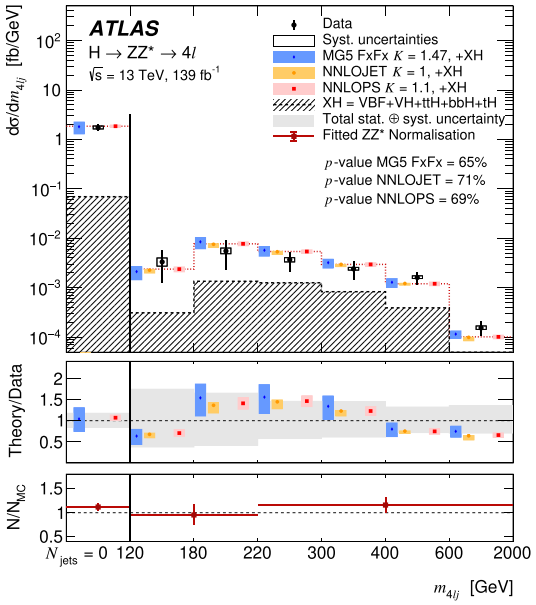

(a)

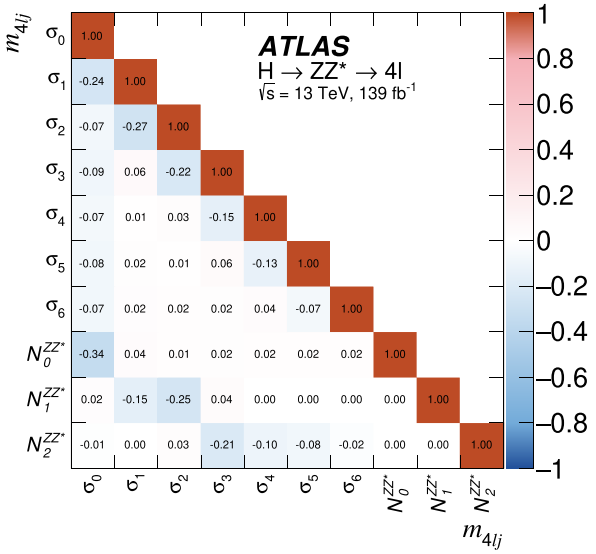

(b)

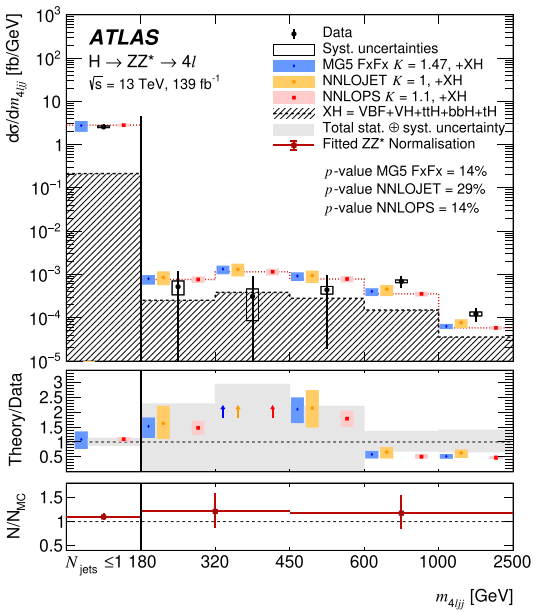

(c)

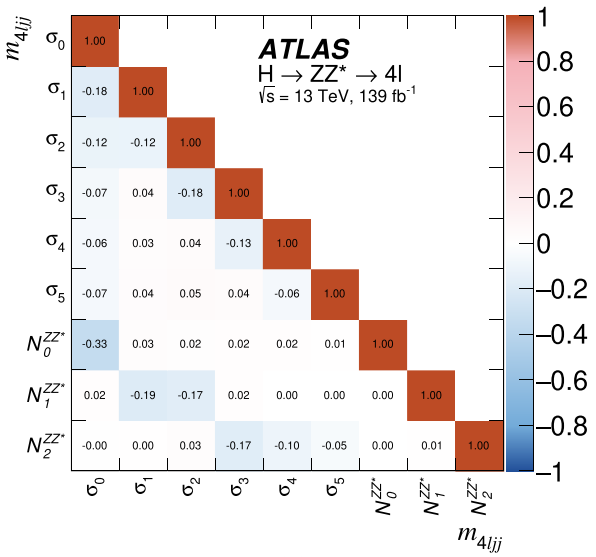

(d)

Fig. 30 Differential fiducial cross sections for **a** the invariant mass of the four-lepton plus jet system, in events with at least one jet, and **c** the invariant mass of the four-lepton plus dijet system, in events with at least two jets. The corresponding correlation matrices between the measured cross sections and the ZZ^* background normalisation factors are also shown (**b** and **d**)

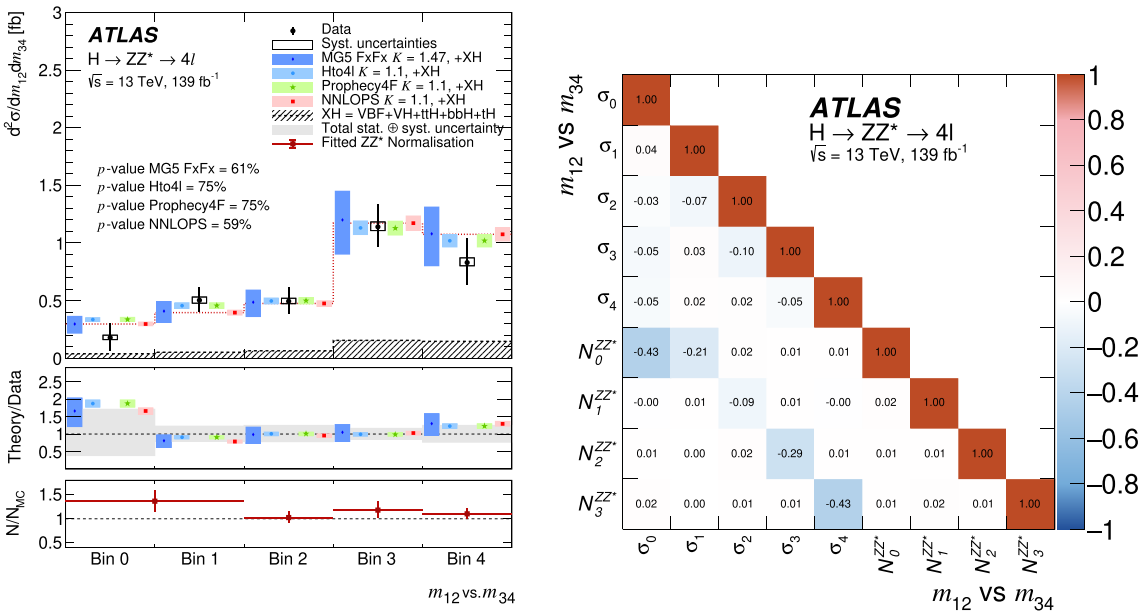

Fig. 31 **a** Differential fiducial cross section for the leading vs. subleading Z boson mass, m_{12} vs. m_{34}, and **b** the corresponding correlation matrix between the measured cross sections and the ZZ^* background normalisation factors. The bin boundaries are defined in Fig. 12

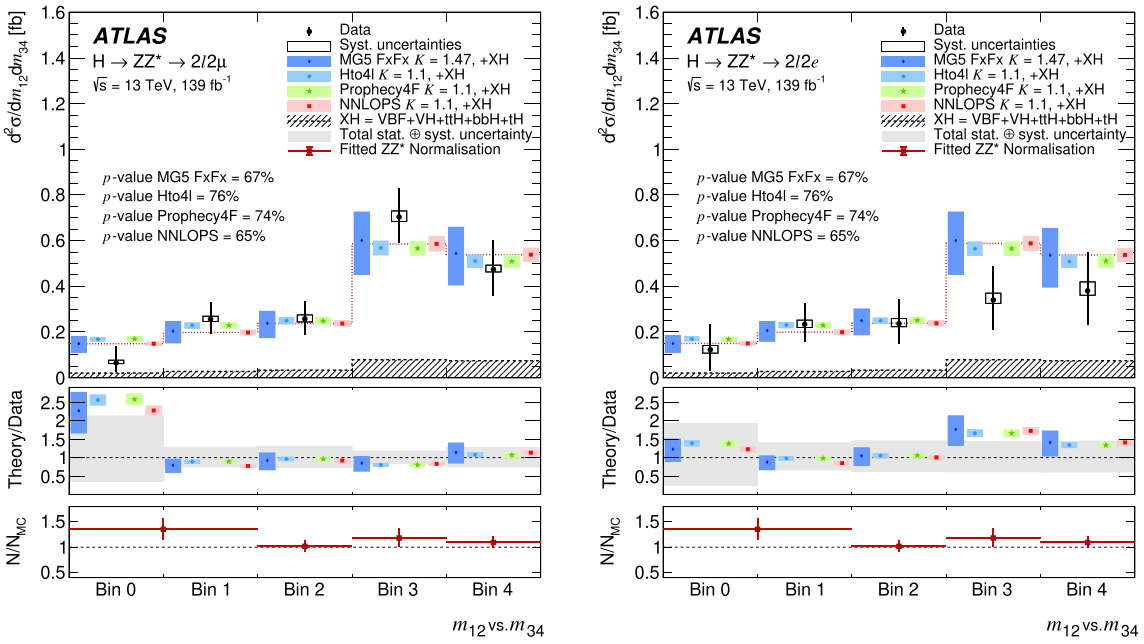

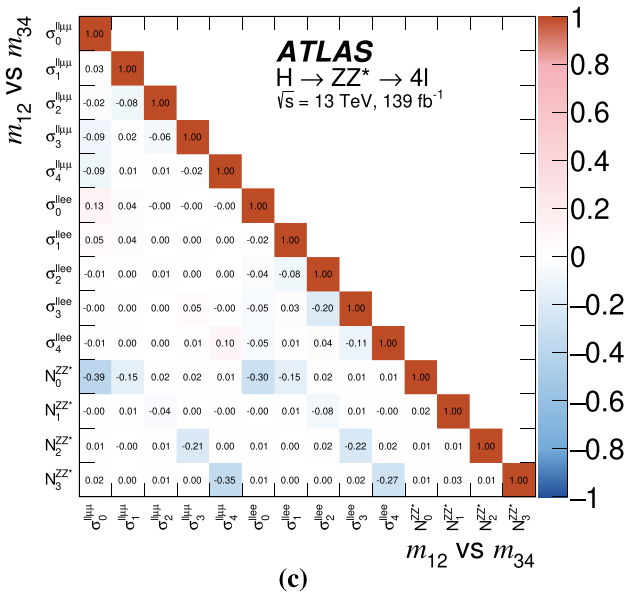

Fig. 32 Differential fiducial cross sections for the leading vs. subleading Z boson mass, m_{12} vs. m_{34}, in **a** $\ell\ell\mu\mu$ and **b** $\ell\ell ee$ final states, along with **c** their corresponding correlation matrix between the measured cross sections and the ZZ^* background normalisation factors. The bin boundaries are defined in Fig. 12

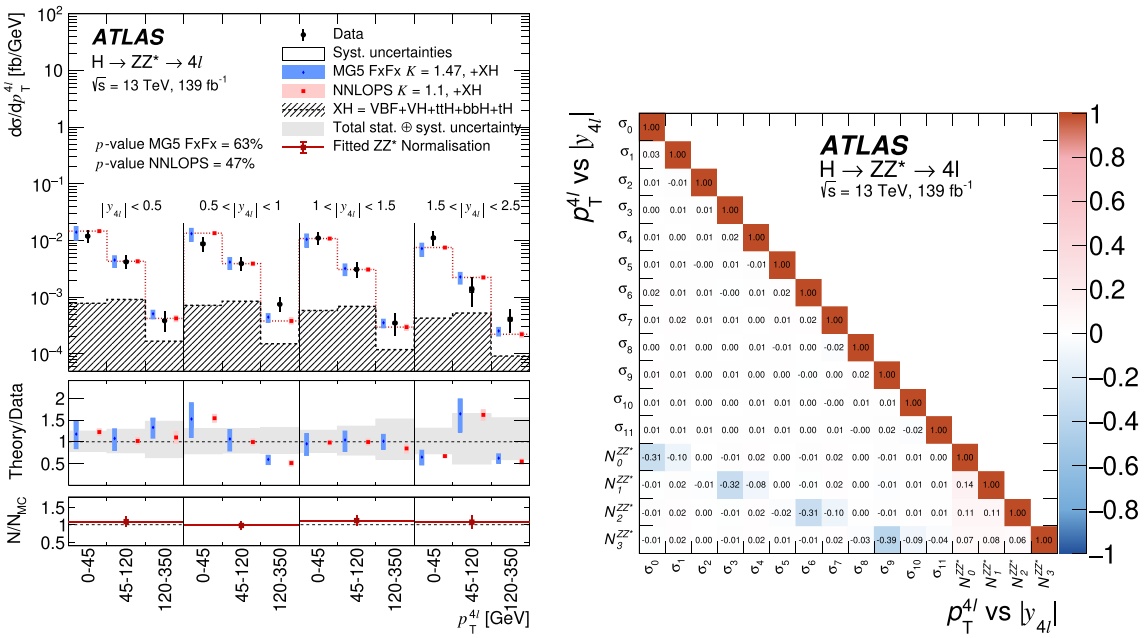

(a) (b)

Fig. 33 **a** Double differential fiducial cross sections of the $p_{\mathrm{T}}^{4\ell}$ distribution in $|y_{4\ell}|$ bins. The corresponding correlation matrix between the measured cross sections and the ZZ^* background normalisation factors is shown in **b**. The p-values shown are calculated for all bins across both $p_{\mathrm{T}}^{4\ell}$ and $|y_{4\ell}|$ simultaneously

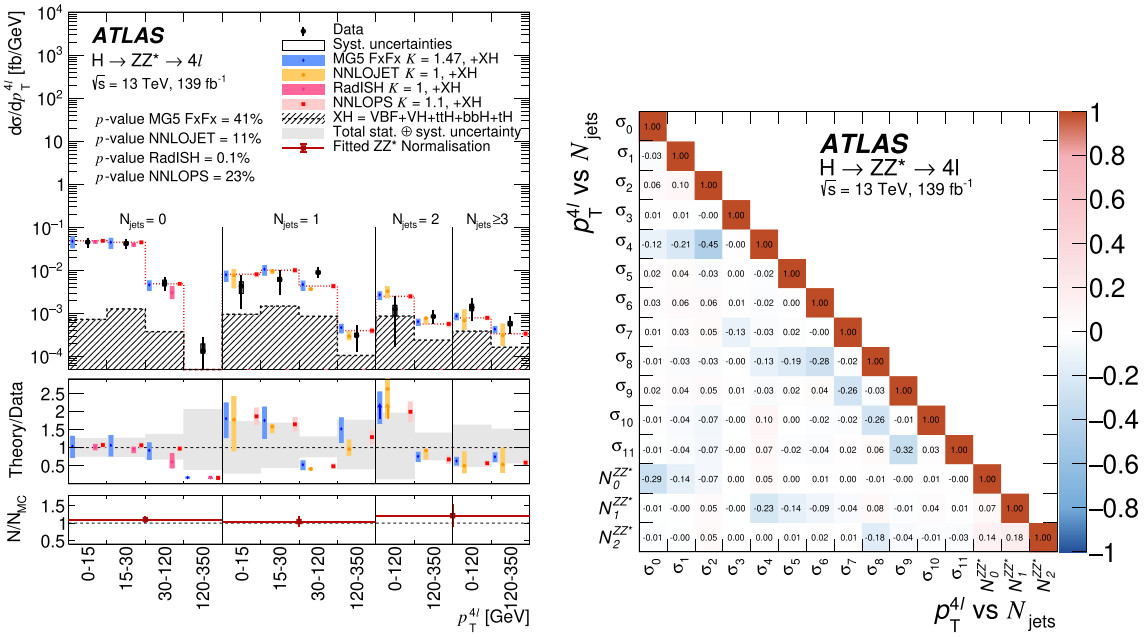

(a) (b)

Fig. 34 **a** Double differential fiducial cross sections of the $p_{\mathrm{T}}^{4\ell}$ distribution in N_{jets} bins. The corresponding correlation matrix between the measured cross sections and the ZZ^* background normalisation factors is shown in **b**. The p values shown are calculated for all bins across both $p_{\mathrm{T}}^{4\ell}$ and N_{jets} simultaneously

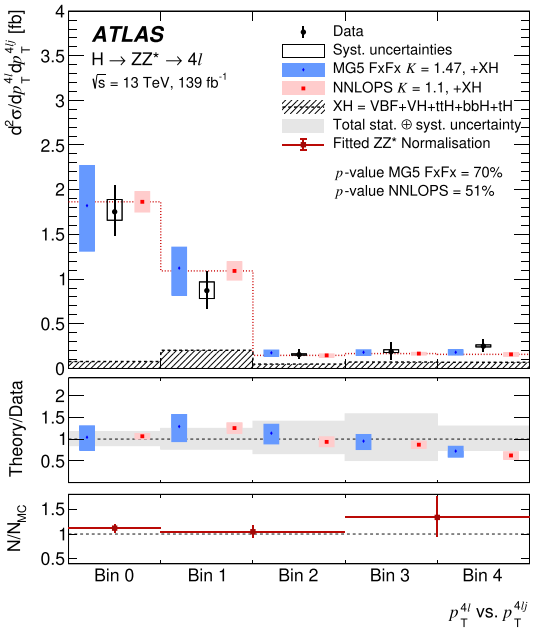

(a)

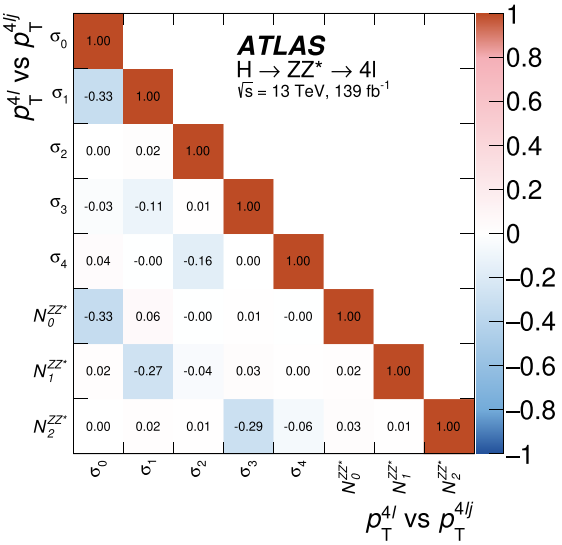

(b)

Fig. 35 **a** Differential fiducial cross section for the transverse momentum of the four-lepton system vs. the transverse momentum of the four-lepton plus jet system, $p_{\mathrm{T}}^{4\ell}$ vs. $p_{\mathrm{T}}^{4\ell\mathrm{j}}$ and **b** the corresponding correlation matrix between the measured cross sections and the ZZ^* background normalisation factors. The bin boundaries are defined in Fig. 14

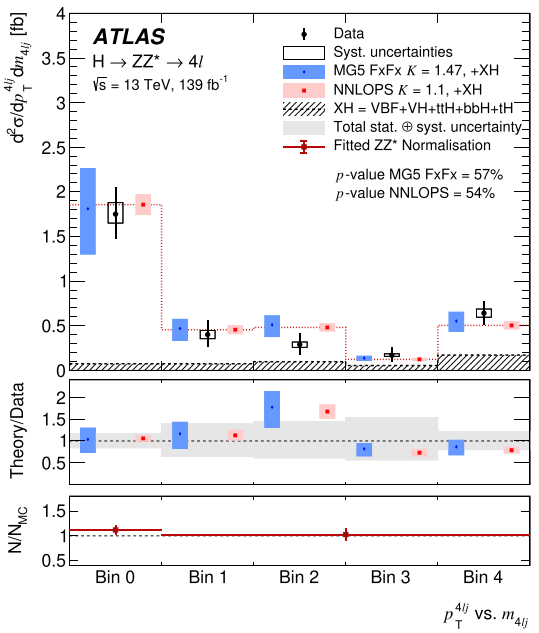

(a)

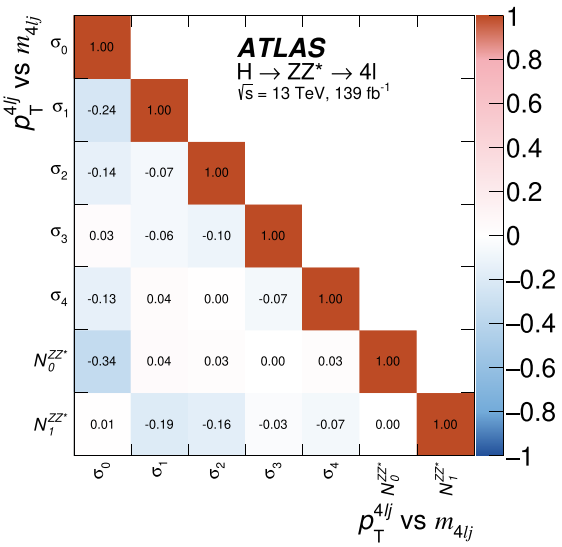

(b)

Fig. 36 **a** Double differential fiducial cross section for the transverse momentum of the four-lepton plus jet system vs. the invariant mass of the four-lepton plus jet system, $p_{\mathrm{T}}^{4\ell\mathrm{j}}$ vs. $m_{4\ell\mathrm{j}}$ and **b** the corresponding correlation matrix between the measured cross sections and the ZZ^* background normalisation factors. The bin boundaries are defined in Fig. 13

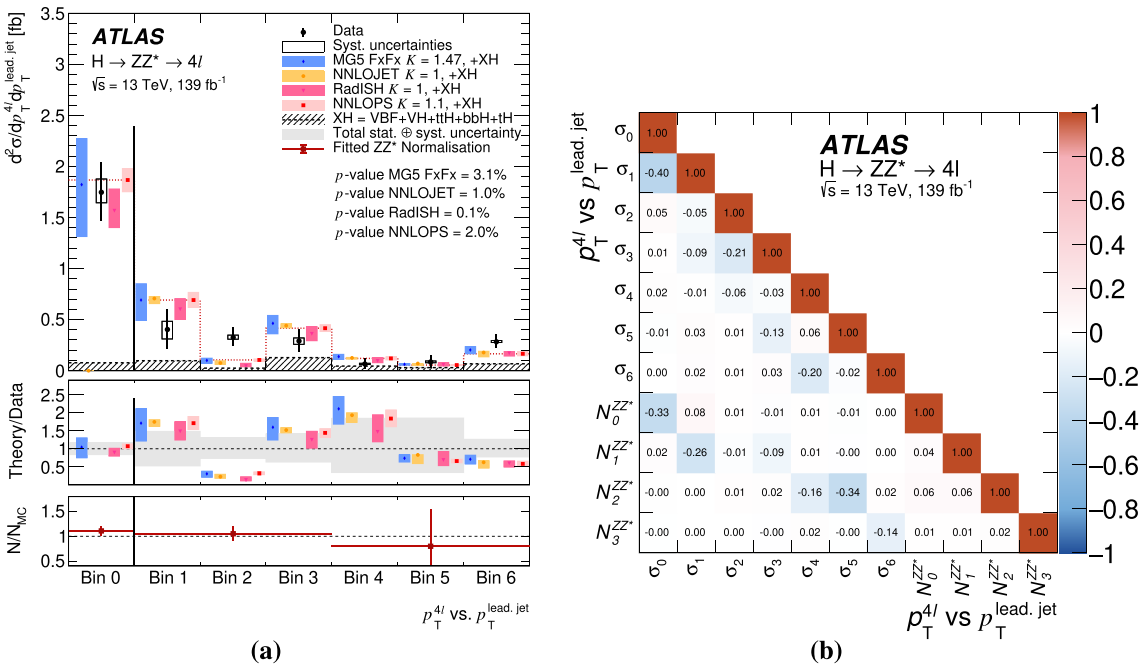

Fig. 37 **a** Double differential fiducial cross section for the transverse momentum of the four-lepton system vs. the transverse momentum of the leading jet, $p_{\mathrm{T}}^{4\ell}$ vs. $p_{\mathrm{T}}^{\text{lead. jet}}$, and **b** the corresponding correlation matrix between the measured cross sections and the ZZ^* background normalisation factors. The bin boundaries are defined in Fig. 15

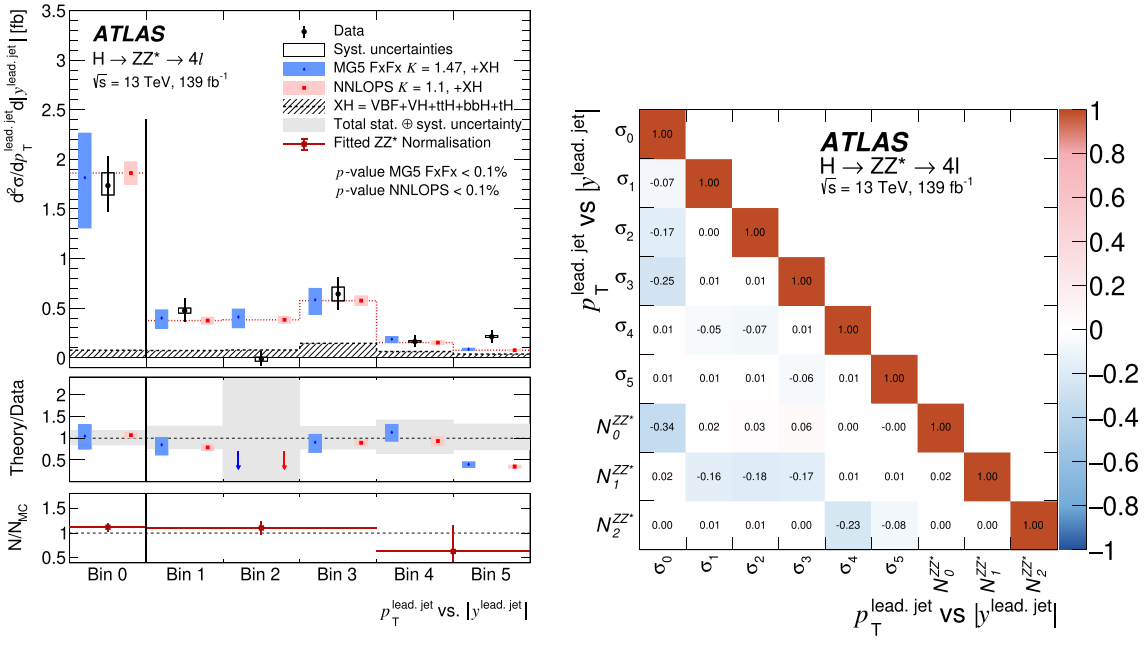

Fig. 38 **a** Double differential fiducial cross section for the transverse momentum of the leading jet vs. the rapidity of the leading jet, $p_{\mathrm{T}}^{\text{lead. jet}}$ vs. $|y^{\text{lead. jet}}|$, and **b** the corresponding correlation matrix between the measured cross sections and the ZZ^* background normalisation factors. The bin boundaries are defined in Fig. 17

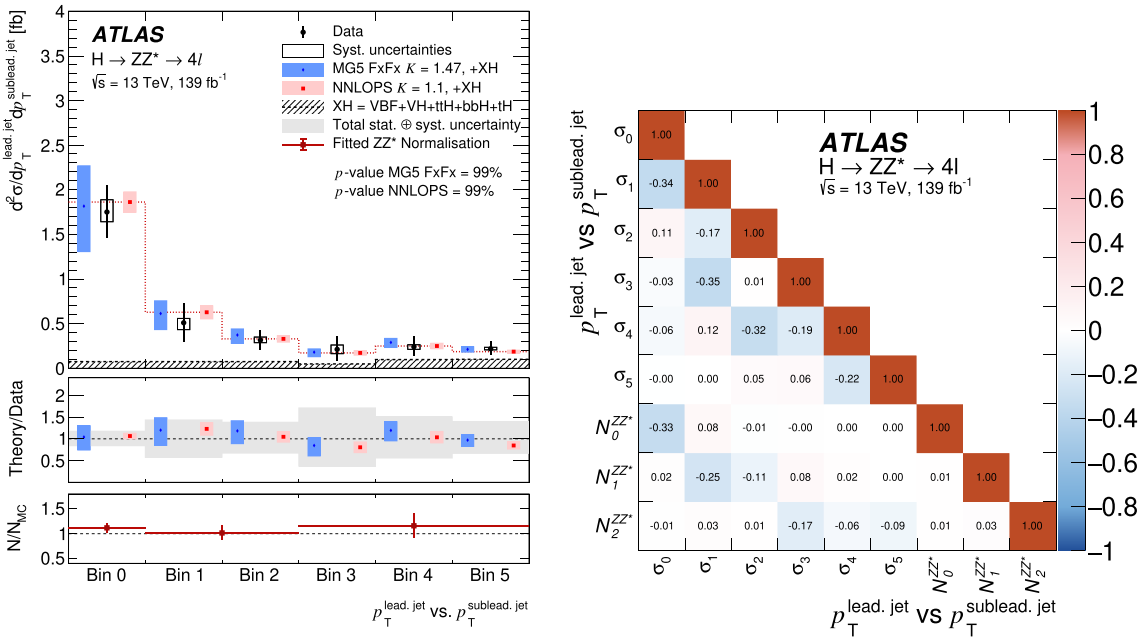

Fig. 39 **a** Double differential fiducial cross section for the transverse momentum of leading vs. subleading jet, $p_{\mathrm{T}}^{\text{lead. jet}}$ vs. $p_{\mathrm{T}}^{\text{sublead. jet}}$, and **b** the corresponding correlation matrix between the measured cross sections and the ZZ^* background normalisation factor. The bin boundaries are defined in Fig. 16

10 Interpretation of differential distributions

The measured differential fiducial cross sections can be used to probe possible effects of physics beyond the SM. Two possible interpretations of the results are presented. In Sect. 10.1, the m_{12} vs. m_{34} double differential cross section is used to probe several BSM scenarios within the framework of pseudo-observables [142], while in Sect. 10.2, the $p_{\mathrm{T}}^{4\ell}$ differential cross section is used to constrain the Yukawa couplings of the Higgs boson with the b- and c-quarks [143].

10.1 Constraints on BSM effects within the pseudo-observables framework

In this interpretation, the couplings related to the BSM contact interactions of the Higgs boson decaying into four leptons are considered. As defined in Ref. [109], the pseudo-observables framework introduces modified contact terms between the Higgs boson, the Z boson, and the left- or right-handed leptons ϵ_{Z,ℓ_L} and ϵ_{Z,ℓ_R}. In order to reduce the number of independent parameters considered in the pseudo-observables framework for the $H \to 4\ell$ decay amplitudes, specific symmetries are imposed [109]. In all the scenarios considered, the parameters associated with other pseudo-observables affecting the angular distributions, such as $\epsilon_{ZZ}^{(CP)}$, $\epsilon_{Z\gamma}^{(CP)}$ and $\epsilon_{\gamma\gamma}^{(CP)}$, are set to zero. Thus, the contact terms considered have the same Lorentz structure as the SM term and only affect the dilepton invariant mass distributions.

Four scenarios are investigated [109]. In the first scenario, referred to as the *flavour-universal contact terms*, the parameters of interest are the ϵ_{Z,ℓ_L} and the ϵ_{Z,ℓ_R} couplings, where the interactions described by these contact terms have the same strength for electrons and muons. The second scenario considered is *linear EFT-inspired*, where lepton-flavour universality is again imposed and the Higgs boson is assumed to be part of a $SU(2)_L$ doublet. This is reflected in the condition $\epsilon_R = 0.48\epsilon_L$ [109]. The parameters of interest are ϵ_L and the coupling strength of the Higgs boson to the Z boson, κ_{ZZ}. In the following two scenarios, lepton-flavour universality can be violated. For the third scenario, referred to as *flavour non-universal vector contact terms*, the helicity structure of the couplings is fixed to be vector ($\epsilon_{Z,e_L} = \epsilon_{Z,e_R}$, $\epsilon_{Z,\mu_L} = \epsilon_{Z,\mu_R}$) and the independent parameters are the couplings to electrons ϵ_{Z,e_R} and muons ϵ_{Z,μ_R}. Finally, a fourth scenario with *flavour non-universal axial-vector contact terms* is considered. In this case the helicity structure of the couplings is fixed to be axial-vector, with the parameters of interest being the couplings to electrons ϵ_{Z,e_R} and muons ϵ_{Z,μ_R} and the condition $\epsilon_{Z,\ell_L} = -\epsilon_{Z,\ell_R}$ is imposed. Using the m_{12} vs. m_{34} double differential cross sections for these interpretations provides sensitivity to distinguish between potential contributions from the contact terms and those from changes to the coupling strength of the Higgs boson to the Z boson.

The variation of the fiducial cross section as a function of the BSM couplings is computed relative to the SM by MadGraph5_aMC@NLO in each of the bins of the measured m_{12} vs. m_{34} differential cross section. This is done for a grid of points in the BSM parameter space in each scenario. These relative variations are then fit to a two-dimensional quadratic function. The parameterisation, which also includes any changes in the acceptance, is then encoded into the likelihood and corresponding limits are set for each scenario.

Figure 40 shows the limits on BSM interactions of the Higgs boson for the four considered cases. The corresponding 95% confidence intervals for each of the parameters are listed in Table 8.

10.2 Constraints on Yukawa couplings

Although the couplings of the Higgs boson to the top and bottom quarks have been established recently, obtaining evidence for the coupling of the Higgs boson to the charm quark is more challenging. Direct methods are limited either by low branching fraction ($H \to J/\psi\gamma \to \mu^+\mu^-\gamma$) or by large backgrounds ($H \to c\bar{c}$). Nevertheless, it has been shown recently that it is possible to indirectly constrain the Yukawa coupling to quarks by analysing the p_{T}^{H} spectrum [19,143]. In particular, the effects of BSM contributions to the coupling modifiers for the Higgs boson to charm quarks, κ_c, and for the Higgs boson to bottom quarks, κ_b, are investigated.

The fiducial cross section is parameterised as a function of the κ_c and κ_b values in each measured bin of $p_{\mathrm{T}}^{4\ell}$. Both the gluon-initiated and quark-initiated components of the prediction show a larger variation, different in size and shape, of the cross section especially at $p_{\mathrm{T}}^{4\ell} < 10$ GeV. The theoretical uncertainties of these predictions are calculated separately for the gluon-initiated and quark-initiated components by varying the normalisation and factorisation scales by factors of two. The configuration with largest uncertainty across all the $p_{\mathrm{T}}^{4\ell}$ bins across $\kappa_c \in [-10, 10]$ and $\kappa_b \in [-2, 2]$ ranges is used to define the systematic uncertainty for the predictions. These uncertainties are uncorrelated for each component. The impact of this uncertainty is about 20% on the expected limits.

Three different scenarios are considered, with an increasing level of model dependency. In the first case, the modified fiducial cross sections in each bin due to the value of the b- and c-quark Yukawa couplings are fit to the data together with a global normalisation factor. The corresponding observed limits on κ_c and κ_b are shown in Fig. 41a. The sensitivity in this case comes mainly from the modification of the shape induced by κ_c and κ_b, while possible overall nor-

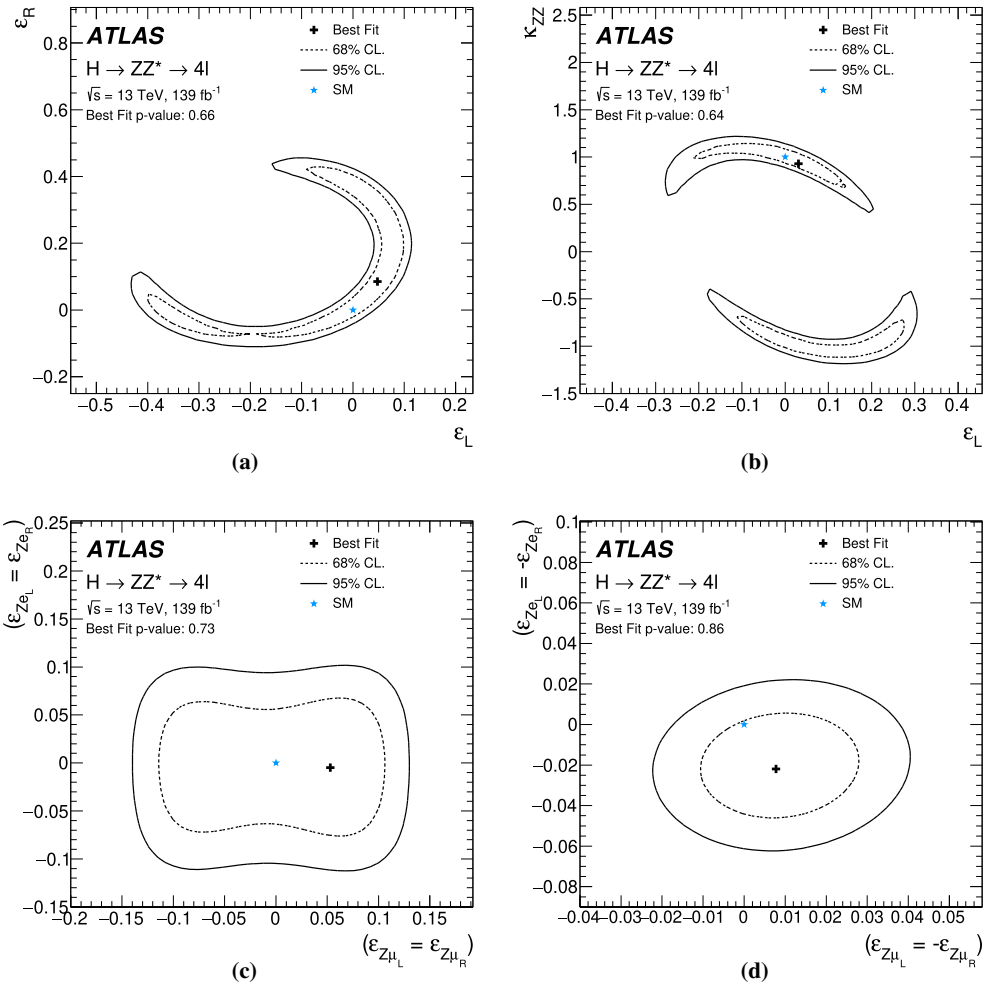

Fig. 40 Observed limits at 68% and 95% CL on the modified Higgs boson decays within the framework of the pseudo-observables: **a** flavour universal contact terms; **b** linear EFT-inspired; **c** flavour non-universal vector contact terms; **d** flavour non-universal axial-vector contact terms. The p values shown represent the probability of compatibility between the data and the m_{12} vs. m_{34} prediction corresponding to the best-fit values of the parameters of interest for each of the four scenarios considered. The SM predictions ($*$) and the observed best-fit values (+) are indicated on the plots

malisation effects are factorised out. In a second scenario, no additional normalisation factor is introduced in the likelihood and the obtained limits for the Yukawa couplings are shown in Fig. 41b. Finally, in a third scenario, a modification to the total width, and correspondingly to the branching ratio as function of the modified Yukawa couplings, is also encoded in the likelihood and the corresponding limits are shown in Fig. 41c. The 95% confidence intervals for the first and second scenarios are also listed in Table 9. These are comparable to results from direct searches in VH, $H \to c\bar{c}$ [144,145]. Constraining κ_b to the results from Ref. [146] leads to a less than 5% improvement in the observed limits for κ_c for the scenarios considered.

Table 8 Confidence intervals for the scenarios considered in the pseudo-observables framework. Based on the observed 2D exclusion contours, 1D exclusion intervals are provided for the EFT-inspired, flavour non-universal vector, and flavour non-universal axial-vector scenarios. The observed limits are calculated while profiling the other parameters of interest. For the EFT-inspired interpretation, the limits are derived assuming $\kappa_{ZZ} \geq 0$. This constraint has no impact on the limit as the analysis is not sensitive to the sign of this parameter

Interpretation	Parameter best-fit value	95% confidence interval
EFT-inspired	$\epsilon_L = 0.03$	$[-0.25, 0.17]$
	$\kappa_{ZZ} = 0.93$	$[0.51, 1.16]$
Flavour non-universal vector	$\epsilon_{Ze} = -0.005$	$[-0.097, 0.082]$
	$\epsilon_{Z\mu} = 0.054$	$[-0.131, 0.114]$
Flavour non-universal axial-vector	$\epsilon_{Ze} = -0.022$	$[-0.056, 0.012]$
	$\epsilon_{Z\mu} = 0.008$	$[-0.016, 0.033]$

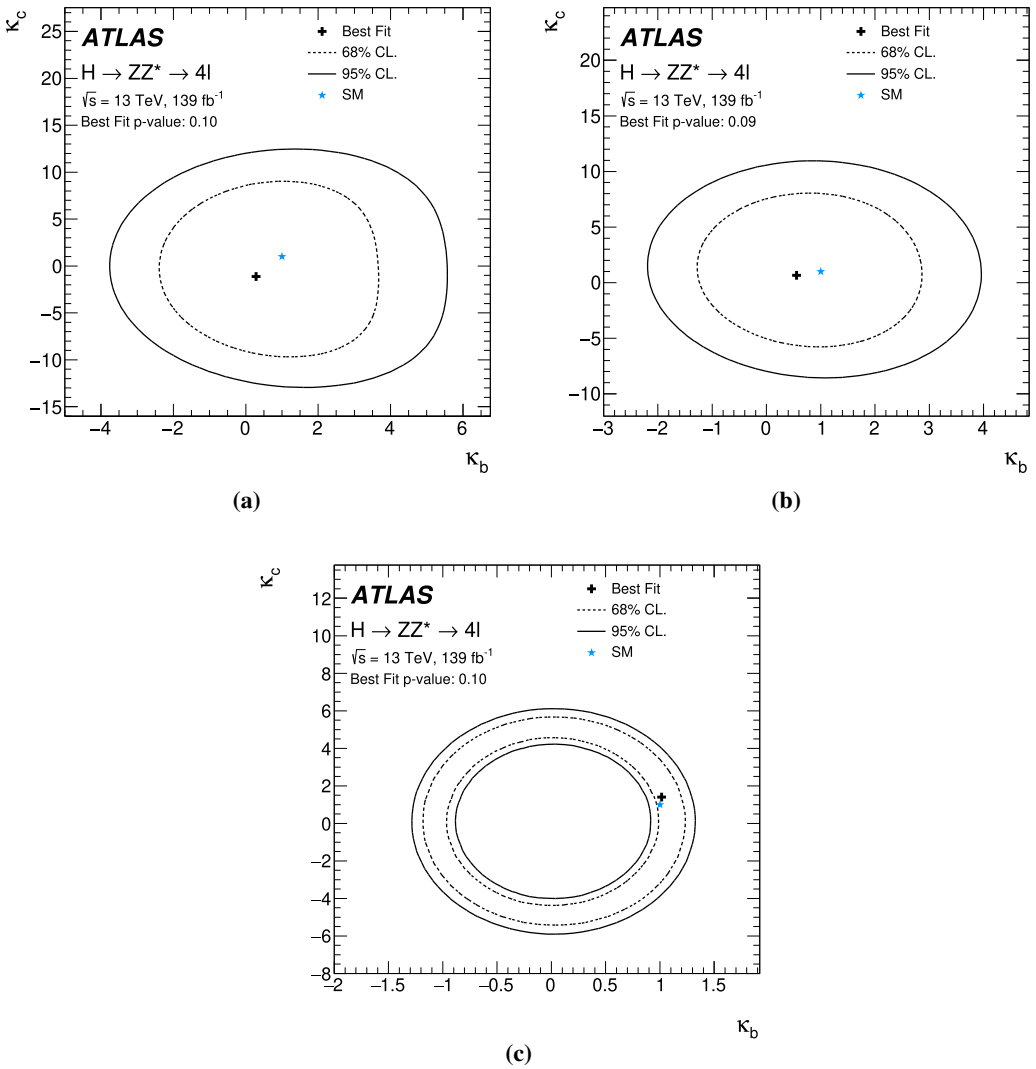

Fig. 41 Observed limits at 95% CL on Yukawa couplings κ_c and κ_b for the three scenarios considered: **a** only the $p_{\mathrm{T}}^{4\ell}$ shape is used to constrain κ_c and κ_b; **b** the predicted $p_{\mathrm{T}}^{4\ell}$ differential cross section is used; **c** both the prediction of the $p_{\mathrm{T}}^{4\ell}$ differential cross section and the modification to the branching ratio due to the κ_c and κ_b values are used. The p values shown represent the probability of compatibility between the data and the $p_{\mathrm{T}}^{4\ell}$ prediction corresponding to the best-fit values of κ_c and κ_b. The SM predictions ($*$) and the observed best-fit values (+) are indicated on the plots

Table 9 Confidence intervals for the Yukawa couplings. Based on the observed 2D exclusion contours, 1D exclusion intervals are only provided for interpretations where modification to the $p_{\mathrm{T}}^{4\ell}$ shape and predictions are considered. The observed limits are calculated while profiling the other parameter of interest

Interpretation	Parameter best-fit value	95% confidence interval
Modifications to only $p_{\mathrm{T}}^{4\ell}$ shape	$\kappa_c = -1.1$	$[-11.7,\ 10.5]$
	$\kappa_b = 0.28$	$[-3.21,\ 4.50]$
Modifications to $p_{\mathrm{T}}^{4\ell}$ predictions	$\kappa_c = 0.66$	$[-7.46,\ 9.27]$
	$\kappa_b = 0.55$	$[-1.82,\ 3.34]$

11 Summary

Fiducial inclusive and differential cross-section measurements of the Higgs boson in the $H \to ZZ^* \to 4\ell$ decay channel are presented. They are based on 139 fb^{-1} of $\sqrt{s} =$ 13 TeV proton-proton collisions recorded by the ATLAS detector at the LHC in 2015−2018. The inclusive fiducial cross section in the $H \to ZZ^* \to 4\ell$ decay channel is measured to be $\sigma_{\mathrm{fid}} = 3.28 \pm 0.30$ (stat.) ± 0.11 (syst.) fb, in agreement with the Standard Model prediction $\sigma_{\mathrm{fid,SM}} = 3.41 \pm 0.18$ fb. The measurement is about 40% more precise than the previous ATLAS result. The inclusive fiducial cross section is also extrapolated to the full phase space. Differential cross sections defined in a fiducial region close

to the reconstructed event selection are measured for several variables sensitive to the Higgs boson production and decay such as the transverse momentum of the Higgs boson, the number of jets produced in association with the Higgs boson, the leading and subleading invariant masses of the lepton pairs. The measured cross sections are compared with different Standard Model predictions and in general good agreement is found. The results are also used to set new and more stringent constraints on BSM scenarios where contact term interactions in the $H \to 4\ell$ amplitudes are introduced. In addition, the $p_{\mathrm{T}}^{4\ell}$ spectrum is used to constrain the b- and c-quark Yukawa couplings of the Higgs boson. In the scenario with minimal assumptions, values of κ_c outside the range $\kappa_c \in [-12, +11]$ are excluded at 95% CL.

Acknowledgements We thank CERN for the very successful operation of the LHC, as well as the support staff from our institutions without whom ATLAS could not be operated efficiently. We acknowledge the support of ANPCyT, Argentina; YerPhI, Armenia; ARC, Australia; BMWFW and FWF, Austria; ANAS, Azerbaijan; SSTC, Belarus; CNPq and FAPESP, Brazil; NSERC, NRC and CFI, Canada; CERN; CONICYT, Chile; CAS, MOST and NSFC, China; COLCIENCIAS, Colombia; MSMT CR, MPO CR and VSC CR, Czech Republic; DNRF and DNSRC, Denmark; IN2P3-CNRS and CEA-DRF/IRFU, France; SRNSFG, Georgia; BMBF, HGF and MPG, Germany; GSRT, Greece; RGC and Hong Kong SAR, China; ISF and Benoziyo Center, Israel; INFN, Italy; MEXT and JSPS, Japan; CNRST, Morocco; NWO, The Netherlands; RCN, Norway; MNiSW and NCN, Poland; FCT, Portugal; MNE/IFA, Romania; MES of Russia and NRC KI, Russia Federation; JINR; MESTD, Serbia; MSSR, Slovakia; ARRS and MIZŠ, Slovenia; DST/NRF, South Africa; MINECO, Spain; SRC and Wallenberg Foundation, Sweden; SERI, SNSF and Cantons of Bern and Geneva, Switzerland; MOST, Taiwan; TAEK, Turkey; STFC, United Kingdom; DOE and NSF, United States of America. In addition, individual groups and members have received support from BCKDF, CANARIE, Compute Canada and CRC, Canada; ERC, ERDF, Horizon 2020, Marie Skłodowska-Curie Actions and COST, European Union; Investissements d'Avenir Labex, Investissements d'Avenir Idex and ANR, France; DFG and AvH Foundation, Germany; Herakleitos, Thales and Aristeia programmes co-financed by EU-ESF and the Greek NSRF, Greece; BSF-NSF and GIF, Israel; CERCA Programme Generalitat de Catalunya and PROMETEO Programme Generalitat Valenciana, Spain; Göran Gustafssons Stiftelse, Sweden; The Royal Society and Leverhulme Trust, United Kingdom. The crucial computing support from all WLCG partners is acknowledged gratefully, in particular from CERN, the ATLAS Tier-1 facilities at TRIUMF (Canada), NDGF (Denmark, Norway, Sweden), CC-IN2P3 (France), KIT/GridKA (Germany), INFN-CNAF (Italy), NL-T1 (The Netherlands), PIC (Spain), ASGC (Taiwan), RAL (UK) and BNL (USA), the Tier-2 facilities worldwide and large non-WLCG resource providers. Major contributors of computing resources are listed in Ref. [149].

Data Availability Statement This manuscript has no associated data or the data will not be deposited. [Authors' comment: All ATLAS scientific output is published in journals, and preliminary results are made available in Conference Notes. All are openly available, without restriction on use by external parties beyond copyright law and the standard conditions agreed by CERN. Data associated with journal publications are also made available: tables and data from plots (e.g. cross section values, likelihood profiles, selection efficiencies, cross section limits, ...) are stored in appropriate repositories such as HEPDATA (http://hepdata.cedar.ac.uk/). ATLAS also strives to make additional material related to the paper available that allows a reinterpretation of the data in the context of new theoretical models. For example, an extended encapsulation of the analysis is often provided for measurements in the framework of RIVET (http://rivet.hepforge.org/)". This information is taken from the ATLAS Data Access Policy, which is a public document that can be downloaded from http://opendata.cern.ch/record/413 [opendata.cern.ch].]

Funded by SCOAP[3].

Appendix

A Results with regularised unfolding

For all the variables investigated in this paper, the unfolding matrix used is well conditioned and no regularisation is required, as discussed in Sect. 7. Nevertheless, a Tikhonov regularisation has been tested for the N_{jets} and $p_{\mathrm{T}}^{\text{lead. jet}}$ observables where perceptible off-diagonal terms in the response matrix are observed. In the Tikhonov regularisation [147], a prior assumption about the final result of the measurement is added to the PDF, where the impact of this assumption is controlled by a tunable parameter, τ. In practice, this method is implemented by adding a penalty term to the negative log-likelihood that is minimised in the fit as

$$\tau \cdot \sum_{i=2}^{n-1} \left(\left(\frac{\sigma_{i+1}}{\sigma_{i+1,\mathrm{truth}}} - \frac{\sigma_i}{\sigma_{i,\mathrm{truth}}} \right) - \left(\frac{\sigma_i}{\sigma_{i,\mathrm{truth}}} - \frac{\sigma_{i-1}}{\sigma_{i-1,\mathrm{truth}}} \right) \right)^2,$$

where σ_i is the cross section in bin i. Therefore, a second-derivative expression for the curvature is used, with the parameters normalised by their expected values from the MC simulation as done in the SVD unfolding method [148]. As is done for the main results, only the signal is unfolded.

The unfolded N_{jets} and $p_{\mathrm{T}}^{\text{lead. jet}}$ distributions using the regularised unfolding with a τ parameter set to $\tau = 0.6$ and 0.7, respectively, are shown in Fig. 42. The uncertainty which accounts for a possible bias in this regularisation ranges from less than 1% to about 10%, depending on the differential bin. As expected, the comparison of Figs. 42a with 24a and Figs. 42c with 26a shows that the regularisation tends to reduce the off-diagonal anti-correlation terms of the correlation matrix among the measured cross sections, reducing its uncertainty. Nevertheless, the p-values for the different

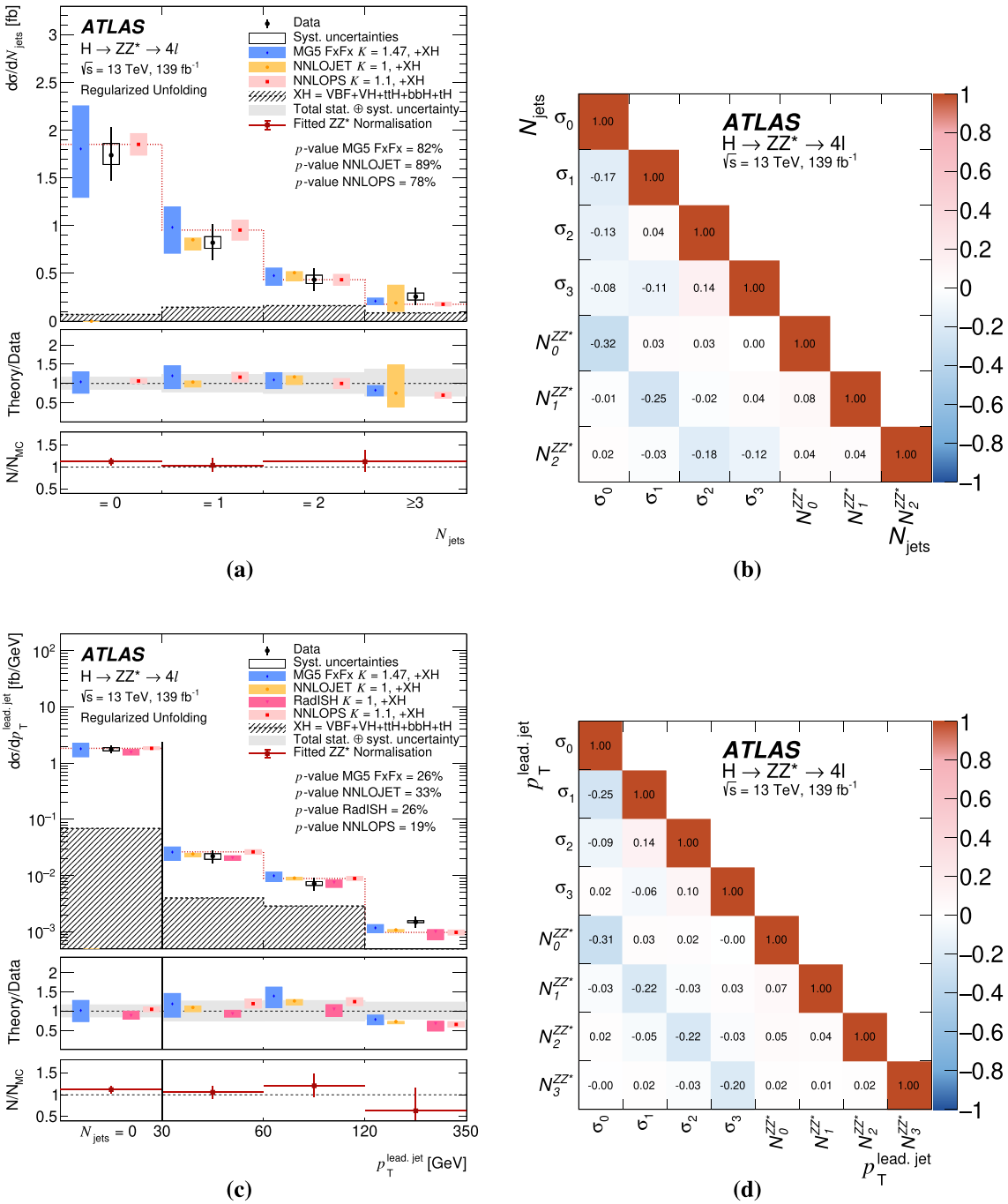

Fig. 42 **a**, **c** Differential fiducial cross sections as a function of the jet multiplicity, N_{jets}, and leading jet p_{T} in events with at least one jet, using a regularised matrix unfolding with the τ parameters set to 0.6 and 0.7 respectively. The corresponding correlation matrix between the measured cross sections and the ZZ^* background normalisation factors are also shown in **b** and **d**

predictions are close to the ones obtained with the matrix unfolding without any regularisation.

B Invariant mass of the leading lepton pair in same-flavour and opposite-flavour final states

Figure 43 presents results for the invariant mass of the leading lepton pair in same-flavour and different-flavour final states.

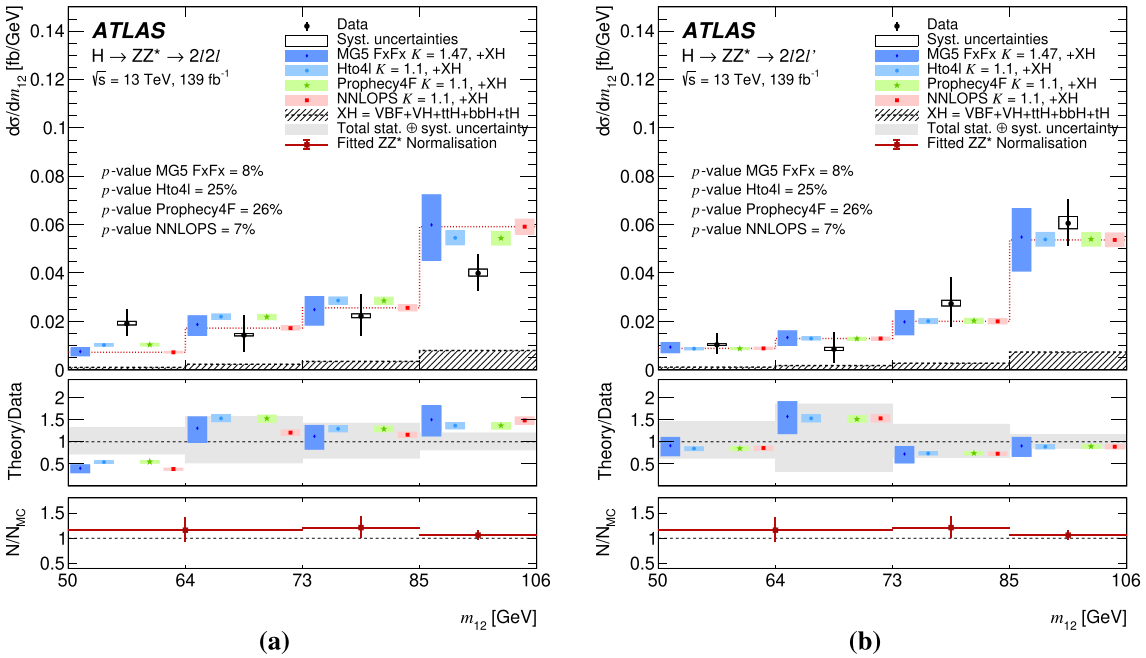

Fig. 43 Differential fiducial cross sections for the invariant mass m_{12} of the leading Z boson in **a** the 4μ and $4e$ decay channels and **b** the $2e2\mu$ and $2\mu2e$ decay channels. The corresponding correlation matrix is shown in **c**

References

1. ATLAS Collaboration, Observation of a new particle in the search for the Standard Model Higgs boson with the ATLAS detector at the LHC. Phys. Lett. B **716**, 1 (2012). arXiv:1207.7214 [hep-ex]
2. CMS Collaboration, Observation of a new boson at a mass of 125 GeV with the CMS experiment at the LHC. Phys. Lett. B **716**, 30 (2012). https://doi.org/10.1016/j.physletb.2012.08.021. arXiv:1207.7235 [hep-ex]
3. F. Englert, R. Brout, Broken symmetry and the mass of gauge vector mesons. Phys. Rev. Lett. **13**, 321 (1964). https://doi.org/10.1103/PhysRevLett.13.321
4. P.W. Higgs, Broken symmetries and the masses of gauge Bosons. Phys. Rev. Lett. **13**, 508 (1964). https://doi.org/10.1103/PhysRevLett.13.508
5. G. Guralnik, C. Hagen, T. Kibble, Global conservation laws and massless particles. Phys. Rev. Lett. **13**, 585 (1964). https://doi.org/10.1103/PhysRevLett.13.585
6. ATLAS Collaboration, Study of the spin and parity of the Higgs boson in Diboson decays with the ATLAS detector. Eur. Phys. J. C **75**, 476 (2015). https://doi.org/10.1140/epjc/s10052-015-3685-1. arXiv:1506.05669 [hep-ex] [**Erratum: Eur. Phys. J. C 76 (2016) 152**]
7. CMS Collaboration, Constraints on the spin-parity and anomalous HVV couplings of the Higgs boson in proton collisions at 7 and 8 TeV. Phys. Rev. D **92**, 012004 (2015). https://doi.org/10.1103/PhysRevD.92.012004. arXiv:1411.3441 [hep-ex]
8. ATLAS Collaboration, Measurements of the Higgs boson production and decay rates and coupling strengths using pp collision data at $\sqrt{s} = 7$ and 8 TeV in the ATLAS experiment. Eur. Phys. J. C **76**, 6 (2016). https://doi.org/10.1140/epjc/s10052-015-3769-y. arXiv:1507.04548 [hep-ex]
9. CMS Collaboration, Precise determination of the mass of the Higgs boson and tests of compatibility of its couplings with the standard model predictions using proton collisions at 7 and 8 TeV. Eur. Phys. J. C **75**, 212 (2015). https://doi.org/10.1140/epjc/s10052-015-3351-7. arXiv:1412.8662 [hep-ex]
10. ATLAS and CMS Collaborations, Measurements of the Higgs boson production and decay rates and constraints on its couplings from a combined ATLAS and CMS analysis of the LHC pp collision data at $\sqrt{s} = 7$ and 8 TeV. JHEP **08**, 045 (2016). https://doi.org/10.1007/JHEP08(2016)045. arXiv:1606.02266 [hep-ex]
11. ATLAS Collaboration, Measurement of inclusive and differential cross sections in the $H \to ZZ^* \to 4\ell$ decay channel in pp collisions at $\sqrt{s} = 13$ TeV with the ATLAS detector. JHEP **10**, 132 (2017). https://doi.org/10.1007/JHEP10(2017)132. arXiv:1708.02810 [hep-ex]
12. ATLAS Collaboration, Measurement of the Higgs boson coupling properties in the $H \to ZZ^* \to 4\ell$ decay channel at $\sqrt{s} = 13$ TeV with the ATLAS detector. JHEP **03**, 095 (2018). https://doi.org/10.1007/JHEP03(2018)095. arXiv:1712.02304 [hep-ex]
13. ATLAS Collaboration, Evidence for the $H \to b\bar{b}$ decay with the ATLAS detector, JHEP **12**, 024 (2017). https://doi.org/10.1007/JHEP12(2017)024. arXiv:1708.03299 [hep-ex]
14. ATLAS Collaboration, Evidence for the associated production of the Higgs boson and a top quark pair with the ATLAS detector. Phys. Rev. D **97**, 072003 (2018). https://doi.org/10.1103/PhysRevD.97.072003. arXiv:1712.08891 [hep-ex]
15. ATLAS and CMS Collaborations, Combined Measurement of the Higgs Boson Mass in pp Collisions at $\sqrt{s} = 7$ and 8 TeV with the ATLAS and CMS Experiments. Phys. Rev. Lett. **114**, 191803 (2015). https://doi.org/10.1103/PhysRevLett.114.191803. arXiv:1503.07589 [hep-ex]
16. ATLAS Collaboration, Measurements of Higgs boson properties in the diphoton decay channel with $36 fb^{-1}$ of pp collision data at $\sqrt{s} = 13$ TeV with the ATLAS detector. Phys. Rev. D **98**, 052005 (2018). https://doi.org/10.1103/PhysRevD.98.052005. arXiv:1802.04146 [hep-ex]
17. CMS Collaboration, Measurements of properties of the Higgs boson decaying into the four-lepton final state in pp collisions at $\sqrt{s} = 13$ TeV. JHEP **11**, 047 (2017). https://doi.org/10.1007/JHEP11(2017)047. arXiv:1706.09936 [hep-ex]
18. CMS Collaboration, Constraints on anomalous Higgs boson couplings using production and decay information in the four-lepton final state. Phys. Lett. B **775**, 1 (2017). https://doi.org/10.1016/j.physletb.2017.10.021. arXiv:1707.00541 [hep-ex]
19. CMS Collaboration, Measurement and interpretation of differential cross sections for Higgs boson production at $\sqrt{s} = 13$ TeV. Phys. Lett. B **792**, 369 (2019). https://doi.org/10.1016/j.physletb.2019.03.059. arXiv:1812.06504 [hep-ex]
20. ATLAS Collaboration, Measurement of the production cross section for a Higgs boson in association with a vector boson in the $H \to WW^* \to \ell\nu\ell\nu$ channel in pp collisions at $\sqrt{s} = 13$ TeV with the ATLAS detector (2019). arXiv:1903.10052 [hep-ex]
21. ATLAS Collaboration, Measurement of the four-lepton invariant mass spectrum in 13 TeV proton-proton collisions with the ATLAS detector. JHEP **04**, 048 (2019). https://doi.org/10.1007/JHEP04(2019)048. arXiv:1902.05892 [hep-ex]
22. ATLAS Collaboration, Cross-section measurements of the Higgs boson decaying into a pair of τ-leptons in proton-proton collisions at $\sqrt{s} = 13$ TeV with the ATLAS detector. Phys. Rev. D **99**, 072001 (2019). https://doi.org/10.1103/PhysRevD.99.072001. arXiv:1811.08856 [hep-ex]
23. ATLAS Collaboration, Measurements of gluon-gluon fusion and vector-boson fusion Higgs boson production cross-sections in the $H \to WW^* \to e\nu\mu\nu$ decay channel in pp collisions at $\sqrt{s} = 13$ TeV with the ATLAS detector. Phys. Lett. B **789**, 508 (2019). https://doi.org/10.1016/j.physletb.2018.11.064. arXiv:1808.09054 [hep-ex]
24. ATLAS Collaboration, Observation of $H \to b\bar{b}$ decays and VH production with the ATLAS detector, Phys. Lett. B **786**, 59 (2018). https://doi.org/10.1016/j.physletb.2018.09.013. arXiv:1808.08238 [hep-ex]
25. ATLAS Collaboration, Constraints on off-shell Higgs boson production and the Higgs boson total width in $ZZ \to 4\ell$ and $ZZ \to 2\ell 2\nu$ final states with the ATLAS detector. Phys. Lett. B **786**, 223 (2018). https://doi.org/10.1016/j.physletb.2018.09.048. arXiv:1808.01191 [hep-ex]
26. ATLAS Collaboration, Observation of Higgs boson production in association with a top quark pair at the LHC with the ATLAS detector. Phys. Lett. B **784**, 173 (2018). https://doi.org/10.1016/j.physletb.2018.07.035. arXiv:1806.00425 [hep-ex]
27. ATLAS Collaboration, Measurement of the Higgs boson mass in the $H \to ZZ^* \to 4\ell$ and $H \to \gamma\gamma$ channels with $\sqrt{s} = 13$ TeV pp collisions using the ATLAS detector. Phys. Lett. B **784**, 345 (2018). https://doi.org/10.1016/j.physletb.2018.07.050. arXiv:1806.00242 [hep-ex]
28. ATLAS Collaboration, Combined measurement of differential and total cross sections in the $H \to \gamma\gamma$ and the $H \to ZZ^* \to 4\ell$ decay channels at $\sqrt{s} = 13$ TeV with the ATLAS detector. Phys. Lett. B **786**, 114 (2018). https://doi.org/10.1016/j.physletb.2018.09.019. arXiv:1805.10197 [hep-ex]
29. ATLAS Collaboration, Electron and photon reconstruction and performance in ATLAS using a dynamical, topological cell clustering-based approach, ATL-PHYS-PUB-2017-022 (2017).https://cds.cern.ch/record/2298955
30. ATLAS Collaboration, Electron and photon performance measurements with the ATLAS detector using the 2015–2017 LHC proton–proton collision data (2019). arXiv:1908.00005 [hep-ex]
31. ATLAS Collaboration, Higgs boson production cross section measurements and their EFT interpretation in the 4ℓ decay chan-

nel at $\sqrt{s} = 13$ TeV with the ATLAS detector, Eur. Phys. J. C. (2020). https://doi.org/10.1140/epjc/s10052-020-8227-9
32. ATLAS Collaboration, The ATLAS Experiment at the CERN Large Hadron Collider. JINST **3**, S08003 (2008). https://doi.org/10.1088/1748-0221/3/08/S08003
33. ATLAS Collaboration, ATLAS Insertable B-Layer Technical Design Report, ATLAS-TDR-19 (2010). https://cds.cern.ch/record/1291633, https://cds.cern.ch/record/1451888 [**Addendum: ATLAS-TDR-19-ADD-1, 2012**]
34. B. Abbott et al., Production and integration of the ATLAS Insertable B-Layer. JINST **13**, T05008 (2018). https://doi.org/10.1088/1748-0221/13/05/T05008. arXiv:1803.00844 [physics.ins-det]
35. ATLAS Collaboration, Performance of the ATLAS trigger system in 2015, Eur. Phys. J. C **77**, 317 (2017). https://doi.org/10.1140/epjc/s10052-017-4852-3. arXiv:1611.09661 [hep-ex]
36. S. Alioli, P. Nason, C. Oleari, E. Re, A general framework for implementing NLO calculations in shower Monte Carlo programs: the POWHEG BOX. JHEP **06**, 043 (2010). https://doi.org/10.1007/JHEP06(2010)043. arXiv:1002.2581 [hep-ph]
37. S. Frixione, P. Nason, C. Oleari, Matching NLO QCD computations with parton shower simulations: the POWHEG method. JHEP **11**, 070 (2007). https://doi.org/10.1088/1126-6708/2007/11/070. arXiv:0709.2092 [hep-ph]
38. P. Nason, A new method for combining NLO QCD with shower Monte Carlo algorithms. JHEP **11**, 040 (2004). https://doi.org/10.1088/1126-6708/2004/11/040. arXiv:hep-ph/0409146
39. E. Bagnaschi, G. Degrassi, P. Slavich, A. Vicini, Higgs production via gluon fusion in the POWHEG approach in the SM and in the MSSM. JHEP **02**, 088 (2012). https://doi.org/10.1007/JHEP02(2012)088. arXiv:1111.2854 [hep-ph]
40. U. Aglietti, R. Bonciani, G. Degrassi, A. Vicini, Two-loop light fermion contribution to Higgs production and decays. Phys. Lett. B **595**, 432 (2004). https://doi.org/10.1016/j.physletb.2004.06.063. arXiv:hep-ph/0404071
41. K. Hamilton, P. Nason, G. Zanderighi, Finite quark-mass effects in the NNLOPSPOWHEG+MiNLO Higgs generator. JHEP **05**, 140 (2015). https://doi.org/10.1007/JHEP05(2015)140. arXiv:1501.04637 [hep-ph]
42. P. Nason, C. Oleari, NLO Higgs boson production via vector-boson fusion matched with shower in POWHEG. JHEP **02**, 037 (2010). https://doi.org/10.1007/JHEP02(2010)037. arXiv:0911.5299 [hep-ph]
43. G. Luisoni, P. Nason, C. Oleari, F. Tramontano, $HW^{\pm}/HZ + 0$ and 1 jet at NLO with the POWHEG BOX interfaced to GoSam and their merging within MiNLO. JHEP **10**, 083 (2013). https://doi.org/10.1007/JHEP10(2013)083. arXiv:1306.2542 [hep-ph]
44. LHC Higgs Cross Section Working Group, Handbook of LHC Higgs Cross Sections: 1. Inclusive Observables, CERN-2011-002 (2011). https://doi.org/10.5170/CERN-2011-002. arXiv:1101.0593 [hep-ph]
45. LHC Higgs Cross SectionWorking Group, Handbook of LHC Higgs Cross Sections: 2. Differential Distributions, CERN-2012-002 (2012). https://doi.org/10.5170/CERN-2012-002. arXiv:1201.3084 [hep-ph]
46. LHC Higgs Cross Section Working Group, Handbook of LHC Higgs Cross Sections: 3. Higgs Properties, CERN-2013-004 (CERN, Geneva, 2013). https://doi.org/10.5170/CERN-2013-004. arXiv:1307.1347 [hep-ph]
47. C. Anastasiou, C. Duhr, F. Dulat, F. Herzog, B. Mistlberger, Higgs boson gluon-fusion production in QCD at three loops. Phys. Rev. Lett. **114**, 212001 (2015). https://doi.org/10.1103/PhysRevLett.114.212001. arXiv:1503.06056 [hep-ph]
48. C. Anastasiou et al., High precision determination of the gluon fusion Higgs boson cross-section at the LHC. JHEP **05**, 058 (2016). https://doi.org/10.1007/JHEP05(2016)058. arXiv:1602.00695 [hep-ph]
49. S. Actis, G. Passarino, C. Sturm, S. Uccirati, NLO electroweak corrections to Higgs boson production at Hadron colliders. Phys. Lett. B **670**, 12 (2008). https://doi.org/10.1016/j.physletb.2008.10.018. arXiv:0809.1301 [hep-ph]
50. C. Anastasiou, R. Boughezal, F. Petriello, Mixed QCD-electroweak corrections to Higgs boson production in gluon fusion. JHEP **04**, 003 (2009). https://doi.org/10.1088/1126-6708/2009/04/003. arXiv:0811.3458 [hep-ph]
51. M. Grazzini, H. Sargsyan, Heavy-quark mass effects in Higgs boson production at the LHC. JHEP **09**, 129 (2013). https://doi.org/10.1007/JHEP09(2013)129. arXiv:1306.4581 [hep-ph]
52. I.W. Stewart, F.J. Tackmann, Theory uncertainties for Higgs mass and other searches using jet bins. Phys. Rev. D **85**, 034011 (2012). https://doi.org/10.1103/PhysRevD.85.034011. arXiv:1107.2117 [hep-ph]
53. M. Ciccolini, A. Denner, S. Dittmaier, Strong and electroweak corrections to the production of a Higgs Boson + 2 jets via weak interactions at the large Hadron collider. Phys. Rev. Lett. **99**, 161803 (2007). https://doi.org/10.1103/PhysRevLett.99.161803. arXiv:0707.0381 [hep-ph]
54. M. Ciccolini, A. Denner, S. Dittmaier, Electroweak and QCD corrections to Higgs production via vector-boson fusion at the LHC. Phys. Rev. D **77**, 013002 (2008). https://doi.org/10.1103/PhysRevD.77.013002. arXiv:0710.4749 [hep-ph]
55. P. Bolzoni, F. Maltoni, S.-O. Moch, M. Zaro, Higgs Boson production via vector-Boson fusion at next-to-next-to-leading order in QCD. Phys. Rev. Lett. **105**, 011801 (2010). https://doi.org/10.1103/PhysRevLett.105.011801. arXiv:1003.4451 [hep-ph]
56. O. Brein, A. Djouadi, R. Harlander, NNLO QCD corrections to the Higgs-strahlung processes at hadron colliders. Phys. Lett. B **579**, 149 (2004). https://doi.org/10.1016/j.physletb.2003.10.112. arXiv:hep-ph/0307206
57. A. Denner, S. Dittmaier, S. Kallweit, A. Mück, Electroweak corrections to Higgs-strahlung off W/Z bosons at the Tevatron and the LHC with HAWK. JHEP **03**, 075 (2012). https://doi.org/10.1007/JHEP03(2012)075. arXiv:1112.5142 [hep-ph]
58. L. Altenkamp, S. Dittmaier, R.V. Harlander, H. Rzehak, T.J.E. Zirke, Gluon-induced Higgs-strahlung at next-to-leading order QCD. JHEP **02**, 078 (2013). https://doi.org/10.1007/JHEP02(2013)078. arXiv:1211.5015 [hep-ph]
59. W. Beenakker et al., NLO QCD corrections to $t\bar{t}H$ production in hadron collisions. Nucl. Phys. B **653**, 151 (2003). https://doi.org/10.1016/S0550-3213(03)00044-0. arXiv:hep-ph/0211352
60. S. Dawson, C. Jackson, L. Orr, L. Reina, D. Wackeroth, Associated Higgs production with top quarks at the large hadron collider: NLO QCD corrections. Phys. Rev. D **68**, 034022 (2003). https://doi.org/10.1103/PhysRevD.68.034022. arXiv:hep-ph/0305087
61. Y. Zhang, W.-G. Ma, R.-Y. Zhang, C. Chen, L. Guo, QCD NLO and EW NLO corrections to $t\bar{t}H$ production with top quark decays at hadron collider. Phys. Lett. B **738**, 1 (2014). https://doi.org/10.1016/j.physletb.2014.09.022. arXiv:1407.1110 [hep-ph]
62. S. Frixione, V. Hirschi, D. Pagani, H.-S. Shao, M. Zaro, Electroweak and QCD corrections to top-pair hadroproduction in association with heavy bosons. JHEP **06**, 184 (2015). https://doi.org/10.1007/JHEP06(2015)184. arXiv:1504.03446 [hep-ph]
63. S. Dawson, C. Jackson, L. Reina, D. Wackeroth, Exclusive Higgs boson production with bottom quarks at hadron colliders. Phys. Rev. D **69**, 074027 (2004). https://doi.org/10.1103/PhysRevD.69.074027. arXiv:hep-ph/0311067
64. S. Dittmaier, M. Krämer, M. Spira, Higgs radiation off bottom quarks at the Fermilab Tevatron and the CERN LHC. Phys. Rev. D **70**, 074010 (2004). https://doi.org/10.1103/PhysRevD.70.074010. arXiv:hep-ph/0309204

65. R.V. Harlander, W.B. Kilgore, Higgs boson production in bottom quark fusion at next-to-next-to leading order. Phys. Rev. D **68**, 013001 (2003). https://doi.org/10.1103/PhysRevD.68.013001. arXiv:hep-ph/0304035
66. A. Djouadi, J. Kalinowski, M. Spira, HDECAY: a program for Higgs boson decays in the standard model and its supersymmetric extension. Comput. Phys. Commun. **108**, 56 (1998). https://doi.org/10.1016/S0010-4655(97)00123-9. arXiv:hep-ph/9704448
67. A. Djouadi, M.M. Mühlleitner, M. Spira, Decays of supersymmetric particles: The Program SUSY-HIT (SUspect-SdecaY-Hdecay-InTerface). Acta Phys. Polon. B **38**, 635 (2007). arXiv:hep-ph/0609292 [hep-ph]
68. A. Bredenstein, A. Denner, S. Dittmaier, M.M. Weber, Precise predictions for the Higgs-boson decay $H \to WW/ZZ \to 4$ leptons. Phys. Rev. D **74**, 013004 (2006). https://doi.org/10.1103/PhysRevD.74.013004. arXiv:0604011 [hep-ph]
69. A. Bredenstein, A. Denner, S. Dittmaier, M.M. Weber, Radiative corrections to the semileptonic and hadronic Higgs-boson decays $H \to WW/ZZ \to 4$ fermions. JHEP **02**, 080 (2007). https://doi.org/10.1088/1126-6708/2007/02/080. arXiv:0611234 [hep-ph]
70. S. Boselli, C.M. Carloni Calame, G. Montagna, O. Nicrosini, F. Piccinini, Higgs boson decay into four leptons at NLOPS electroweak accuracy. JHEP **06**, 023 (2015). https://doi.org/10.1007/JHEP06(2015)023. arXiv: 1503.07394 [hep-ph]
71. J. Butterworth et al., PDF4LHC recommendations for LHC Run II. J. Phys. G **43**, 023001 (2016). https://doi.org/10.1088/0954-3899/43/2/023001. arXiv:1510.03865 [hep-ph]
72. S. Dulat et al., New parton distribution functions from a global analysis of quantum chromodynamics. Phys. Rev. D **93**, 033006 (2016). https://doi.org/10.1103/PhysRevD.93.033006. arXiv:1506.07443 [hep-ph]
73. L.A. Harland-Lang, A.D. Martin, P. Motylinski, R.S. Thorne, Parton distributions in the LHC era: MMHT 2014 PDFs. Eur. Phys. J. C **75**, 204 (2015). https://doi.org/10.1140/epjc/s10052-015-3397-6. arXiv:1412.3989 [hep-ph]
74. R.D. Ball et al., Parton distributions for the LHC Run II. JHEP **04**, 040 (2015). https://doi.org/10.1007/JHEP04(2015)040. arXiv:1410.8849 [hep-ph]
75. K. Hamilton, P. Nason, C. Oleari, G. Zanderighi, Merging H/W/Z + 0 and 1 jet at NLO with no merging scale: a path to parton shower + NNLO matching. JHEP **05**, 082 (2013). https://doi.org/10.1007/JHEP05(2013)082. arXiv:1212.4504 [hep-ph]
76. K. Hamilton, P. Nason, E. Re, G. Zanderighi, NNLOPS simulation of Higgs boson production. JHEP **10**, 222 (2013). https://doi.org/10.1007/JHEP10(2013)222. arXiv:1309.0017 [hep-ph]
77. S. Catani, M. Grazzini, Next-to-next-to-leading-order subtraction formalism in Hadron collisions and its application to higgs-Boson production at the large hadron collider. Phys. Rev. Lett. **98**, 222002 (2007). https://doi.org/10.1103/PhysRevLett.98.222002. arXiv:hep-ph/0703012
78. M. Grazzini, NNLO predictions for the Higgs boson signal in the $H \to WW \to l\nu l\nu$ and $H \to ZZ \to 4l$ decay channels. JHEP **02**, 043 (2008). https://doi.org/10.1088/1126-6708/2008/02/043. arXiv:0801.3232 [hep-ph]
79. M. Wiesemann et al., Higgs production in association with bottom quarks. JHEP **02**, 132 (2015). https://doi.org/10.1007/JHEP02(2015)132. arXiv:1409.5301 [hep-ph]
80. H.-L. Lai et al., New parton distributions for collider physics. Phys. Rev. D **82**, 074024 (2010). https://doi.org/10.1103/PhysRevD.82.074024. arXiv:1007.2241 [hep-ph]
81. T. Sjöstrand, S. Mrenna, P.Z. Skands, A brief introduction to PYTHIA 8.1. Comput. Phys. Commun. **178**, 852 (2008). https://doi.org/10.1016/j.cpc.2008.01.036. arXiv:0710.3820 [hep-ph]
82. ATLAS Collaboration, Measurement of the Z/γ^* boson transverse momentum distribution in pp collisions at $\sqrt{s} = 7$ TeV with the ATLAS detector. JHEP **09**,145 (2014). https://doi.org/10.1007/JHEP09(2014)145. arXiv:1406.3660 [hep-ex]
83. ATLAS Collaboration, ATLAS Run 1 Pythia8 tunes, tech. rep. ATL-PHYS-PUB-2014-021, CERN (2014). https://cds.cern.ch/record/1966419
84. D.J. Lange, The EvtGen particle decay simulation package. Nucl. Instrum. Methods A **462**, 152 (2001). https://doi.org/10.1016/S0168-9002(01)00089-4
85. J. Alwall et al., The automated computation of tree-level and next-to-leading order differential cross sections, and their matching to parton shower simulations. JHEP **07**, 079 (2014). https://doi.org/10.1007/JHEP07(2014)079. arXiv:1405.0301 [hep-ph]
86. R. Frederix, S. Frixione, Merging meets matching in MC@NLO. JHEP **12**, 061 (2012). https://doi.org/10.1007/JHEP12(2012)061. arXiv:1209.6215 [hep-ph]
87. R. Frederix, S. Frixione, E. Vryonidou, M. Wiesemann, Heavy-quark mass effects in Higgs plus jets production. JHEP **08**, 006 (2016). https://doi.org/10.1007/JHEP08(2016)006. arXiv:1604.03017 [hep-ph]
88. H. Mantler, M. Wiesemann, Hadronic Higgs production through NLO + PS in the SM, the 2HDM and the MSSM. Eur. Phys. J. C **75**, 257 (2015). https://doi.org/10.1140/epjc/s10052-015-3462-1. arXiv:1504.06625 [hep-ph]
89. H. Mantler, M. Wiesemann, Top- and bottom-mass effects in hadronic Higgs production at small transverse momenta through LO+NLL. Eur. Phys. J. C **73**, 2467 (2013). https://doi.org/10.1140/epjc/s10052-013-2467-x. arXiv:1210.8263 [hep-ph]
90. S. Frixione, E. Laenen, P. Motylinski, B.R. Webber, Angular correlations of lepton pairs from vector boson and top quark decays in Monte Carlo simulations. JHEP **04**, 081 (2007). https://doi.org/10.1088/1126-6708/2007/04/081. arXiv:hep-ph/0702198
91. P. Artoisenet, R. Frederix, O. Mattelaer, R. Rietkerk, Automatic spin-entangled decays of heavy resonances in Monte Carlo simulations. JHEP **03**, 015 (2013). https://doi.org/10.1007/JHEP03(2013)015. arXiv:1212.3460 [hep-ph]
92. A. Banfi, P.F. Monni, G.P. Salam, G. Zanderighi, Higgs- and Z-boson production with a jet veto. Phys. Rev. Lett. **109**, 202001 (2012). https://doi.org/10.1103/PhysRevLett.109.202001. arXiv:1206.4998 [hep-ph]
93. A. Banfi et al., Jet-vetoed Higgs cross section in gluon fusion at $N^3LO + NNLL$ with small-R resummation. JHEP **04**, 049 (2016). https://doi.org/10.1007/JHEP04(2016)049. arXiv:1511.02886 [hep-ph]
94. P.F. Monni, E. Re, P. Torrielli, Higgs transverse-momentum resummation in direct space. Phys. Rev. Lett. **116**, 242001 (2016). https://doi.org/10.1103/PhysRevLett.116.242001. arXiv:1604.02191 [hep-ph]
95. W. Bizon, P.F. Monni, E. Re, L. Rottoli, P. Torrielli, Momentum-space resummation for transverse observables and the Higgs $p\perp$ at $N^3LL + NNLO$. JHEP **02**, 108 (2018). https://doi.org/10.1007/JHEP02(2018)108. arXiv:1705.09127 [hep-ph]
96. P.F. Monni, L. Rottoli, P. Torrielli, Higgs transverse momentum with a jet veto: a double-differential resummation (2019). arXiv:1909.04704 [hep-ph]
97. M. Grazzini, S. Kallweit, M. Wiesemann, Fully differential NNLO computations with MATRIX. Eur. Phys. J. C **78**, 537 (2018). https://doi.org/10.1140/epjc/s10052-018-5771-7. arXiv:1711.06631 [hep-ph]
98. M. Grazzini, S. Kallweit, D. Rathlev, M. Wiesemann, Transverse-momentum resummation for vector-boson pair production at NNLL+NNLO. JHEP **08**, 154 (2015). https://doi.org/10.1007/JHEP08(2015)154. arXiv:1507.02565 [hep-ph]
99. X. Chen, T. Gehrmann, E.W.N. Glover, M. Jaquier, Precise QCD predictions for the production of Higgs + jet final states. Phys. Lett. B **740**, 147 (2015). https://doi.org/10.1016/j.physletb.2014.11.021. arXiv:1408.5325 [hep-ph]

100. X. Chen, J. Cruz-Martinez, T. Gehrmann, E.W.N. Glover, M. Jaquier, NNLO QCD corrections to Higgs boson production at large transverse momentum. JHEP **10**, 066 (2016). https://doi.org/10.1007/JHEP10(2016)066. arXiv:1607.08817 [hep-ph]
101. X. Chen, T. Gehrmann, E.W.N. Glover, A. Huss, Fiducial cross sections for the four-lepton decay mode in Higgs-plus-jet production up to NNLO QCD. JHEP **07**, 052 (2019). https://doi.org/10.1007/JHEP07(2019)052. arXiv:1905.13738 [hep-ph]
102. S. Boselli et al., Higgs decay into four charged leptons in the presence of dimension-six operators. JHEP **01**, 096 (2018). https://doi.org/10.1007/JHEP01(2018)096. arXiv:1703.06667 [hep-ph]
103. A. Bredenstein, A. Denner, S. Dittmaier, M.M. Weber, Precision calculations for the Higgs decays $H \to ZZ/WW \to 4$ leptons. Nucl. Phys. Proc. Suppl. **160**, 131 (2006). https://doi.org/10.1016/j.nuclphysbps.2006.09.104. arXiv:0607060 [hep-ph]
104. L. Altenkamp, S. Dittmaier, H. Rzehak, Renormalization schemes for the two-Higgs-doublet model and applications to $h \to WW/ZZ \to 4$ fermions. JHEP **09**, 134 (2017). https://doi.org/10.1007/JHEP09(2017)134. arXiv:1704.02645 [hep-ph]
105. L. Altenkamp, S. Dittmaier, H. Rzehak, Precision calculations for $h \to WW/ZZ \to 4$ fermions in the Two-Higgs-Doublet Model with Prophecy4f. JHEP **03**, 110 (2018). https://doi.org/10.1007/JHEP03(2018)110. arXiv:1710.07598 [hep-ph]
106. L. Altenkamp, M. Boggia, S. Dittmaier, Precision calculations for $h \to WW/ZZ \to 4$ fermions in a singlet extension of the Standard Model with PROPHECY4F. JHEP **04**, 062 (2018). https://doi.org/10.1007/JHEP04(2018)062. arXiv:1801.07291 [hep-ph]
107. A. Denner, S. Dittmaier, J.-N. Lang, Renormalization of mixing angles. JHEP **11**, 104 (2018). https://doi.org/10.1007/JHEP11(2018)104. arXiv:1808.03466 [hep-ph]
108. LHC Higgs Cross SectionWorking Group, Handbook of LHC Higgs Cross Sections: 4. Deciphering the nature of the Higgs sector, CERN-2017-002-M (CERN, Geneva, 2016). https://doi.org/10.23731/CYRM-2017-002. arXiv:1610.07922 [hep-ph]
109. J.S. Gainer et al., Adding pseudo-observables to the four-lepton experimentalist's toolbox. JHEP **10**, 073 (2018). https://doi.org/10.1007/JHEP10(2018)073. arXiv:1808.00965 [hep-ph]
110. A. Alloul, N.D. Christensen, C. Degrande, C. Duhr, B. Fuks, FeynRules 2.0—A complete toolbox for tree-level phenomenology, Comput. Phys. Commun. **185**, 2250 (2014). arXiv:1310.1921 [hep-ph]. https://doi.org/10.1016/j.cpc.2014.04.012
111. T. Gleisberg et al., Event generation with SHERPA 1.1, JHEP 02, 007 (2009). https://doi.org/10.1088/1126-6708/2009/02/007. arXiv:0811.4622 [hep-ph]
112. T. Gleisberg, S. Höche, Comix, a new matrix element generator. JHEP **12**, 039 (2008). https://doi.org/10.1088/1126-6708/2008/12/039. arXiv:0808.3674 [hep-ph]
113. F. Cascioli, P. Maierhofer, S. Pozzorini, Scattering amplitudes with open loops. Phys. Rev. Lett. **108**, 111601 (2012). https://doi.org/10.1103/PhysRevLett.108.111601. arXiv:1111.5206 [hep-ph]
114. S. Schumann, F. Krauss, A parton shower algorithm based on Catani–Seymour dipole factorisation. JHEP **03**, 038 (2008). https://doi.org/10.1088/1126-6708/2008/03/038. arXiv:0709.1027 [hep-ph]
115. S. Höche, F. Krauss, M. Schönherr, F. Siegert, QCD matrix elements + parton showers. The NLO case. JHEP **04**, 027 (2013). https://doi.org/10.1007/JHEP04(2013)027. arXiv:1207.5030 [hep-ph]
116. B. Biedermann, A. Denner, S. Dittmaier, L. Hofer, B. Jäger, Electroweak corrections to $pp \to \mu^+\mu^- e^+ e^- + X$ at the LHC: A Higgs Boson Background Study. Phys. Rev. Lett. **116**, 161803 (2016). https://doi.org/10.1103/PhysRevLett.116.161803. arXiv:1601.07787 [hep-ph]
117. B. Biedermann, A. Denner, S. Dittmaier, L. Hofer, B. Jäger, Next-to-leading-order electroweak corrections to the production of four charged leptons at the LHC. JHEP **01**, 033 (2017). https://doi.org/10.1007/JHEP01(2017)033. arXiv:1611.05338 [hep-ph]
118. F. Caola, K. Melnikov, R. Röntsch, L. Tancredi, QCD corrections to ZZ production in gluon fusion at the LHC. Phys. Rev. D **92**, 094028 (2015). https://doi.org/10.1103/PhysRevD.92.094028. arXiv:1509.06734 [hep-ph]
119. F. Caola, K. Melnikov, R. Röntsch, L. Tancredi, QCD corrections to W^+W^- production through gluon fusion. Phys. Lett. B **754**, 275 (2016). https://doi.org/10.1016/j.physletb.2016.01.046. arXiv:1511.08617 [hep-ph]
120. J.M. Campbell, R.K. Ellis, M. Czakon, S. Kirchner, Two loop correction to interference in $gg \to ZZ$. JHEP **08**, 011 (2016). https://doi.org/10.1007/JHEP08(2016)011. arXiv:1605.01380 [hep-ph]
121. K. Melnikov, M. Dowling, Production of two Z-bosons in gluon fusion in the heavy top quark approximation. Phys. Lett. B **744**, 43 (2015). https://doi.org/10.1016/j.physletb.2015.03.030. arXiv:1503.01274 [hep-ph]
122. M. Bonvini, F. Caola, S. Forte, K. Melnikov, G. Ridolfi, Signal-background interference effects for $gg \to H \to W^+W^-$ beyond leading order. Phys. Rev. D **88**, 034032 (2013). https://doi.org/10.1103/PhysRevD.88.034032. arXiv:1304.3053 [hep-ph]
123. C.S. Li, H.T. Li, D.Y. Shao, J. Wang, Soft gluon resummation in the signal-background interference process of $gg(\to h^*) \to ZZ$. JHEP **08**, 065 (2015). https://doi.org/10.1007/JHEP08(2015)065. arXiv:1504.02388 [hep-ph]
124. ATLAS Collaboration, Studies on top-quark Monte Carlo modelling for Top2016, ATL-PHYSPUB-2016-020 (2016). https://cds.cern.ch/record/2216168
125. ATLAS Collaboration, The ATLAS Simulation Infrastructure, Eur. Phys. J. C **70**, 823 (2010). https://doi.org/10.1140/epjc/s10052-010-1429-9. arXiv:1005.4568 [physics.ins-det]
126. S. Agostinelli et al., GEANT4—a simulation toolkit. Nucl. Instrum. Methods A **506**, 250 (2003). https://doi.org/10.1016/S0168-9002(03)01368-8
127. R.D. Ball et al., Parton distributions with LHC data. Nucl. Phys. B **867**, 244 (2013). https://doi.org/10.1016/j.nuclphysb.2012.10.003. arXiv:1207.1303 [hep-ph]
128. ATLAS Collaboration, The Pythia 8 A3 tune description of ATLAS minimum bias and inelastic measurements incorporating the Donnachie–Landshoff diffractive model. ATL-PHYS-PUB-2016- 017 (2016). https://cds.cern.ch/record/2206965
129. ATLAS Collaboration, Jet reconstruction and performance using particle flow with the ATLAS Detector, Eur. Phys. J. C **77**, 466 (2017). https://doi.org/10.1140/epjc/s10052-017-5031-2. arXiv:1703.10485 [hep-ex]
130. ATLAS Collaboration, Expected performance of the ATLAS b-tagging algorithms in Run-2. ATL-PHYS-PUB-2015-022 (2015). https://cds.cern.ch/record/2037697
131. ATLAS Collaboration, Measurements of b-jet tagging efficiency with the ATLAS detector using $t\bar{t}$ events at $\sqrt{s} = 13$ TeV. JHEP **08**, 089 (2018). https://doi.org/10.1007/JHEP08(2018)089. arXiv:1805.01845 [hep-ex]
132. Y. Gao et al., Spin determination of single-produced resonances at Hadron colliders. Phys. Rev. D **81**, 075022 (2010). https://doi.org/10.1103/PhysRevD.81.075022. arXiv:1001.3396 [hep-ph]
133. M. Pivk, F.R. Le Diberder, SPlot: A statistical tool to unfold data distributions. Nucl. Instrum. Methods A **555**, 356 (2005). https://doi.org/10.1016/j.nima.2005.08.106. arXiv:physics/0402083
134. I.W. Stewart, F.J. Tackmann, J.R. Walsh, S. Zuberi, Jet p_T resummation in Higgs production at $NNLL' + NNLO$. Phys. Rev. D **89**, 054001 (2014). https://doi.org/10.1103/PhysRevD.89.054001. arXiv:1307.1808 [hep-ph]
135. X. Liu, F. Petriello, Reducing theoretical uncertainties for exclusive Higgs-boson plus one-jet production at the LHC. Phys. Rev. D **87**, 094027 (2013). https://doi.org/10.1103/PhysRevD.87.094027. arXiv:1303.4405 [hep-ph]

136. R. Boughezal, X. Liu, F. Petriello, F.J. Tackmann, J.R. Walsh, Combining resummed Higgs predictions across jet bins. Phys. Rev. D **89**, 074044 (2014). https://doi.org/10.1103/PhysRevD.89.074044. arXiv:1312.4535 [hep-ph]
137. S. Gangal, F.J. Tackmann, Next-to-leading-order uncertainties in Higgs+2 jets from gluon fusion. Phys. Rev. D **87**, 093008 (2013). https://doi.org/10.1103/PhysRevD.87.093008. arXiv:1302.5437 [hep-ph]
138. J. Bendavid et al., Les Houches 2017: Physics at TeV colliders standard model working group report (2018). arXiv:1803.07977 [hep-ph]
139. G. Cowan, K. Cranmer, E. Gross, O. Vitells, Asymptotic formulae for likelihood-based tests of new physics. Eur. Phys. J. C **71**, 1554 (2011). https://doi.org/10.1140/epjc/s10052-011-1554-0. arXiv:1007.1727 [hep-ex] [**Erratum: Eur. Phys. J. C 73 (2013) 2501**]
140. D. de Florian, G. Ferrera, M. Grazzini, D. Tommasini, Higgs boson production at the LHC: transverse momentum resummation effects in the $H \to \gamma\gamma, H \to WW \to \ell\nu\ell\nu$ and $H \to ZZ \to 4\ell$ decay modes. JHEP **06**, 132 (2012). https://doi.org/10.1007/JHEP06(2012)132. arXiv:1203.6321 [hep-ph]
141. A.L. Read, Presentation of the search results: the CLs technique. J. Phys. G **28**, 2693 (2002). https://doi.org/10.1088/0954-3899/28/10/313
142. M. González-Alonso, A. Greljo, G. Isidori, D. Marzocca, Pseudo-observables in Higgs decays. Eur. Phys. J. C **75**, 128 (2015). https://doi.org/10.1140/epjc/s10052-015-3345-5. arXiv:1412.6038 [hep-ph]
143. F. Bishara, U. Haisch, P.F. Monni, E. Re, Constraining light-quark Yukawa couplings from Higgs distributions. Phys. Rev. Lett. **118**, 121801 (2017). https://doi.org/10.1103/PhysRevLett.118.121801. arXiv:1606.09253 [hep-ph]
144. CMS Collaboration, A search for the standard model Higgs boson decaying to charm quarks (2019). arXiv:1912.01662 [hep-ex]
145. ATLAS Collaboration, Search for the Decay of the Higgs Boson to Charm Quarks with the ATLAS Experiment. Phys. Rev. Lett. 120, 211802 (2018). https://doi.org/10.1103/PhysRevLett.120.211802. arXiv:1802.04329 [hep-ex]
146. ATLAS Collaboration, Combined measurements of Higgs boson production and decay using up to $80\,fb^{-1}$ of proton-proton collision data at $\sqrt{s} = 13$ TeV collected with the ATLAS experiment (2019). arXiv:1909.02845 [hep-ex]
147. A. Tikhonov, Solution of incorrectly formulated problems and the regularization method. Soviet Math. Dokl. **5**, 1035/1038 (1963)
148. A. Höcker, V. Kartvelishvili, SVD approach to data unfolding. Nucl. Instrum. Methods Ar53 **372**, 469 (1996). https://doi.org/10.1016/0168-9002(95)01478-0. arXiv: 9509307 [hep-ph]
149. ATLAS Collaboration, ATLAS Computing Acknowledgements. ATL-GEN-PUB-2016-002 (2016). https://cds.cern.ch/record/2202407

ATLAS Collaboration

G. Aad[102], B. Abbott[128], D. C. Abbott[103], A. Abed Abud[36], K. Abeling[53], D. K. Abhayasinghe[94], S. H. Abidi[166], O. S. AbouZeid[40], N. L. Abraham[155], H. Abramowicz[160], H. Abreu[159], Y. Abulaiti[6], B. S. Acharya[67a,67b,n], B. Achkar[53], L. Adam[100], C. Adam Bourdarios[5], L. Adamczyk[84a], L. Adamek[166], J. Adelman[121], M. Adersberger[114], A. Adiguzel[12c], S. Adorni[54], T. Adye[143], A. A. Affolder[145], Y. Afik[159], C. Agapopoulou[65], M. N. Agaras[38], A. Aggarwal[119], C. Agheorghiesei[27c], J. A. Aguilar-Saavedra[139a,ad,139f], A. Ahmad[36], F. Ahmadov[80], W. S. Ahmed[104], X. Ai[18], G. Aielli[74a,74b], S. Akatsuka[86], T. P. A. Åkesson[97], E. Akilli[54], A. V. Akimov[111], K. Al Khoury[65], G. L. Alberghi[23a,23b], J. Albert[175], M. J. Alconada Verzini[160], S. Alderweireldt[36], M. Aleksa[36], I. N. Aleksandrov[80], C. Alexa[27b], T. Alexopoulos[10], A. Alfonsi[120], F. Alfonsi[23a,23b], M. Alhroob[128], B. Ali[141], S. Ali[157], M. Aliev[165], G. Alimonti[69a], C. Allaire[36], B. M. M. Allbrooke[155], B. W. Allen[131], P. P. Allport[21], A. Aloisio[70a,70b], F. Alonso[89], C. Alpigiani[147], E. Alunno Camelia[74a,74b], M. Alvarez Estevez[99], M. G. Alviggi[70a,70b], Y. Amaral Coutinho[81b], A. Ambler[104], L. Ambroz[134], C. Amelung[26], D. Amidei[106], S. P. Amor Dos Santos[139a], S. Amoroso[46], C. S. Amrouche[54], F. An[79], C. Anastopoulos[148], N. Andari[144], T. Andeen[11], J. K. Anders[20], S. Y. Andrean[45a,45b], A. Andreazza[69a,69b], V. Andrei[61a], C. R. Anelli[175], S. Angelidakis[9], A. Angerami[39], A. V. Anisenkov[122a,122b], A. Annovi[72a], C. Antel[54], M. T. Anthony[148], E. Antipov[129], M. Antonelli[51], D. J. A. Antrim[170], F. Anulli[73a], M. Aoki[82], J. A. Aparisi Pozo[173], M. A. Aparo[155], L. Aperio Bella[46], N. Aranzabal Barrio[36], V. Araujo Ferraz[81a], R. Araujo Pereira[81b], C. Arcangeletti[51], A. T. H. Arce[49], F. A. Arduh[89], J-F. Arguin[110], S. Argyropoulos[52], J.-H. Arling[46], A. J. Armbruster[36], A. Armstrong[170], O. Arnaez[166], H. Arnold[120], Z. P. Arrubarrena Tame[114], G. Artoni[134], K. Asai[126], S. Asai[162], T. Asawatavonvanich[164], N. Asbah[59], E. M. Asimakopoulou[171], L. Asquith[155], J. Assahsah[35d], K. Assamagan[29], R. Astalos[28a], R. J. Atkin[33a], M. Atkinson[172], N. B. Atlay[19], H. Atmani[65], K. Augsten[141], V. A. Austrup[181], G. Avolio[36], M. K. Ayoub[15a], G. Azuelos[110,al], H. Bachacou[144], K. Bachas[161], M. Backes[134], F. Backman[45a,45b], P. Bagnaia[73a,73b], M. Bahmani[85], H. Bahrasemani[151], A. J. Bailey[173], V. R. Bailey[172], J. T. Baines[143], C. Bakalis[10], O. K. Baker[182], P. J. Bakker[120], E. Bakos[16], D. Bakshi Gupta[8], S. Balaji[156], E. M. Baldin[122a,122b], P. Balek[179], F. Balli[144], W. K. Balunas[134], J. Balz[100], E. Banas[85], M. Bandieramonte[138], A. Bandyopadhyay[24], Sw. Banerjee[180,i], L. Barak[160], W. M. Barbe[38], E. L. Barberio[105], D. Barberis[55a,55b], M. Barbero[102], G. Barbour[95], T. Barillari[115], M-S. Barisits[36], J. Barkeloo[131], T. Barklow[152], R. Barnea[159], B. M. Barnett[143], R. M. Barnett[18], Z. Barnovska-Blenessy[60a], A. Baroncelli[60a], G. Barone[29], A. J. Barr[134], L. Barranco Navarro[45a,45b],

F. Barreiro[99], J. Barreiro Guimarães da Costa[15a], U. Barron[160], S. Barsov[137], F. Bartels[61a], R. Bartoldus[152], G. Bartolini[102], A. E. Barton[90], P. Bartos[28a], A. Basalaev[46], A. Basan[100], A. Bassalat[65,ai], M. J. Basso[166], R. L. Bates[57], S. Batlamous[35e], J. R. Batley[32], B. Batool[150], M. Battaglia[145], M. Bauce[73a,73b], F. Bauer[144], K. T. Bauer[170], H. S. Bawa[31], A. Bayirli[12c], J. B. Beacham[49], T. Beau[135], P. H. Beauchemin[169], F. Becherer[52], P. Bechtle[24], H. C. Beck[53], H. P. Beck[20,p], K. Becker[177], C. Becot[46], A. Beddall[12d], A. J. Beddall[12a], V. A. Bednyakov[80], M. Bedognetti[120], C. P. Bee[154], T. A. Beermann[181], M. Begalli[81b], M. Begel[29], A. Behera[154], J. K. Behr[46], F. Beisiegel[24], M. Belfkir[5], A. S. Bell[95], G. Bella[160], L. Bellagamba[23b], A. Bellerive[34], P. Bellos[9], K. Beloborodov[122b,122a], K. Belotskiy[112], N. L. Belyaev[112], D. Benchekroun[35a], N. Benekos[10], Y. Benhammou[160], D. P. Benjamin[6], M. Benoit[54], J. R. Bensinger[26], S. Bentvelsen[120], L. Beresford[134], M. Beretta[51], D. Berge[19], E. Bergeaas Kuutmann[171], N. Berger[5], B. Bergmann[141], L. J. Bergsten[26], J. Beringer[18], S. Berlendis[7], G. Bernardi[135], C. Bernius[152], F. U. Bernlochner[24], T. Berry[94], P. Berta[100], C. Bertella[15a], A. Berthold[48], I. A. Bertram[90], O. Bessidskaia Bylund[181], N. Besson[144], A. Bethani[101], S. Bethke[115], A. Betti[42], A. J. Bevan[93], J. Beyer[115], D. S. Bhattacharya[176], P. Bhattarai[26], V. S. Bhopatkar[6], R. Bi[138], R. M. Bianchi[138], O. Biebel[114], D. Biedermann[19], R. Bielski[36], K. Bierwagen[100], N. V. Biesuz[72a,72b], M. Biglietti[75a], T. R. V. Billoud[110], M. Bindi[53], A. Bingul[12d], C. Bini[73a,73b], S. Biondi[23a,23b], C. J. Birch-sykes[101], M. Birman[179], T. Bisanz[53], J. P. Biswal[3], D. Biswas[180,i], A. Bitadze[101], C. Bittrich[48], K. Bjørke[133], T. Blazek[28a], I. Bloch[46], C. Blocker[26], A. Blue[57], U. Blumenschein[93], G. J. Bobbink[120], V. S. Bobrovnikov[122a,122b], S. S. Bocchetta[97], D. Boerner[46], D. Bogavac[14], A. G. Bogdanchikov[122a,122b], C. Bohm[45a], V. Boisvert[94], P. Bokan[53,171], T. Bold[84a], A. E. Bolz[61b], M. Bomben[135], M. Bona[93], J. S. Bonilla[131], M. Boonekamp[144], C. D. Booth[94], H. M. Borecka-Bielska[91], L. S. Borgna[95], A. Borisov[123], G. Borissov[90], J. Bortfeldt[36], D. Bortoletto[134], D. Boscherini[23b], M. Bosman[14], J. D. Bossio Sola[104], K. Bouaouda[35a], J. Boudreau[138], E. V. Bouhova-Thacker[90], D. Boumediene[38], S. K. Boutle[57], A. Boveia[127], J. Boyd[36], D. Boye[33c], I. R. Boyko[80], A. J. Bozson[94], J. Bracinik[21], N. Brahimi[60d], G. Brandt[181], O. Brandt[32], F. Braren[46], B. Brau[103], J. E. Brau[131], W. D. Breaden Madden[57], K. Brendlinger[46], L. Brenner[36], R. Brenner[171], S. Bressler[179], B. Brickwedde[100], D. L. Briglin[21], D. Britton[57], D. Britzger[115], I. Brock[24], R. Brock[107], G. Brooijmans[39], W. K. Brooks[146d], E. Brost[29], P. A. Bruckman de Renstrom[85], B. Brüers[46], D. Bruncko[28b], A. Bruni[23b], G. Bruni[23b], L. S. Bruni[120], S. Bruno[74a,74b], M. Bruschi[23b], N. Bruscino[73a,73b], L. Bryngemark[152], T. Buanes[17], Q. Buat[36], P. Buchholz[150], A. G. Buckley[57], I. A. Budagov[80], M. K. Bugge[133], F. Bührer[52], O. Bulekov[112], B. A. Bullard[59], T. J. Burch[121], S. Burdin[91], C. D. Burgard[120], A. M. Burger[129], B. Burghgrave[8], J. T. P. Burr[46], C. D. Burton[11], J. C. Burzynski[103], V. Büscher[100], E. Buschmann[53], P. J. Bussey[57], J. M. Butler[25], C. M. Buttar[57], J. M. Butterworth[95], P. Butti[36], W. Buttinger[36], C. J. Buxo Vazquez[107], A. Buzatu[157], A. R. Buzykaev[122a,122b], G. Cabras[23a,23b], S. Cabrera Urbán[173], D. Caforio[56], H. Cai[138], V. M. M. Cairo[152], O. Cakir[4a], N. Calace[36], P. Calafiura[18], G. Calderini[135], P. Calfayan[66], G. Callea[57], L. P. Caloba[81b], A. Caltabiano[74a,74b], S. Calvente Lopez[99], D. Calvet[38], S. Calvet[38], T. P. Calvet[102], M. Calvetti[72a,72b], R. Camacho Toro[135], S. Camarda[36], D. Camarero Munoz[99], P. Camarri[74a,74b], M. T. Camerlingo[75a,75b], D. Cameron[133], C. Camincher[36], S. Campana[36], M. Campanelli[95], A. Camplani[40], V. Canale[70a,70b], A. Canesse[104], M. Cano Bret[78], J. Cantero[129], T. Cao[160], Y. Cao[172], M. D. M. Capeans Garrido[36], M. Capua[41b,41a], R. Cardarelli[74a], F. Cardillo[148], G. Carducci[41a,41b], I. Carli[142], T. Carli[36], G. Carlino[70a], B. T. Carlson[138], E. M. Carlson[167a,175], L. Carminati[69a,69b], R. M. D. Carney[152], S. Caron[119], E. Carquin[146d], S. Carrá[46], G. Carratta[23a,23b], J. W. S. Carter[166], T. M. Carter[50], M. P. Casado[14,f], A. F. Casha[166], F. L. Castillo[173], L. Castillo Garcia[14], V. Castillo Gimenez[173], N. F. Castro[139a,139e], A. Catinaccio[36], J. R. Catmore[133], A. Cattai[36], V. Cavaliere[29], V. Cavasinni[72a,72b], E. Celebi[12b], F. Celli[134], K. Cerny[130], A. S. Cerqueira[81a], A. Cerri[155], L. Cerrito[74a,74b], F. Cerutti[18], A. Cervelli[23a,23b], S. A. Cetin[12b], Z. Chadi[35a], D. Chakraborty[121], J. Chan[180], W. S. Chan[120], W. Y. Chan[91], J. D. Chapman[32], B. Chargeishvili[158b], D. G. Charlton[21], T. P. Charman[93], C. C. Chau[34], S. Che[127], S. Chekanov[6], S. V. Chekulaev[167a], G. A. Chelkov[80,ag], B. Chen[79], C. Chen[60a], C. H. Chen[79], H. Chen[29], J. Chen[60a], J. Chen[39], J. Chen[26], S. Chen[136], S. J. Chen[15c], X. Chen[15b], Y. Chen[60a], Y-H. Chen[46], H. C. Cheng[63a], H. J. Cheng[15a], A. Cheplakov[80], E. Cheremushkina[123], R. Cherkaoui El Moursli[35e], E. Cheu[7], K. Cheung[64], T. J. A. Chevalérias[144], L. Chevalier[144], V. Chiarella[51], G. Chiarelli[72a], G. Chiodini[68a], A. S. Chisholm[21], A. Chitan[27b], I. Chiu[162], Y. H. Chiu[175], M. V. Chizhov[80], K. Choi[11], A. R. Chomont[73a,73b], Y. S. Chow[120], L. D. Christopher[33e], M. C. Chu[63a], X. Chu[15a,15d], J. Chudoba[140], J. J. Chwastowski[85], L. Chytka[130], D. Cieri[115], K. M. Ciesla[85], D. Cinca[47], V. Cindro[92], I. A. Cioară[27b], A. Ciocio[18],

F. Cirotto[70a,70b], Z. H. Citron[179,j], M. Citterio[69a], D. A. Ciubotaru[27b], B. M. Ciungu[166], A. Clark[54], M. R. Clark[39], P. J. Clark[50], S. E. Clawson[101], C. Clement[45a,45b], Y. Coadou[102], M. Cobal[67a,67c], A. Coccaro[55b], J. Cochran[79], R. Coelho Lopes De Sa[103], H. Cohen[160], A. E. C. Coimbra[36], B. Cole[39], A. P. Colijn[120], J. Collot[58], P. Conde Muiño[139a,139h], S. H. Connell[33c], I. A. Connelly[57], S. Constantinescu[27b], F. Conventi[70a,am], A. M. Cooper-Sarkar[134], F. Cormier[174], K. J. R. Cormier[166], L. D. Corpe[95], M. Corradi[73a,73b], E. E. Corrigan[97], F. Corriveau[104,ab], M. J. Costa[173], F. Costanza[5], D. Costanzo[148], G. Cowan[94], J. W. Cowley[32], J. Crane[101], K. Cranmer[125], R. A. Creager[136], S. Crépé-Renaudin[58], F. Crescioli[135], M. Cristinziani[24], V. Croft[169], G. Crosetti[41a,41b], A. Cueto[5], T. Cuhadar Donszelmann[170], H. Cui[15a,15d], A. R. Cukierman[152], W. R. Cunningham[57], S. Czekierda[85], P. Czodrowski[36], M. M. Czurylo[61b], M. J. Da Cunha Sargedas De Sousa[60b], J. V. Da Fonseca Pinto[81b], C. Da Via[101], W. Dabrowski[84a], F. Dachs[36], T. Dado[47], S. Dahbi[33e], T. Dai[106], C. Dallapiccola[103], M. Dam[40], G. D'amen[29], V. D'Amico[75a,75b], J. Damp[100], J. R. Dandoy[136], M. F. Daneri[30], M. Danninger[151], V. Dao[36], G. Darbo[55b], O. Dartsi[5], A. Dattagupta[131], T. Daubney[46], S. D'Auria[69a,69b], C. David[167b], T. Davidek[142], D. R. Davis[49], I. Dawson[148], K. De[8], R. De Asmundis[70a], M. De Beurs[120], S. De Castro[23a,23b], N. De Groot[119], P. de Jong[120], H. De la Torre[107], A. De Maria[15c], D. De Pedis[73a], A. De Salvo[73a], U. De Sanctis[74a,74b], M. De Santis[74a,74b], A. De Santo[155], J. B. De Vivie De Regie[65], C. Debenedetti[145], D. V. Dedovich[80], A. M. Deiana[42], J. Del Peso[99], Y. Delabat Diaz[46], D. Delgove[65], F. Deliot[144], C. M. Delitzsch[7], M. Della Pietra[70a,70b], D. Della Volpe[54], A. Dell'Acqua[36], L. Dell'Asta[74a,74b], M. Delmastro[5], C. Delporte[65], P. A. Delsart[58], D. A. DeMarco[166], S. Demers[182], M. Demichev[80], G. Demontigny[110], S. P. Denisov[123], L. D'Eramo[121], D. Derendarz[85], J. E. Derkaoui[35d], F. Derue[135], P. Dervan[91], K. Desch[24], K. Dette[166], C. Deutsch[24], M. R. Devesa[30], P. O. Deviveiros[36], F. A. Di Bello[73a,73b], A. Di Ciaccio[74a,74b], L. Di Ciaccio[5], W. K. Di Clemente[136], C. Di Donato[70a,70b], A. Di Girolamo[36], G. Di Gregorio[72a,72b], B. Di Micco[75a,75b], R. Di Nardo[75a,75b], K. F. Di Petrillo[59], R. Di Sipio[166], C. Diaconu[102], F. A. Dias[40], T. Dias Do Vale[139a], M. A. Diaz[146a], F. G. Diaz Capriles[24], J. Dickinson[18], M. Didenko[165], E. B. Diehl[106], J. Dietrich[19], S. Díez Cornell[46], A. Dimitrievska[18], W. Ding[15b], J. Dingfelder[24], S. J. Dittmeier[61b], F. Dittus[36], F. Djama[102], T. Djobava[158b], J. I. Djuvsland[17], M. A. B. Do Vale[81c], M. Dobre[27b], D. Dodsworth[26], C. Doglioni[97], J. Dolejsi[142], Z. Dolezal[142], M. Donadelli[81d], B. Dong[60c], J. Donini[38], A. D'onofrio[15c], M. D'Onofrio[91], J. Dopke[143], A. Doria[70a], M. T. Dova[89], A. T. Doyle[57], E. Drechsler[151], E. Dreyer[151], T. Dreyer[53], A. S. Drobac[169], D. Du[60b], T. A. du Pree[120], Y. Duan[60d], F. Dubinin[111], M. Dubovsky[28a], A. Dubreuil[54], E. Duchovni[179], G. Duckeck[114], O. A. Ducu[36], D. Duda[115], A. Dudarev[36], A. C. Dudder[100], E. M. Duffield[18], M. D'uffizi[101], L. Duflot[65], M. Dührssen[36], C. Dülsen[181], M. Dumancic[179], A. E. Dumitriu[27b], M. Dunford[61a], A. Duperrin[102], H. Duran Yildiz[4a], M. Düren[56], A. Durglishvili[158b], D. Duschinger[48], B. Dutta[46], D. Duvnjak[1], G. I. Dyckes[136], M. Dyndal[36], S. Dysch[101], B. S. Dziedzic[85], M. G. Eggleston[49], T. Eifert[8], G. Eigen[17], K. Einsweiler[18], T. Ekelof[171], H. El Jarrari[35e], V. Ellajosyula[171], M. Ellert[171], F. Ellinghaus[181], A. A. Elliot[93], N. Ellis[36], J. Elmsheuser[29], M. Elsing[36], D. Emeliyanov[143], A. Emerman[39], Y. Enari[162], M. B. Epland[49], J. Erdmann[47], A. Ereditato[20], P. A. Erland[85], M. Errenst[36], M. Escalier[65], C. Escobar[173], O. Estrada Pastor[173], E. Etzion[160], H. Evans[66], M. O. Evans[155], A. Ezhilov[137], F. Fabbri[57], L. Fabbri[23b,23a], V. Fabiani[119], G. Facini[177], R. M. Faisca Rodrigues Pereira[139a], R. M. Fakhrutdinov[123], S. Falciano[73a], P. J. Falke[24], S. Falke[36], J. Faltova[142], Y. Fang[15a], Y. Fang[15a], G. Fanourakis[44], M. Fanti[69a,69b], M. Faraj[67a,67c,q], A. Farbin[8], A. Farilla[75a], E. M. Farina[71a,71b], T. Farooque[107], S. M. Farrington[50], P. Farthouat[36], F. Fassi[35e], P. Fassnacht[36], D. Fassouliotis[9], M. Faucci Giannelli[50], W. J. Fawcett[32], L. Fayard[65], O. L. Fedin[137,o], W. Fedorko[174], A. Fehr[20], M. Feickert[172], L. Feligioni[102], A. Fell[148], C. Feng[60b], M. Feng[49], M. J. Fenton[170], A. B. Fenyuk[123], S. W. Ferguson[43], J. Ferrando[46], A. Ferrante[172], A. Ferrari[171], P. Ferrari[120], R. Ferrari[71a], D. E. Ferreira de Lima[61b], A. Ferrer[173], D. Ferrere[54], C. Ferretti[106], F. Fiedler[100], A. Filipčič[92], F. Filthaut[119], K. D. Finelli[25], M. C. N. Fiolhais[139a,139c,a], L. Fiorini[173], F. Fischer[114], J. Fischer[100], W. C. Fisher[107], T. Fitschen[21], I. Fleck[150], P. Fleischmann[106], T. Flick[181], B. M. Flierl[114], L. Flores[136], L. R. Flores Castillo[63a], F. M. Follega[76a,76b], N. Fomin[17], J. H. Foo[166], G. T. Forcolin[76a,76b], B. C. Forland[66], A. Formica[144], F. A. Förster[14], A. C. Forti[101], E. Fortin[102], M. G. Foti[134], D. Fournier[65], H. Fox[90], P. Francavilla[72a,72b], S. Francescato[73a,73b], M. Franchini[23a,23b], S. Franchino[61a], D. Francis[36], L. Franco[5], L. Franconi[20], M. Franklin[59], G. Frattari[73a,73b], A. N. Fray[93], P. M. Freeman[21], B. Freund[110], W. S. Freund[81b], E. M. Freundlich[47], D. C. Frizzell[128], D. Froidevaux[36], J. A. Frost[134], M. Fujimoto[126], C. Fukunaga[163], E. Fullana Torregrosa[173], T. Fusayasu[116], J. Fuster[173], A. Gabrielli[23b,23a], A. Gabrielli[36], S. Gadatsch[54], P. Gadow[115], G. Gagliardi[55b,55a], L. G. Gagnon[110], G. E. Gallardo[134],

E. J. Gallas[134], B. J. Gallop[143], G. Galster[40], R. Gamboa Goni[93], K. K. Gan[127], S. Ganguly[179], J. Gao[60a], Y. Gao[50], Y. S. Gao[31,l], F. M. Garay Walls[146a], C. García[173], J. E. García Navarro[173], J. A. García Pascual[15a], C. Garcia-Argos[52], M. Garcia-Sciveres[18], R. W. Gardner[37], N. Garelli[152], S. Gargiulo[52], C. A. Garner[166], V. Garonne[133], S. J. Gasiorowski[147], P. Gaspar[81b], A. Gaudiello[55a,55b], G. Gaudio[71a], I. L. Gavrilenko[111], A. Gavrilyuk[124], C. Gay[174], G. Gaycken[46], E. N. Gazis[10], A. A. Geanta[27b], C. M. Gee[145], C. N. P. Gee[143], J. Geisen[97], M. Geisen[100], C. Gemme[55b], M. H. Genest[58], C. Geng[106], S. Gentile[73a,73b], S. George[94], T. Geralis[44], L. O. Gerlach[53], P. Gessinger-Befurt[100], G. Gessner[47], S. Ghasemi[150], M. Ghasemi Bostanabad[175], M. Ghneimat[150], A. Ghosh[65], A. Ghosh[78], B. Giacobbe[23b], S. Giagu[73a,73b], N. Giangiacomi[23a,23b], P. Giannetti[72a], A. Giannini[70a,70b], G. Giannini[14], S. M. Gibson[94], M. Gignac[145], D. T. Gil[84b], D. Gillberg[34], G. Gilles[181], D. M. Gingrich[3,al], M. P. Giordani[67a,67c], P. F. Giraud[144], G. Giugliarelli[67a,67c], D. Giugni[69a], F. Giuli[74a,74b], S. Gkaitatzis[161], I. Gkialas[9,g], E. L. Gkougkousis[14], P. Gkountoumis[10], L. K. Gladilin[113], C. Glasman[99], J. Glatzer[14], P. C. F. Glaysher[46], A. Glazov[46], G. R. Gledhill[131], I. Gnesi[41b,b], M. Goblirsch-Kolb[26], D. Godin[110], S. Goldfarb[105], T. Golling[54], D. Golubkov[123], A. Gomes[139a,139b], R. Goncalves Gama[53], R. Gonçalo[139a,139c], G. Gonella[131], L. Gonella[21], A. Gongadze[80], F. Gonnella[21], J. L. Gonski[39], S. González de la Hoz[173], S. Gonzalez Fernandez[14], R. Gonzalez Lopez[91], C. Gonzalez Renteria[18], R. Gonzalez Suarez[171], S. Gonzalez-Sevilla[54], G. R. Gonzalvo Rodriguez[173], L. Goossens[36], N. A. Gorasia[21], P. A. Gorbounov[124], H. A. Gordon[29], B. Gorini[36], E. Gorini[68a,68b], A. Gorišek[92], A. T. Goshaw[49], M. I. Gostkin[80], C. A. Gottardo[119], M. Gouighri[35b], A. G. Goussiou[147], N. Govender[33c], C. Goy[5], I. Grabowska-Bold[84a], E. C. Graham[91], J. Gramling[170], E. Gramstad[133], S. Grancagnolo[19], M. Grandi[155], V. Gratchev[137], P. M. Gravila[27f], F. G. Gravili[68a,68b], C. Gray[57], H. M. Gray[18], C. Grefe[24], K. Gregersen[97], I. M. Gregor[46], P. Grenier[152], K. Grevtsov[46], C. Grieco[14], N. A. Grieser[128], A. A. Grillo[145], K. Grimm[31,k], S. Grinstein[14,w], J.-F. Grivaz[65], S. Groh[100], E. Gross[179], J. Grosse-Knetter[53], Z. J. Grout[95], C. Grud[106], A. Grummer[118], J. C. Grundy[134], L. Guan[106], W. Guan[180], C. Gubbels[174], J. Guenther[36], A. Guerguichon[65], J. G. R. Guerrero Rojas[173], F. Guescini[115], D. Guest[170], R. Gugel[100], T. Guillemin[5], S. Guindon[36], U. Gul[57], J. Guo[60c], W. Guo[106], Y. Guo[60a], Z. Guo[102], R. Gupta[46], S. Gurbuz[12c], G. Gustavino[128], M. Guth[52], P. Gutierrez[128], C. Gutschow[95], C. Guyot[144], C. Gwenlan[134], C. B. Gwilliam[91], E. S. Haaland[133], A. Haas[125], C. Haber[18], H. K. Hadavand[8], A. Hadef[60a], M. Haleem[176], J. Haley[129], J. J. Hall[148], G. Halladjian[107], G. D. Hallewell[102], K. Hamano[175], H. Hamdaoui[35e], M. Hamer[24], G. N. Hamity[50], K. Han[60a,v], L. Han[60a], S. Han[18], Y. F. Han[166], K. Hanagaki[82,t], M. Hance[145], D. M. Handl[114], M. D. Hank[37], R. Hankache[135], E. Hansen[97], J. B. Hansen[40], J. D. Hansen[40], M. C. Hansen[24], P. H. Hansen[40], E. C. Hanson[101], K. Hara[168], T. Harenberg[181], S. Harkusha[108], P. F. Harrison[177], N. M. Hartman[152], N. M. Hartmann[114], Y. Hasegawa[149], A. Hasib[50], S. Hassani[144], S. Haug[20], R. Hauser[107], L. B. Havener[39], M. Havranek[141], C. M. Hawkes[21], R. J. Hawkings[36], S. Hayashida[117], D. Hayden[107], C. Hayes[106], R. L. Hayes[174], C. P. Hays[134], J. M. Hays[93], H. S. Hayward[91], S. J. Haywood[143], F. He[60a], Y. He[164], M. P. Heath[50], V. Hedberg[97], S. Heer[24], A. L. Heggelund[133], C. Heidegger[52], K. K. Heidegger[52], W. D. Heidorn[79], J. Heilman[34], S. Heim[46], T. Heim[18], B. Heinemann[46,aj], J. J. Heinrich[131], L. Heinrich[36], J. Hejbal[140], L. Helary[46], A. Held[125], S. Hellesund[133], C. M. Helling[145], S. Hellman[45a,45b], C. Helsens[36], R. C. W. Henderson[90], Y. Heng[180], L. Henkelmann[32], A. M. Henriques Correia[36], H. Herde[26], Y. Hernández Jiménez[33e], H. Herr[100], M. G. Herrmann[114], T. Herrmann[48], G. Herten[52], R. Hertenberger[114], L. Hervas[36], T. C. Herwig[136], G. G. Hesketh[95], N. P. Hessey[167a], H. Hibi[83], A. Higashida[162], S. Higashino[82], E. Higón-Rodriguez[173], K. Hildebrand[37], J. C. Hill[32], K. K. Hill[29], K. H. Hiller[46], S. J. Hillier[21], M. Hils[48], I. Hinchliffe[18], F. Hinterkeuser[24], M. Hirose[132], S. Hirose[52], D. Hirschbuehl[181], B. Hiti[92], O. Hladik[140], D. R. Hlaluku[33e], J. Hobbs[154], N. Hod[179], M. C. Hodgkinson[148], A. Hoecker[36], D. Hohn[52], D. Hohov[65], T. Holm[24], T. R. Holmes[37], M. Holzbock[114], L. B. A. H. Hommels[32], T. M. Hong[138], J. C. Honig[52], A. Hönle[115], B. H. Hooberman[172], W. H. Hopkins[6], Y. Horii[117], P. Horn[48], L. A. Horyn[37], S. Hou[157], A. Hoummada[35a], J. Howarth[57], J. Hoya[89], M. Hrabovsky[130], J. Hrdinka[77], J. Hrivnac[65], A. Hrynevich[109], T. Hryn'ova[5], P. J. Hsu[64], S.-C. Hsu[147], Q. Hu[29], S. Hu[60c], Y. F. Hu[15a,15d,an], D. P. Huang[95], Y. Huang[60a], Y. Huang[15a], Z. Hubacek[141], F. Hubaut[102], M. Huebner[24], F. Huegging[24], T. B. Huffman[134], M. Huhtinen[36], R. Hulsken[58], R. F. H. Hunter[34], P. Huo[154], N. Huseynov[80,ac], J. Huston[107], J. Huth[59], R. Hyneman[106], S. Hyrych[28a], G. Iacobucci[54], G. Iakovidis[29], I. Ibragimov[150], L. Iconomidou-Fayard[65], P. Iengo[36], R. Ignazzi[40], O. Igonkina[120,y,*], R. Iguchi[162], T. Iizawa[54], Y. Ikegami[82], M. Ikeno[82], D. Iliadis[161], N. Ilic[119,166,ab], F. Iltzsche[48], H. Imam[35a], G. Introzzi[71a,71b], M. Iodice[75a], K. Iordanidou[167a], V. Ippolito[73a,73b], M. F. Isacson[171], M. Ishino[162], W. Islam[129], C. Issever[19,46], S. Istin[159], F. Ito[168], J. M. Iturbe Ponce[63a],

R. Iuppa[76a,76b], A. Ivina[179], H. Iwasaki[82], J. M. Izen[43], V. Izzo[70a], P. Jacka[140], P. Jackson[1], R. M. Jacobs[46], B. P. Jaeger[151], V. Jain[2], G. Jäkel[181], K. B. Jakobi[100], K. Jakobs[52], T. Jakoubek[179], J. Jamieson[57], K. W. Janas[84a], R. Jansky[54], M. Janus[53], P. A. Janus[84a], G. Jarlskog[97], A. E. Jaspan[91], N. Javadov[80,ac], T. Javůrek[36], M. Javurkova[103], F. Jeanneau[144], L. Jeanty[131], J. Jejelava[158a], P. Jenni[52,c], N. Jeong[46], S. Jézéquel[5], H. Ji[180], J. Jia[154], H. Jiang[79], Y. Jiang[60a], Z. Jiang[152], S. Jiggins[52], F. A. Jimenez Morales[38], J. Jimenez Pena[115], S. Jin[15c], A. Jinaru[27b], O. Jinnouchi[164], H. Jivan[33e], P. Johansson[148], K. A. Johns[7], C. A. Johnson[66], R. W. L. Jones[90], S. D. Jones[155], T. J. Jones[91], J. Jongmanns[61a], J. Jovicevic[36], X. Ju[18], J. J. Junggeburth[115], A. Juste Rozas[14,w], A. Kaczmarska[85], M. Kado[73a,73b], H. Kagan[127], M. Kagan[152], A. Kahn[39], C. Kahra[100], T. Kaji[178], E. Kajomovitz[159], C. W. Kalderon[29], A. Kaluza[100], A. Kamenshchikov[123], M. Kaneda[162], N. J. Kang[145], S. Kang[79], Y. Kano[117], J. Kanzaki[82], L. S. Kaplan[180], D. Kar[33e], K. Karava[134], M. J. Kareem[167b], I. Karkanias[161], S. N. Karpov[80], Z. M. Karpova[80], V. Kartvelishvili[90], A. N. Karyukhin[123], A. Kastanas[45a,45b], C. Kato[60c,60d], J. Katzy[46], K. Kawade[149], K. Kawagoe[88], T. Kawaguchi[117], T. Kawamoto[144], G. Kawamura[53], E. F. Kay[175], S. Kazakos[14], V. F. Kazanin[122b,122a], R. Keeler[175], R. Kehoe[42], J. S. Keller[34], E. Kellermann[97], D. Kelsey[155], J. J. Kempster[21], J. Kendrick[21], K. E. Kennedy[39], O. Kepka[140], S. Kersten[181], B. P. Kerševan[92], S. Ketabchi Haghighat[166], M. Khader[172], F. Khalil-Zada[13], M. Khandoga[144], A. Khanov[129], A. G. Kharlamov[122a,122b], T. Kharlamova[122a,122b], E. E. Khoda[174], A. Khodinov[165], T. J. Khoo[54], G. Khoriauli[176], E. Khramov[80], J. Khubua[158b], S. Kido[83], M. Kiehn[54], C. R. Kilby[94], E. Kim[164], Y. K. Kim[37], N. Kimura[95], A. Kirchhoff[53], D. Kirchmeier[48], J. Kirk[143], A. E. Kiryunin[115], T. Kishimoto[162], D. P. Kisliuk[166], V. Kitali[46], C. Kitsaki[10], O. Kivernyk[24], T. Klapdor-Kleingrothaus[52], M. Klassen[61a], C. Klein[34], M. H. Klein[106], M. Klein[91], U. Klein[91], K. Kleinknecht[100], P. Klimek[121], A. Klimentov[29], T. Klingl[24], T. Klioutchnikova[36], F. F. Klitzner[114], P. Kluit[120], S. Kluth[115], E. Kneringer[77], E. B. F. G. Knoops[102], A. Knue[52], D. Kobayashi[88], T. Kobayashi[162], M. Kobel[48], M. Kocian[152], T. Kodama[162], P. Kodys[142], D. M. Koeck[155], P. T. Koenig[24], T. Koffas[34], N. M. Köhler[36], M. Kolb[144], I. Koletsou[5], T. Komarek[130], T. Kondo[82], K. Köneke[52], A. X. Y. Kong[1], A. C. König[119], T. Kono[126], V. Konstantinides[95], N. Konstantinidis[95], B. Konya[97], R. Kopeliansky[66], S. Koperny[84a], K. Korcyl[85], K. Kordas[161], G. Koren[160], A. Korn[95], I. Korolkov[14], E. V. Korolkova[148], N. Korotkova[113], O. Kortner[115], S. Kortner[115], V. V. Kostyukhin[148,165], A. Kotsokechagia[65], A. Kotwal[49], A. Koulouris[10], A. Kourkoumeli-Charalampidi[71a,71b], C. Kourkoumelis[9], E. Kourlitis[6], V. Kouskoura[29], R. Kowalewski[175], W. Kozanecki[101], A. S. Kozhin[123], V. A. Kramarenko[113], G. Kramberger[92], D. Krasnopevtsev[60a], M. W. Krasny[135], A. Krasznahorkay[36], D. Krauss[115], J. A. Kremer[100], J. Kretzschmar[91], P. Krieger[166], F. Krieter[114], A. Krishnan[61b], K. Krizka[18], K. Kroeninger[47], H. Kroha[115], J. Kroll[140], J. Kroll[136], K. S. Krowpman[107], U. Kruchonak[80], H. Krüger[24], N. Krumnack[79], M. C. Kruse[49], J. A. Krzysiak[85], O. Kuchinskaia[165], S. Kuday[4b], J. T. Kuechler[46], S. Kuehn[36], T. Kuhl[46], V. Kukhtin[80], Y. Kulchitsky[108,ae], S. Kuleshov[146b], Y. P. Kulinich[172], M. Kuna[58], T. Kunigo[86], A. Kupco[140], T. Kupfer[47], O. Kuprash[52], H. Kurashige[83], L. L. Kurchaninov[167a], Y. A. Kurochkin[108], A. Kurova[112], M. G. Kurth[15a,15d], E. S. Kuwertz[36], M. Kuze[164], A. K. Kvam[147], J. Kvita[130], T. Kwan[104], F. La Ruffa[41a,41b], C. Lacasta[173], F. Lacava[73a,73b], D. P. J. Lack[101], H. Lacker[19], D. Lacour[135], E. Ladygin[80], R. Lafaye[5], B. Laforge[135], T. Lagouri[146b], S. Lai[53], I. K. Lakomiec[84a], J. E. Lambert[128], S. Lammers[66], W. Lampl[7], C. Lampoudis[161], E. Lançon[29], U. Landgraf[52], M. P. J. Landon[93], M. C. Lanfermann[54], V. S. Lang[52], J. C. Lange[53], R. J. Langenberg[103], A. J. Lankford[170], F. Lanni[29], K. Lantzsch[24], A. Lanza[71a], A. Lapertosa[55a,55b], S. Laplace[135], J. F. Laporte[144], T. Lari[69a], F. Lasagni Manghi[23a,23b], M. Lassnig[36], T. S. Lau[63a], A. Laudrain[65], A. Laurier[34], M. Lavorgna[70a,70b], S. D. Lawlor[94], M. Lazzaroni[69a,69b], B. Le[101], E. Le Guirriec[102], A. Lebedev[79], M. LeBlanc[7], T. LeCompte[6], F. Ledroit-Guillon[58], A. C. A. Lee[95], C. A. Lee[29], G. R. Lee[17], L. Lee[59], S. C. Lee[157], S. Lee[79], B. Lefebvre[167a], H. P. Lefebvre[94], M. Lefebvre[175], C. Leggett[18], K. Lehmann[151], N. Lehmann[20], G. Lehmann Miotto[36], W. A. Leight[46], A. Leisos[161,u], M. A. L. Leite[81d], C. E. Leitgeb[114], R. Leitner[142], D. Lellouch[179,*], K. J. C. Leney[42], T. Lenz[24], S. Leone[72a], C. Leonidopoulos[50], A. Leopold[135], C. Leroy[110], R. Les[107], C. G. Lester[32], M. Levchenko[137], J. Levêque[5], D. Levin[106], L. J. Levinson[179], D. J. Lewis[21], B. Li[15b], B. Li[106], C-Q. Li[60a], F. Li[60c], H. Li[60a], H. Li[60b], J. Li[60c], K. Li[147], L. Li[60c], M. Li[15a,15d], Q. Li[15a,15d], Q. Y. Li[60a], S. Li[60c,60d], X. Li[46], Y. Li[46], Z. Li[60b], Z. Li[134], Z. Li[104], Z. Liang[15a], M. Liberatore[46], B. Liberti[74a], A. Liblong[166], K. Lie[63c], S. Lim[29], C. Y. Lin[32], K. Lin[107], R. A. Linck[66], R. E. Lindley[7], J. H. Lindon[21], A. Linss[46], A. L. Lionti[54], E. Lipeles[136], A. Lipniacka[17], T. M. Liss[172,ak], A. Lister[174], J. D. Little[8], B. Liu[79], B. L. Liu[6], H. B. Liu[29], J. B. Liu[60a], J. K. K. Liu[37], K. Liu[60d], M. Liu[60a], P. Liu[15a], Y. Liu[46], Y. Liu[15a,15d], Y. L. Liu[106], Y. W. Liu[60a], M. Livan[71a,71b], A. Lleres[58], J. Llorente Merino[151],

S. L. Lloyd[93], C. Y. Lo[63b], E. M. Lobodzinska[46], P. Loch[7], S. Loffredo[74a,74b], T. Lohse[19], K. Lohwasser[148], M. Lokajicek[140], J. D. Long[172], R. E. Long[90], I. Longarini[73a,73b], L. Longo[36], K. A. Looper[127], I. Lopez Paz[101], A. Lopez Solis[148], J. Lorenz[114], N. Lorenzo Martinez[5], A. M. Lory[114], P. J. Lösel[114], A. Lösle[52], X. Lou[46], X. Lou[15a], A. Lounis[65], J. Love[6], P. A. Love[90], J. J. Lozano Bahilo[173], M. Lu[60a], Y. J. Lu[64], H. J. Lubatti[147], C. Luci[73a,73b], F. L. Lucio Alves[15c], A. Lucotte[58], F. Luehring[66], I. Luise[135], L. Luminari[73a], B. Lund-Jensen[153], M. S. Lutz[160], D. Lynn[29], H. Lyons[91], R. Lysak[140], E. Lytken[97], F. Lyu[15a], V. Lyubushkin[80], T. Lyubushkina[80], H. Ma[29], L. L. Ma[60b], Y. Ma[95], D. M. Mac Donell[175], G. Maccarrone[51], A. Macchiolo[115], C. M. Macdonald[148], J. C. Macdonald[148], J. Machado Miguens[136], D. Madaffari[173], R. Madar[38], W. F. Mader[48], M. Madugoda Ralalage Don[129], N. Madysa[48], J. Maeda[83], T. Maeno[29], M. Maerker[48], V. Magerl[52], N. Magini[79], J. Magro[67a,67c,q], D. J. Mahon[39], C. Maidantchik[81b], T. Maier[114], A. Maio[139a,139b,139d], K. Maj[84a], O. Majersky[28a], S. Majewski[131], Y. Makida[82], N. Makovec[65], B. Malaescu[135], Pa. Malecki[85], V. P. Maleev[137], F. Malek[58], D. Malito[41a,41b], U. Mallik[78], D. Malon[6], C. Malone[32], S. Maltezos[10], S. Malyukov[80], J. Mamuzic[173], G. Mancini[70a,70b], I. Mandić[92], L. Manhaes de Andrade Filho[81a], I. M. Maniatis[161], J. Manjarres Ramos[48], K. H. Mankinen[97], A. Mann[114], A. Manousos[77], B. Mansoulie[144], I. Manthos[161], S. Manzoni[120], A. Marantis[161], G. Marceca[30], L. Marchese[134], G. Marchiori[135], M. Marcisovsky[140], L. Marcoccia[74a,74b], C. Marcon[97], C. A. Marin Tobon[36], M. Marjanovic[128], Z. Marshall[18], M. U. F. Martensson[171], S. Marti-Garcia[173], C. B. Martin[127], T. A. Martin[177], V. J. Martin[50], B. Martin dit Latour[17], L. Martinelli[75a,75b], M. Martinez[14,w], P. Martinez Agullo[173], V. I. Martinez Outschoorn[103], S. Martin-Haugh[143], V. S. Martoiu[27b], A. C. Martyniuk[95], A. Marzin[36], S. R. Maschek[115], L. Masetti[100], T. Mashimo[162], R. Mashinistov[111], J. Masik[101], A. L. Maslennikov[122a,122b], L. Massa[23a,23b], P. Massarotti[70a,70b], P. Mastrandrea[72a,72b], A. Mastroberardino[41a,41b], T. Masubuchi[162], D. Matakias[29], A. Matic[114], N. Matsuzawa[162], P. Mättig[24], J. Maurer[27b], B. Maček[92], D. A. Maximov[122a,122b], R. Mazini[157], I. Maznas[161], S. M. Mazza[145], J. P. Mc Gowan[104], S. P. Mc Kee[106], T. G. McCarthy[115], W. P. McCormack[18], E. F. McDonald[105], J. A. Mcfayden[36], G. Mchedlidze[158b], M. A. McKay[42], K. D. McLean[175], S. J. McMahon[143], P. C. McNamara[105], C. J. McNicol[177], R. A. McPherson[175,ab], J. E. Mdhluli[33e], Z. A. Meadows[103], S. Meehan[36], T. Megy[38], S. Mehlhase[114], A. Mehta[91], B. Meirose[43], D. Melini[159], B. R. Mellado Garcia[33e], J. D. Mellenthin[53], M. Melo[28a], F. Meloni[46], A. Melzer[24], E. D. Mendes Gouveia[139a,139e], L. Meng[36], X. T. Meng[106], S. Menke[115], E. Meoni[41b,41a], S. Mergelmeyer[19], S. A. M. Merkt[138], C. Merlassino[134], P. Mermod[54], L. Merola[70a,70b], C. Meroni[69a], G. Merz[106], O. Meshkov[113,111], J. K. R. Meshreki[150], J. Metcalfe[6], A. S. Mete[6], C. Meyer[66], J-P. Meyer[144], M. Michetti[19], R. P. Middleton[143], L. Mijović[50], G. Mikenberg[179], M. Mikestikova[140], M. Mikuž[92], H. Mildner[148], A. Milic[166], C. D. Milke[42], D. W. Miller[37], A. Milov[179], D. A. Milstead[45a,45b], R. A. Mina[152], A. A. Minaenko[123], I. A. Minashvili[158b], A. I. Mincer[125], B. Mindur[84a], M. Mineev[80], Y. Minegishi[162], L. M. Mir[14], M. Mironova[134], A. Mirto[68a,68b], K. P. Mistry[136], T. Mitani[178], J. Mitrevski[114], V. A. Mitsou[173], M. Mittal[60c], O. Miu[166], A. Miucci[20], P. S. Miyagawa[93], A. Mizukami[82], J. U. Mjörnmark[97], T. Mkrtchyan[61a], M. Mlynarikova[142], T. Moa[45a,45b], S. Mobius[53], K. Mochizuki[110], P. Mogg[114], S. Mohapatra[39], R. Moles-Valls[24], K. Mönig[46], E. Monnier[102], A. Montalbano[151], J. Montejo Berlingen[36], M. Montella[95], F. Monticelli[89], S. Monzani[69a], N. Morange[65], D. Moreno[22a], M. Moreno Llácer[173], C. Moreno Martinez[14], P. Morettini[55b], M. Morgenstern[159], S. Morgenstern[48], D. Mori[151], M. Morii[59], M. Morinaga[178], V. Morisbak[133], A. K. Morley[36], G. Mornacchi[36], A. P. Morris[95], L. Morvaj[154], P. Moschovakos[36], B. Moser[120], M. Mosidze[158b], T. Moskalets[144], H. J. Moss[148], J. Moss[31,m], E. J. W. Moyse[103], S. Muanza[102], J. Mueller[138], R. S. P. Mueller[114], D. Muenstermann[90], G. A. Mullier[97], D. P. Mungo[69a,69b], J. L. Munoz Martinez[14], F. J. Munoz Sanchez[101], P. Murin[28b], W. J. Murray[177,143], A. Murrone[69a,69b], J. M. Muse[128], M. Muškinja[18], C. Mwewa[33a], A. G. Myagkov[123,ag], A. A. Myers[138], J. Myers[131], M. Myska[141], B. P. Nachman[18], O. Nackenhorst[47], A.Nag Nag[48], K. Nagai[134], K. Nagano[82], Y. Nagasaka[62], J. L. Nagle[29], E. Nagy[102], A. M. Nairz[36], Y. Nakahama[117], K. Nakamura[82], T. Nakamura[162], H. Nanjo[132], F. Napolitano[61a], R. F. Naranjo Garcia[46], R. Narayan[42], I. Naryshkin[137], T. Naumann[46], G. Navarro[22a], P. Y. Nechaeva[111], F. Nechansky[46], T. J. Neep[21], A. Negri[71a,71b], M. Negrini[23b], C. Nellist[119], C. Nelson[104], M. E. Nelson[45a,45b], S. Nemecek[140], M. Nessi[36,e], M. S. Neubauer[172], F. Neuhaus[100], M. Neumann[181], R. Newhouse[174], P. R. Newman[21], C. W. Ng[138], Y. S. Ng[19], Y. W. Y. Ng[170], B. Ngair[35e], H. D. N. Nguyen[102], T. Nguyen Manh[110], E. Nibigira[38], R. B. Nickerson[134], R. Nicolaidou[144], D. S. Nielsen[40], J. Nielsen[145], M. Niemeyer[53], N. Nikiforou[11], V. Nikolaenko[123,ag], I. Nikolic-Audit[135], K. Nikolopoulos[21], P. Nilsson[29], H. R. Nindhito[54], Y. Ninomiya[82], A. Nisati[73a], N. Nishu[60c], R. Nisius[115],

I. Nitsche[47], T. Nitta[178], T. Nobe[162], D. L. Noel[32], Y. Noguchi[86], I. Nomidis[135], M. A. Nomura[29], M. Nordberg[36], J. Novak[92], T. Novak[92], O. Novgorodova[48], R. Novotny[141], L. Nozka[130], K. Ntekas[170], E. Nurse[95], F. G. Oakham[34,al], H. Oberlack[115], J. Ocariz[135], A. Ochi[83], I. Ochoa[39], J. P. Ochoa-Ricoux[146a], K. O'Connor[26], S. Oda[88], S. Odaka[82], S. Oerdek[53], A. Ogrodnik[84a], A. Oh[101], S. H. Oh[49], C. C. Ohm[153], H. Oide[164], M. L. Ojeda[166], H. Okawa[168], Y. Okazaki[86], M. W. O'Keefe[91], Y. Okumura[162], T. Okuyama[82], A. Olariu[27b], L. F. Oleiro Seabra[139a], S. A. Olivares Pino[146a], D. Oliveira Damazio[29], J. L. Oliver[1], M. J. R. Olsson[170], A. Olszewski[85], J. Olszowska[85], O. Öncel[24], D. C. O'Neil[151], A. P. O'neill[134], A. Onofre[139a,139e], P. U. E. Onyisi[11], H. Oppen[133], R. G. Oreamuno Madriz[121], M. J. Oreglia[37], G. E. Orellana[89], D. Orestano[75a,75b], N. Orlando[14], R. S. Orr[166], V. O'Shea[57], R. Ospanov[60a], G. Otero y Garzon[30], H. Otono[88], P. S. Ott[61a], G. J. Ottino[18], M. Ouchrif[35d], J. Ouellette[29], F. Ould-Saada[133], A. Ouraou[144], Q. Ouyang[15a], M. Owen[57], R. E. Owen[143], V. E. Ozcan[12c], N. Ozturk[8], J. Pacalt[130], H. A. Pacey[32], K. Pachal[49], A. Pacheco Pages[14], C. Padilla Aranda[14], S. Pagan Griso[18], G. Palacino[66], S. Palazzo[50], S. Palestini[36], M. Palka[84b], P. Palni[84a], C. E. Pandini[54], J. G. Panduro Vazquez[94], P. Pani[46], G. Panizzo[67a,67c], L. Paolozzi[54], C. Papadatos[110], K. Papageorgiou[9,g], S. Parajuli[42], A. Paramonov[6], C. Paraskevopoulos[10], D. Paredes Hernandez[63b], S. R. Paredes Saenz[134], B. Parida[179], T. H. Park[166], A. J. Parker[31], M. A. Parker[32], F. Parodi[55b,55a], E. W. Parrish[121], J. A. Parsons[39], U. Parzefall[52], L. Pascual Dominguez[135], V. R. Pascuzzi[18], J. M. P. Pasner[145], F. Pasquali[120], E. Pasqualucci[73a], S. Passaggio[55b], F. Pastore[94], P. Pasuwan[45a,45b], S. Pataraia[100], J. R. Pater[101], A. Pathak[180,i], J. Patton[91], T. Pauly[36], J. Pearkes[152], B. Pearson[115], M. Pedersen[133], L. Pedraza Diaz[119], R. Pedro[139a], T. Peiffer[53], S. V. Peleganchuk[122a,122b], O. Penc[140], H. Peng[60a], B. S. Peralva[81a], M. M. Perego[65], A. P. Pereira Peixoto[139a], L. Pereira Sanchez[45a,45b], D. V. Perepelitsa[29], E. Perez Codina[167a], F. Peri[19], L. Perini[69a,69b], H. Pernegger[36], S. Perrella[36], A. Perrevoort[120], K. Peters[46], R. F. Y. Peters[101], B. A. Petersen[36], T. C. Petersen[40], E. Petit[102], V. Petousis[141], A. Petridis[1], C. Petridou[161], P. Petroff[65], F. Petrucci[75a,75b], M. Pettee[182], N. E. Pettersson[103], K. Petukhova[142], A. Peyaud[144], R. Pezoa[146d], L. Pezzotti[71a,71b], T. Pham[105], F. H. Phillips[107], P. W. Phillips[143], M. W. Phipps[172], G. Piacquadio[154], E. Pianori[18], A. Picazio[103], R. H. Pickles[101], R. Piegaia[30], D. Pietreanu[27b], J. E. Pilcher[37], A. D. Pilkington[101], M. Pinamonti[67a,67c], J. L. Pinfold[3], C. Pitman Donaldson[95], M. Pitt[160], L. Pizzimento[74a,74b], M.-A. Pleier[29], V. Pleskot[142], E. Plotnikova[80], P. Podberezko[122a,122b], R. Poettgen[97], R. Poggi[54], L. Poggioli[135], I. Pogrebnyak[107], D. Pohl[24], I. Pokharel[53], G. Polesello[71a], A. Poley[151,167a], A. Policicchio[73a,73b], R. Polifka[142], A. Polini[23b], C. S. Pollard[46], V. Polychronakos[29], D. Ponomarenko[112], L. Pontecorvo[36], S. Popa[27a], G. A. Popeneciu[27d], L. Portales[5], D. M. Portillo Quintero[58], S. Pospisil[141], K. Potamianos[46], I. N. Potrap[80], C. J. Potter[32], H. Potti[11], T. Poulsen[97], J. Poveda[173], T. D. Powell[148], G. Pownall[46], M. E. Pozo Astigarraga[36], P. Pralavorio[102], S. Prell[79], D. Price[101], M. Primavera[68a], M. L. Proffitt[147], N. Proklova[112], K. Prokofiev[63c], F. Prokoshin[80], S. Protopopescu[29], J. Proudfoot[6], M. Przybycien[84a], D. Pudzha[137], A. Puri[172], P. Puzo[65], D. Pyatiizbyantseva[112], J. Qian[106], Y. Qin[101], A. Quadt[53], M. Queitsch-Maitland[36], A. Qureshi[1], M. Racko[28a], F. Ragusa[69a,69b], G. Rahal[98], J. A. Raine[54], S. Rajagopalan[29], A. Ramirez Morales[93], K. Ran[15a,15d], D. M. Rauch[46], F. Rauscher[114], S. Rave[100], B. Ravina[148], I. Ravinovich[179], J. H. Rawling[101], M. Raymond[36], A. L. Read[133], N. P. Readioff[58], M. Reale[68a,68b], D. M. Rebuzzi[71a,71b], G. Redlinger[29], K. Reeves[43], J. Reichert[136], D. Reikher[160], A. Reiss[100], A. Rej[150], C. Rembser[36], A. Renardi[46], M. Renda[27b], M. B. Rendel[115], S. Resconi[69a], E. D. Resseguie[18], S. Rettie[95], B. Reynolds[127], E. Reynolds[21], O. L. Rezanova[122a,122b], P. Reznicek[142], E. Ricci[76a,76b], R. Richter[115], S. Richter[46], E. Richter-Was[84b], M. Ridel[135], P. Rieck[115], O. Rifki[46], M. Rijssenbeek[154], A. Rimoldi[71a,71b], M. Rimoldi[46], L. Rinaldi[23b], T. T. Rinn[172], G. Ripellino[153], I. Riu[14], P. Rivadeneira[46], J. C. Rivera Vergara[175], F. Rizatdinova[129], E. Rizvi[93], C. Rizzi[36], S. H. Robertson[104,ab], M. Robin[46], D. Robinson[32], C. M. Robles Gajardo[146d], M. Robles Manzano[100], A. Robson[57], A. Rocchi[74a,74b], E. Rocco[100], C. Roda[72a,72b], S. Rodriguez Bosca[173], A. M. Rodríguez Vera[167b], S. Roe[36], J. Roggel[181], O. Røhne[133], R. Röhrig[115], R. A. Rojas[146d], B. Roland[52], C. P. A. Roland[66], J. Roloff[29], A. Romaniouk[112], M. Romano[23a,23b], N. Rompotis[91], M. Ronzani[125], L. Roos[135], S. Rosati[73a], G. Rosin[103], B. J. Rosser[136], E. Rossi[46], E. Rossi[75a,75b], E. Rossi[70a,70b], L. P. Rossi[55b], L. Rossini[69a,69b], R. Rosten[14], M. Rotaru[27b], B. Rottler[52], D. Rousseau[65], G. Rovelli[71a,71b], A. Roy[11], D. Roy[33e], A. Rozanov[102], Y. Rozen[159], X. Ruan[33e], F. Rühr[52], A. Ruiz-Martinez[173], A. Rummler[36], Z. Rurikova[52], N. A. Rusakovich[80], H. L. Russell[104], L. Rustige[38,47], J. P. Rutherfoord[7], E. M. Rüttinger[148], M. Rybar[39], G. Rybkin[65], E. B. Rye[133], A. Ryzhov[123], J. A. Sabater Iglesias[46], P. Sabatini[53], L. Sabetta[73a,73b], S. Sacerdoti[65],

H.F-W. Sadrozinski[145], R. Sadykov[80], F. Safai Tehrani[73a], B. Safarzadeh Samani[155], M. Safdari[152], P. Saha[121], S. Saha[104], M. Sahinsoy[115], A. Sahu[181], M. Saimpert[36], M. Saito[162], T. Saito[162], H. Sakamoto[162], D. Salamani[54], G. Salamanna[75a,75b], A. Salnikov[152], J. Salt[173], A. Salvador Salas[14], D. Salvatore[41a,41b], F. Salvatore[155], A. Salvucci[63a,63b,63c], A. Salzburger[36], J. Samarati[36], D. Sammel[52], D. Sampsonidis[161], D. Sampsonidou[161], J. Sánchez[173], A. Sanchez Pineda[36,67a,67c], H. Sandaker[133], C. O. Sander[46], I. G. Sanderswood[90], M. Sandhoff[181], C. Sandoval[22a], D. P. C. Sankey[143], M. Sannino[55a,55b], Y. Sano[117], A. Sansoni[51], C. Santoni[38], H. Santos[139a,139b], S. N. Santpur[18], A. Santra[173], K. A. Saoucha[148], A. Sapronov[80], J. G. Saraiva[139a,139d], O. Sasaki[82], K. Sato[168], F. Sauerburger[52], E. Sauvan[5], P. Savard[166,al], R. Sawada[162], C. Sawyer[143], L. Sawyer[96,af], I. Sayago Galvan[173], C. Sbarra[23b], A. Sbrizzi[67a,67c], T. Scanlon[95], J. Schaarschmidt[147], P. Schacht[115], D. Schaefer[37], L. Schaefer[136], S. Schaepe[36], U. Schäfer[100], A. C. Schaffer[65], D. Schaile[114], R. D. Schamberger[154], E. Schanet[114], N. Scharmberg[101], V. A. Schegelsky[137], D. Scheirich[142], F. Schenck[19], M. Schernau[170], C. Schiavi[55b,55a], L. K. Schildgen[24], Z. M. Schillaci[26], E. J. Schioppa[68a,68b], M. Schioppa[41b,41a], K. E. Schleicher[52], S. Schlenker[36], K. R. Schmidt-Sommerfeld[115], K. Schmieden[36], C. Schmitt[100], S. Schmitt[46], J. C. Schmoeckel[46], L. Schoeffel[144], A. Schoening[61b], P. G. Scholer[52], E. Schopf[134], M. Schott[100], J. F. P. Schouwenberg[119], J. Schovancova[36], S. Schramm[54], F. Schroeder[181], A. Schulte[100], H-C. Schultz-Coulon[61a], M. Schumacher[52], B. A. Schumm[145], Ph. Schune[144], A. Schwartzman[152], T. A. Schwarz[106], Ph. Schwemling[144], R. Schwienhorst[107], A. Sciandra[145], G. Sciolla[26], M. Scornajenghi[41a,41b], F. Scuri[72a], F. Scutti[105], L. M. Scyboz[115], C. D. Sebastiani[91], P. Seema[19], S. C. Seidel[118], A. Seiden[145], B. D. Seidlitz[29], T. Seiss[37], C. Seitz[46], J. M. Seixas[81b], G. Sekhniaidze[70a], S. J. Sekula[42], N. Semprini-Cesari[23a,23b], S. Sen[49], C. Serfon[29], L. Serin[65], L. Serkin[67a,67b], M. Sessa[60a], H. Severini[128], S. Sevova[152], F. Sforza[55a,55b], A. Sfyrla[54], E. Shabalina[53], J. D. Shahinian[145], N. W. Shaikh[45a,45b], D. Shaked Renous[179], L. Y. Shan[15a], M. Shapiro[18], A. Sharma[134], A. S. Sharma[1], P. B. Shatalov[124], K. Shaw[155], S. M. Shaw[101], M. Shehade[179], Y. Shen[128], A. D. Sherman[25], P. Sherwood[95], L. Shi[95], S. Shimizu[82], C. O. Shimmin[182], Y. Shimogama[178], M. Shimojima[116], I. P. J. Shipsey[134], S. Shirabe[164], M. Shiyakova[80,z], J. Shlomi[179], A. Shmeleva[111], M. J. Shochet[37], J. Shojaii[105], D. R. Shope[128], S. Shrestha[127], E. M. Shrif[33e], E. Shulga[179], P. Sicho[140], A. M. Sickles[172], E. Sideras Haddad[33e], O. Sidiropoulou[36], A. Sidoti[23a,23b], F. Siegert[48], Dj. Sijacki[16], M. Jr. Silva[180], M. V. Silva Oliveira[36], S. B. Silverstein[45a], S. Simion[65], R. Simoniello[100], C. J. Simpson-allsop[21], S. Simsek[12b], P. Sinervo[166], V. Sinetckii[113], S. Singh[151], M. Sioli[23b,23a], I. Siral[131], S. Yu. Sivoklokov[113], J. Sjölin[45a,45b], A. Skaf[53], E. Skorda[97], P. Skubic[128], M. Slawinska[85], K. Sliwa[169], R. Slovak[142], V. Smakhtin[179], B. H. Smart[143], J. Smiesko[28b], N. Smirnov[112], S. Yu. Smirnov[112], Y. Smirnov[112], L. N. Smirnova[113,r], O. Smirnova[97], H. A. Smith[134], M. Smizanska[90], K. Smolek[141], A. Smykiewicz[85], A. A. Snesarev[111], H. L. Snoek[120], I. M. Snyder[131], S. Snyder[29], R. Sobie[175,ab], A. Soffer[160], A. Søgaard[50], F. Sohns[53], C. A. Solans Sanchez[36], E. Yu. Soldatov[112], U. Soldevila[173], A. A. Solodkov[123], A. Soloshenko[80], O. V. Solovyanov[123], V. Solovyev[137], P. Sommer[148], H. Son[169], W. Song[143], W. Y. Song[167b], A. Sopczak[141], A. L. Sopio[95], F. Sopkova[28b], S. Sottocornola[71a,71b], R. Soualah[67a,67c], A. M. Soukharev[122a,122b], D. South[46], S. Spagnolo[68a,68b], M. Spalla[115], M. Spangenberg[177], F. Spanò[94], D. Sperlich[52], T. M. Spieker[61a], G. Spigo[36], M. Spina[155], D. P. Spiteri[57], M. Spousta[142], A. Stabile[69a,69b], B. L. Stamas[121], R. Stamen[61a], M. Stamenkovic[120], E. Stanecka[85], B. Stanislaus[134], M. M. Stanitzki[46], M. Stankaityte[134], B. Stapf[120], E. A. Starchenko[123], G. H. Stark[145], J. Stark[58], P. Staroba[140], P. Starovoitov[61a], S. Stärz[104], R. Staszewski[85], G. Stavropoulos[44], M. Stegler[46], P. Steinberg[29], A. L. Steinhebel[131], B. Stelzer[151,167a], H. J. Stelzer[138], O. Stelzer-Chilton[167a], H. Stenzel[56], T. J. Stevenson[155], G. A. Stewart[36], M. C. Stockton[36], G. Stoicea[27b], M. Stolarski[139a], S. Stonjek[115], A. Straessner[48], J. Strandberg[153], S. Strandberg[45a,45b], M. Strauss[128], T. Strebler[102], P. Strizenec[28b], R. Ströhmer[176], D. M. Strom[131], R. Stroynowski[42], A. Strubig[50], S. A. Stucci[29], B. Stugu[17], J. Stupak[128], N. A. Styles[46], D. Su[152], W. Su[60c,147], S. Suchek[61a], V. V. Sulin[111], M. J. Sullivan[91], D. M. S. Sultan[54], S. Sultansoy[4c], T. Sumida[86], S. Sun[106], X. Sun[101], K. Suruliz[155], C. J. E. Suster[156], M. R. Sutton[155], S. Suzuki[82], M. Svatos[140], M. Swiatlowski[167a], S. P. Swift[2], T. Swirski[176], A. Sydorenko[100], I. Sykora[28a], M. Sykora[142], T. Sykora[142], D. Ta[100], K. Tackmann[46,x], J. Taenzer[160], A. Taffard[170], R. Tafirout[167a], R. Takashima[87], K. Takeda[83], T. Takeshita[149], E. P. Takeva[50], Y. Takubo[82], M. Talby[102], A. A. Talyshev[122b,122a], K. C. Tam[63b], N. M. Tamir[160], J. Tanaka[162], R. Tanaka[65], S. Tapia Araya[172], S. Tapprogge[100], A. Tarek Abouelfadl Mohamed[107], S. Tarem[159], K. Tariq[60b], G. Tarna[27b,d], G. F. Tartarelli[69a], P. Tas[142], M. Tasevsky[140], T. Tashiro[86], E. Tassi[41a,41b], A. Tavares Delgado[139a], Y. Tayalati[35e], A. J. Taylor[50], G. N. Taylor[105], W. Taylor[167b], H. Teagle[91], A. S. Tee[90],

R. Teixeira De Lima[152], P. Teixeira-Dias[94], H. Ten Kate[36], J. J. Teoh[120], S. Terada[82], K. Terashi[162], J. Terron[99], S. Terzo[14], M. Testa[51], R. J. Teuscher[166,ab], S. J. Thais[182], N. Themistokleous[50], T. Theveneaux-Pelzer[46], F. Thiele[40], D. W. Thomas[94], J. O. Thomas[42], J. P. Thomas[21], E. A. Thompson[46], P. D. Thompson[21], E. Thomson[136], E. J. Thorpe[93], R. E. Ticse Torres[53], V. O. Tikhomirov[111,ah], Yu. A. Tikhonov[122a,122b], S. Timoshenko[112], P. Tipton[182], S. Tisserant[102], K. Todome[23a,23b], S. Todorova-Nova[142], S. Todt[48], J. Tojo[88], S. Tokár[28a], K. Tokushuku[82], E. Tolley[127], R. Tombs[32], K. G. Tomiwa[33e], M. Tomoto[117], L. Tompkins[152], P. Tornambe[103], E. Torrence[131], H. Torres[48], E. Torró Pastor[147], C. Tosciri[134], J. Toth[102,aa], D. R. Tovey[148], A. Traeet[17], C. J. Treado[125], T. Trefzger[176], F. Tresoldi[155], A. Tricoli[29], I. M. Trigger[167a], S. Trincaz-Duvoid[135], D. A. Trischuk[174], W. Trischuk[166], B. Trocmé[58], A. Trofymov[65], C. Troncon[69a], F. Trovato[155], L. Truong[33c], M. Trzebinski[85], A. Trzupek[85], F. Tsai[46], J.C-L. Tseng[134], P. V. Tsiareshka[108,ae], A. Tsirigotis[161,u], V. Tsiskaridze[154], E. G. Tskhadadze[158a], M. Tsopoulou[161], I. I. Tsukerman[124], V. Tsulaia[18], S. Tsuno[82], D. Tsybychev[154], Y. Tu[63b], A. Tudorache[27b], V. Tudorache[27b], T. T. Tulbure[27a], A. N. Tuna[59], S. Turchikhin[80], D. Turgeman[179], I. Turk Cakir[4b,s], R. J. Turner[21], R. Turra[69a], P. M. Tuts[39], S. Tzamarias[161], E. Tzovara[100], K. Uchida[162], F. Ukegawa[168], G. Unal[36], M. Unal[11], A. Undrus[29], G. Unel[170], F. C. Ungaro[105], Y. Unno[82], K. Uno[162], J. Urban[28b], P. Urquijo[105], G. Usai[8], Z. Uysal[12d], V. Vacek[141], B. Vachon[104], K. O. H. Vadla[133], T. Vafeiadis[36], A. Vaidya[95], C. Valderanis[114], E. Valdes Santurio[45a,45b], M. Valente[54], S. Valentinetti[23a,23b], A. Valero[173], L. Valéry[46], R. A. Vallance[21], A. Vallier[36], J. A. Valls Ferrer[173], T. R. Van Daalen[14], P. Van Gemmeren[6], S. Van Stroud[95], I. Van Vulpen[120], M. Vanadia[74a,74b], W. Vandelli[36], M. Vandenbroucke[144], E. R. Vandewall[129], A. Vaniachine[165], D. Vannicola[73a,73b], R. Vari[73a], E. W. Varnes[7], C. Varni[55a,55b], T. Varol[157], D. Varouchas[65], K. E. Varvell[156], M. E. Vasile[27b], G. A. Vasquez[175], F. Vazeille[38], D. Vazquez Furelos[14], T. Vazquez Schroeder[36], J. Veatch[53], V. Vecchio[101], M. J. Veen[120], L. M. Veloce[166], F. Veloso[139a,139c], S. Veneziano[73a], A. Ventura[68a,68b], A. Verbytskyi[115], V. Vercesi[71a], M. Verducci[72a,72b], C. M. Vergel Infante[79], C. Vergis[24], W. Verkerke[120], A. T. Vermeulen[120], J. C. Vermeulen[120], C. Vernieri[152], M. C. Vetterli[151,al], N. Viaux Maira[146d], T. Vickey[148], O. E. Vickey Boeriu[148], G. H. A. Viehhauser[134], L. Vigani[61b], M. Villa[23a,23b], M. Villaplana Perez[3], E. M. Villhauer[50], E. Vilucchi[51], M. G. Vincter[34], G. S. Virdee[21], A. Vishwakarma[50], C. Vittori[23b,23a], I. Vivarelli[155], M. Vogel[181], P. Vokac[141], S. E. von Buddenbrock[33e], E. Von Toerne[24], V. Vorobel[142], K. Vorobev[112], M. Vos[173], J. H. Vossebeld[91], M. Vozak[101], N. Vranjes[16], M. Vranjes Milosavljevic[16], V. Vrba[141], M. Vreeswijk[120], R. Vuillermet[36], I. Vukotic[37], S. Wada[168], P. Wagner[24], W. Wagner[181], J. Wagner-Kuhr[114], S. Wahdan[181], H. Wahlberg[89], R. Wakasa[168], V. M. Walbrecht[115], J. Walder[90], R. Walker[114], S. D. Walker[94], W. Walkowiak[150], V. Wallangen[45a,45b], A. M. Wang[59], A. Z. Wang[180], C. Wang[60a], C. Wang[60c], F. Wang[180], H. Wang[18], H. Wang[3], J. Wang[63a], P. Wang[42], Q. Wang[128], R.-J. Wang[100], R. Wang[60a], R. Wang[6], S. M. Wang[157], W. T. Wang[60a], W. Wang[15c], W. X. Wang[60a], Y. Wang[60a], Z. Wang[106], C. Wanotayaroj[46], A. Warburton[104], C. P. Ward[32], D. R. Wardrope[95], N. Warrack[57], A. T. Watson[21], M. F. Watson[21], G. Watts[147], B. M. Waugh[95], A. F. Webb[11], C. Weber[29], M. S. Weber[20], S. A. Weber[34], S. M. Weber[61a], A. R. Weidberg[134], J. Weingarten[47], M. Weirich[100], C. Weiser[52], P. S. Wells[36], T. Wenaus[29], B. Wendland[47], T. Wengler[36], S. Wenig[36], N. Wermes[24], M. Wessels[61a], T. D. Weston[20], K. Whalen[131], N. L. Whallon[147], A. M. Wharton[90], A. S. White[106], A. White[8], M. J. White[1], D. Whiteson[170], B. W. Whitmore[90], W. Wiedenmann[180], C. Wiel[48], M. Wielers[143], N. Wieseotte[100], C. Wiglesworth[40], L. A. M. Wiik-Fuchs[52], H. G. Wilkens[36], L. J. Wilkins[94], H. H. Williams[136], S. Williams[32], S. Willocq[103], P. J. Windischhofer[134], I. Wingerter-Seez[5], E. Winkels[155], F. Winklmeier[131], B. T. Winter[52], M. Wittgen[152], M. Wobisch[96], A. Wolf[100], R. Wölker[134], J. Wollrath[52], M. W. Wolter[85], H. Wolters[139a,139c], V. W. S. Wong[174], N. L. Woods[145], S. D. Worm[46], B. K. Wosiek[85], K. W. Woźniak[85], K. Wraight[57], S. L. Wu[180], X. Wu[54], Y. Wu[60a], J. Wuerzinger[134], T. R. Wyatt[101], B. M. Wynne[50], S. Xella[40], L. Xia[177], J. Xiang[63c], X. Xiao[106], X. Xie[60a], I. Xiotidis[155], D. Xu[15a], H. Xu[60a], H. Xu[60a], L. Xu[29], T. Xu[144], W. Xu[106], Z. Xu[60b], Z. Xu[152], B. Yabsley[156], S. Yacoob[33a], K. Yajima[132], D. P. Yallup[95], N. Yamaguchi[88], Y. Yamaguchi[164], A. Yamamoto[82], M. Yamatani[162], T. Yamazaki[162], Y. Yamazaki[83], J. Yan[60c], Z. Yan[25], H. J. Yang[60c,60d], H. T. Yang[18], S. Yang[60a], T. Yang[63c], X. Yang[60b,58], Y. Yang[162], Z. Yang[60a], W-M. Yao[18], Y. C. Yap[46], Y. Yasu[82], E. Yatsenko[60c], H. Ye[15c], J. Ye[42], S. Ye[29], I. Yeletskikh[80], M. R. Yexley[90], E. Yigitbasi[25], P. Yin[39], K. Yorita[178], K. Yoshihara[79], C. J. S. Young[36], C. Young[152], J. Yu[79], R. Yuan[60b,h], X. Yue[61a], M. Zaazoua[35e], B. Zabinski[85], G. Zacharis[10], E. Zaffaroni[54], J. Zahreddine[135], A. M. Zaitsev[123,ag], T. Zakareishvili[158b], N. Zakharchuk[34], S. Zambito[36], D. Zanzi[36], D. R. Zaripovas[57], S. V. Zeißner[47], C. Zeitnitz[181], G. Zemaityte[134], J. C. Zeng[172], O. Zenin[123], T. Ženiš[28a], D. Zerwas[65], M. Zgubič[134],

B. Zhang[15c], D. F. Zhang[15b], G. Zhang[15b], J. Zhang[6], Kaili. Zhang[15a], L. Zhang[15c], L. Zhang[60a], M. Zhang[172], R. Zhang[180], S. Zhang[106], X. Zhang[60c], X. Zhang[60b], Y. Zhang[15a,15d], Z. Zhang[63a], Z. Zhang[65], P. Zhao[49], Z. Zhao[60a], A. Zhemchugov[80], Z. Zheng[106], D. Zhong[172], B. Zhou[106], C. Zhou[180], H. Zhou[7], M. S. Zhou[15a,15d], M. Zhou[154], N. Zhou[60c], Y. Zhou[7], C. G. Zhu[60b], C. Zhu[15a,15d], H. L. Zhu[60a], H. Zhu[15a], J. Zhu[106], Y. Zhu[60a], X. Zhuang[15a], K. Zhukov[111], V. Zhulanov[122a,122b], D. Zieminska[66], N. I. Zimine[80], S. Zimmermann[52], Z. Zinonos[115], M. Ziolkowski[150], L. Živković[16], G. Zobernig[180], A. Zoccoli[23a,23b], K. Zoch[53], T. G. Zorbas[148], R. Zou[37], L. Zwalinski[36]

[1] Department of Physics, University of Adelaide, Adelaide, Australia
[2] Physics Department, SUNY Albany, Albany, NY, USA
[3] Department of Physics, University of Alberta, Edmonton, AB, Canada
[4] [(a)]Department of Physics, Ankara University, Ankara, Turkey; [(b)]Application and Research Center for Advanced Studies, Istanbul Aydin University, Istanbul, Turkey; [(c)]Division of Physics, TOBB University of Economics and Technology, Ankara, Turkey
[5] LAPP, Université Grenoble Alpes, Université Savoie Mont Blanc, CNRS/IN2P3, Annecy, France
[6] High Energy Physics Division, Argonne National Laboratory, Argonne, IL, USA
[7] Department of Physics, University of Arizona, Tucson, AZ, USA
[8] Department of Physics, University of Texas at Arlington, Arlington, TX, USA
[9] Physics Department, National and Kapodistrian University of Athens, Athens, Greece
[10] Physics Department, National Technical University of Athens, Zografou, Greece
[11] Department of Physics, University of Texas at Austin, Austin, TX, USA
[12] [(a)]Bahcesehir University, Faculty of Engineering and Natural Sciences, Istanbul, Turkey; [(b)]Faculty of Engineering and Natural Sciences, Istanbul Bilgi University, Istanbul, Turkey; [(c)]Department of Physics, Bogazici University, Istanbul, Turkey; [(d)]Department of Physics Engineering, Gaziantep University, Gaziantep, Turkey
[13] Institute of Physics, Azerbaijan Academy of Sciences, Baku, Azerbaijan
[14] Institut de Física d'Altes Energies (IFAE), Barcelona Institute of Science and Technology, Barcelona, Spain
[15] [(a)]Institute of High Energy Physics, Chinese Academy of Sciences, Beijing, China; [(b)]Physics Department, Tsinghua University, Beijing, China; [(c)]Department of Physics, Nanjing University, Nanjing, China; [(d)]University of Chinese Academy of Science (UCAS), Beijing, China
[16] Institute of Physics, University of Belgrade, Belgrade, Serbia
[17] Department for Physics and Technology, University of Bergen, Bergen, Norway
[18] Physics Division, Lawrence Berkeley National Laboratory and University of California, Berkeley, CA, USA
[19] Institut für Physik, Humboldt Universität zu Berlin, Berlin, Germany
[20] Albert Einstein Center for Fundamental Physics and Laboratory for High Energy Physics, University of Bern, Bern, Switzerland
[21] School of Physics and Astronomy, University of Birmingham, Birmingham, UK
[22] [(a)]Facultad de Ciencias y Centro de Investigaciónes, Universidad Antonio Nariño, Bogotá, Colombia; [(b)]Departamento de Física, Universidad Nacional de Colombia,, Bogotá Colombia, Colombia
[23] [(a)]INFN Bologna and Universita' di Bologna, Dipartimento di Fisica, Italy; [(b)]INFN Sezione di Bologna, Bologna, Italy
[24] Physikalisches Institut, Universität Bonn, Bonn, Germany
[25] Department of Physics, Boston University, Boston, MA, USA
[26] Department of Physics, Brandeis University, Waltham, MA, USA
[27] [(a)]Transilvania University of Brasov, Brasov, Romania; [(b)]Horia Hulubei National Institute of Physics and Nuclear Engineering, Bucharest, Romania; [(c)]Department of Physics, Alexandru Ioan Cuza University of Iasi, Iasi, Romania; [(d)]National Institute for Research and Development of Isotopic and Molecular Technologies, Physics Department, Cluj-Napoca, Romania; [(d)]University Politehnica Bucharest, Bucharest, Romania; [(e)]West University in Timisoara, Timisoara, Romania
[28] [(a)]Faculty of Mathematics, Physics and Informatics, Comenius University, Bratislava, Slovak Republic; [(b)]Department of Subnuclear Physics, Institute of Experimental Physics of the Slovak Academy of Sciences, Kosice, Slovak Republic
[29] Physics Department, Brookhaven National Laboratory, Upton, NY, USA
[30] Departamento de Física, Universidad de Buenos Aires, Buenos Aires, Argentina
[31] California State University, CA, USA
[32] Cavendish Laboratory, University of Cambridge, Cambridge, UK

[33] [(a)]Department of Physics, University of Cape Town, Cape Town, South Africa; [(b)]iThemba Labs, Western Cape, South Africa; [(c)]Department of Mechanical Engineering Science, University of Johannesburg, Johannesburg, South Africa; [(d)]University of South Africa, Department of Physics, Pretoria, South Africa; [(e)]School of Physics, University of the Witwatersrand, Johannesburg, South Africa
[34] Department of Physics, Carleton University, Ottawa, ON, Canada
[35] [(a)]Faculté des Sciences Ain Chock, Réseau Universitaire de Physique des Hautes Energies - Université Hassan II, Casablanca, Morocco; [(b)]Faculté des Sciences, Université Ibn-Tofail, Kénitra, Morocco; [(c)]Faculté des Sciences Semlalia, Université Cadi Ayyad, LPHEA-Marrakech, Morocco; [(d)]Faculté des Sciences, Université Mohamed Premier and LPTPM, Oujda, Morocco; [(e)]Faculté des sciences, Université Mohammed V, Rabat, Morocco
[36] CERN, Geneva, Switzerland
[37] Enrico Fermi Institute, University of Chicago, Chicago, IL, USA
[38] LPC, Université Clermont Auvergne, CNRS/IN2P3, Clermont-Ferrand, France
[39] Nevis Laboratory, Columbia University, Irvington, NY, USA
[40] Niels Bohr Institute, University of Copenhagen, Copenhagen, Denmark
[41] [(a)]Dipartimento di Fisica, Università della Calabria, Rende, Italy; [(b)]Laboratori Nazionali di Frascati, INFN Gruppo Collegato di Cosenza, Cosenza, Italy
[42] Physics Department, Southern Methodist University, Dallas, TX, USA
[43] Physics Department, University of Texas at Dallas, Richardson, TX, USA
[44] National Centre for Scientific Research "Demokritos", Agia Paraskevi, Greece
[45] [(a)]Department of Physics, Stockholm University, Stockholm, Sweden; [(b)]Oskar Klein Centre, Stockholm, Sweden
[46] Deutsches Elektronen-Synchrotron DESY, Hamburg and Zeuthen, Germany
[47] Lehrstuhl für Experimentelle Physik IV, Technische Universität Dortmund, Dortmund, Germany
[48] Institut für Kern- und Teilchenphysik, Technische Universität Dresden, Dresden, Germany
[49] Department of Physics, Duke University, Durham, NC, USA
[50] SUPA, School of Physics and Astronomy, University of Edinburgh, Edinburgh, UK
[51] INFN e Laboratori Nazionali di Frascati, Frascati, Italy
[52] Physikalisches Institut, Albert-Ludwigs-Universität Freiburg, Freiburg, Germany
[53] II. Physikalisches Institut, Georg-August-Universität Göttingen, Göttingen, Germany
[54] Département de Physique Nucléaire et Corpusculaire, Université de Genève, Genève, Switzerland
[55] [(a)]Dipartimento di Fisica, Università di Genova, Genova, Italy; [(b)]INFN Sezione di Genova, Genoa, Italy
[56] II. Physikalisches Institut, Justus-Liebig-Universität Giessen, Giessen, Germany
[57] SUPA - School of Physics and Astronomy, University of Glasgow, Glasgow, UK
[58] LPSC, Université Grenoble Alpes, CNRS/IN2P3, Grenoble INP, Grenoble, France
[59] Laboratory for Particle Physics and Cosmology, Harvard University, Cambridge, MA, USA
[60] [(a)]Department of Modern Physics and State Key Laboratory of Particle Detection and Electronics, University of Science and Technology of China, Hefei, China; [(b)]Institute of Frontier and Interdisciplinary Science and Key Laboratory of Particle Physics and Particle Irradiation (MOE), Shandong University, Qingdao, China; [(c)]School of Physics and Astronomy, Shanghai Jiao Tong University, KLPPAC-MoE, SKLPPC, Shanghai, China; [(d)]Tsung-Dao Lee Institute, Shanghai, China
[61] [(a)]Kirchhoff-Institut für Physik, Ruprecht-Karls-Universität Heidelberg, Heidelberg, Germany; [(b)]Physikalisches Institut, Ruprecht-Karls-Universität Heidelberg, Heidelberg, Germany
[62] Faculty of Applied Information Science, Hiroshima Institute of Technology, Hiroshima, Japan
[63] [(a)]Department of Physics, Chinese University of Hong Kong, Shatin, N.T., Hong Kong, China; [(b)]Department of Physics, University of Hong Kong, Hong Kong, China; [(c)]Department of Physics and Institute for Advanced Study, Hong Kong University of Science and Technology, Clear Water Bay, Kowloon, Hong Kong, China
[64] Department of Physics, National Tsing Hua University, Hsinchu, Taiwan
[65] IJCLab, Université Paris-Saclay, CNRS/IN2P3, 91405 Orsay, France
[66] Department of Physics, Indiana University, Bloomington, IN, USA
[67] [(a)]INFN Gruppo Collegato di Udine, Sezione di Trieste, Udine, Italy; [(b)]ICTP, Trieste, Italy; [(c)]Dipartimento Politecnico di Ingegneria e Architettura, Università di Udine, Udine, Italy
[68] [(a)]INFN Sezione di Lecce, Lecce, Italy; [(b)]Dipartimento di Matematica e Fisica, Università del Salento, Lecce, Italy
[69] [(a)]INFN Sezione di Milano, Milan, Italy; [(b)]Dipartimento di Fisica, Università di Milano, Milan, Italy
[70] [(a)]INFN Sezione di Napoli, Naples, Italy; [(b)]Dipartimento di Fisica, Università di Napoli, Naples, Italy

[71] [(a)]INFN Sezione di Pavia, Pavia, Italy; [(b)]Dipartimento di Fisica, Università di Pavia, Pavia, Italy
[72] [(a)]INFN Sezione di Pisa, Pisa, Italy; [(b)]Dipartimento di Fisica E. Fermi, Università di Pisa, Pisa, Italy
[73] [(a)]INFN Sezione di Roma, Rome, Italy; [(b)]Dipartimento di Fisica, Sapienza Università di Roma, Rome, Italy
[74] [(a)]INFN Sezione di Roma Tor Vergata, Rome, Italy; [(b)]Dipartimento di Fisica, Università di Roma Tor Vergata, Rome, Italy
[75] [(a)]INFN Sezione di Roma Tre, Rome, Italy; [(b)]Dipartimento di Matematica e Fisica, Università Roma Tre, Rome, Italy
[76] [(a)]INFN-TIFPA, Trento, Italy; [(b)]Università degli Studi di Trento, Trento, Italy
[77] Institut für Astro- und Teilchenphysik, Leopold-Franzens-Universität, Innsbruck, Austria
[78] University of Iowa, Iowa City, IA, USA
[79] Department of Physics and Astronomy, Iowa State University, Ames, IA, USA
[80] Joint Institute for Nuclear Research, Dubna, Russia
[81] [(a)]Departamento de Engenharia Elétrica, Universidade Federal de Juiz de Fora (UFJF), Juiz de Fora, Brazil; [(b)]Universidade Federal do Rio De Janeiro COPPE/EE/IF, Rio de Janeiro, Brazil; [(c)]Universidade Federal de São João del Rei (UFSJ), São João del Rei, Brazil; [(d)]Instituto de Física, Universidade de São Paulo, São Paulo, Brazil
[82] KEK, High Energy Accelerator Research Organization, Tsukuba, Japan
[83] Graduate School of Science, Kobe University, Kobe, Japan
[84] [(a)]AGH University of Science and Technology, Faculty of Physics and Applied Computer Science, Kraków, Poland; [(b)]Marian Smoluchowski Institute of Physics, Jagiellonian University, Kraków, Poland
[85] Institute of Nuclear Physics Polish Academy of Sciences, Kraków, Poland
[86] Faculty of Science, Kyoto University, Kyoto, Japan
[87] Kyoto University of Education, Kyoto, Japan
[88] Research Center for Advanced Particle Physics and Department of Physics, Kyushu University, Fukuoka, Japan
[89] Instituto de Física La Plata, Universidad Nacional de La Plata and CONICET, La Plata, Argentina
[90] Physics Department, Lancaster University, Lancaster, United Kingdom
[91] Oliver Lodge Laboratory, University of Liverpool, Liverpool, UK
[92] Department of Experimental Particle Physics, Jožef Stefan Institute and Department of Physics, University of Ljubljana, Ljubljana, Slovenia
[93] School of Physics and Astronomy, Queen Mary University of London, London, UK
[94] Department of Physics, Royal Holloway University of London, Egham, UK
[95] Department of Physics and Astronomy, University College London, London, UK
[96] Louisiana Tech University, Ruston, LA, USA
[97] Fysiska institutionen, Lunds universitet, Lund, Sweden
[98] Centre de Calcul de l'Institut National de Physique Nucléaire et de Physique des Particules (IN2P3), Villeurbanne, France
[99] Departamento de Física Teorica C-15 and CIAFF, Universidad Autónoma de Madrid, Madrid, Spain
[100] Institut für Physik, Universität Mainz, Mainz, Germany
[101] School of Physics and Astronomy, University of Manchester, Manchester, UK
[102] CPPM, Aix-Marseille Université, CNRS/IN2P3, Marseille, France
[103] Department of Physics, University of Massachusetts, Amherst, MA, USA
[104] Department of Physics, McGill University, Montreal, QC, Canada
[105] School of Physics, University of Melbourne, Victoria, Australia
[106] Department of Physics, University of Michigan, Ann Arbor, MI, USA
[107] Department of Physics and Astronomy, Michigan State University, East Lansing, MI, USA
[108] B.I. Stepanov Institute of Physics, National Academy of Sciences of Belarus, Minsk, Belarus
[109] Research Institute for Nuclear Problems of Byelorussian State University, Minsk, Belarus
[110] Group of Particle Physics, University of Montreal, Montreal, QC, Canada
[111] P.N. Lebedev Physical Institute of the Russian Academy of Sciences, Moscow, Russia
[112] National Research Nuclear University MEPhI, Moscow, Russia
[113] D.V. Skobeltsyn Institute of Nuclear Physics, M.V. Lomonosov Moscow State University, Moscow, Russia
[114] Fakultät für Physik, Ludwig-Maximilians-Universität München, Munich, Germany
[115] Max-Planck-Institut für Physik (Werner-Heisenberg-Institut), Munich, Germany
[116] Nagasaki Institute of Applied Science, Nagasaki, Japan
[117] Graduate School of Science and Kobayashi-Maskawa Institute, Nagoya University, Nagoya, Japan

[118] Department of Physics and Astronomy, University of New Mexico, Albuquerque, NM, USA
[119] Institute for Mathematics, Astrophysics and Particle Physics, Radboud University Nijmegen/Nikhef, Nijmegen, The Netherlands
[120] Nikhef National Institute for Subatomic Physics and University of Amsterdam, Amsterdam, The Netherlands
[121] Department of Physics, Northern Illinois University, DeKalb, IL, USA
[122] [(a)]Budker Institute of Nuclear Physics and NSU, SB RAS, Novosibirsk, Russia; [(b)]Novosibirsk State University Novosibirsk, Novosibirsk, Russia
[123] Institute for High Energy Physics of the National Research Centre Kurchatov Institute, Protvino, Russia
[124] Institute for Theoretical and Experimental Physics named by A.I. Alikhanov of National Research Centre "Kurchatov Institute", Moscow, Russia
[125] Department of Physics, New York University, New York, NY, USA
[126] Ochanomizu University, Otsuka, Bunkyo-ku, Tokyo, Japan
[127] Ohio State University, Columbus, OH, USA
[128] Homer L. Dodge Department of Physics and Astronomy, University of Oklahoma, Norman, OK, USA
[129] Department of Physics, Oklahoma State University, Stillwater, OK, USA
[130] Palacký University, RCPTM, Joint Laboratory of Optics, Olomouc, Czech Republic
[131] Institute for Fundamental Science, University of Oregon, Eugene, OR, USA
[132] Graduate School of Science, Osaka University, Osaka, Japan
[133] Department of Physics, University of Oslo, Oslo, Norway
[134] Department of Physics, Oxford University, Oxford, UK
[135] LPNHE, Sorbonne Université, Université de Paris, CNRS/IN2P3, Paris, France
[136] Department of Physics, University of Pennsylvania, Philadelphia, PA, USA
[137] Konstantinov Nuclear Physics Institute of National Research Centre "Kurchatov Institute", PNPI, St. Petersburg, Russia
[138] Department of Physics and Astronomy, University of Pittsburgh, Pittsburgh, PA, USA
[139] [(a)]Laboratório de Instrumentação e Física Experimental de Partículas - LIP, Lisbon, Portugal; [(b)]Departamento de Física, Faculdade de Ciências, Universidade de Lisboa, Lisbon, Portugal; [(c)]Departamento de Física, Universidade de Coimbra, Coimbra, Portugal; [(d)]Centro de Física Nuclear da Universidade de Lisboa, Lisbon, Portugal; [(e)]Departamento de Física, Universidade do Minho, Braga, Portugal; [(f)]Departamento de Física Teórica y del Cosmos, Universidad de Granada, Granada, Spain; [(g)]Dep Física and CEFITEC of Faculdade de Ciências e Tecnologia, Universidade Nova de Lisboa, Caparica, Portugal; [(h)]Instituto Superior Técnico, Universidade de Lisboa, Lisbon, Portugal
[140] Institute of Physics of the Czech Academy of Sciences, Prague, Czech Republic
[141] Czech Technical University in Prague, Prague, Czech Republic
[142] Faculty of Mathematics and Physics, Charles University, Prague, Czech Republic
[143] Particle Physics Department, Rutherford Appleton Laboratory, Didcot, UK
[144] IRFU, CEA, Université Paris-Saclay, Gif-sur-Yvette, France
[145] Santa Cruz Institute for Particle Physics, University of California Santa Cruz, Santa Cruz, CA, USA
[146] [(a)]Departamento de Física, Pontificia Universidad Católica de Chile, Santiago, Chile; [(b)]Department of Physics, Universidad Andres Bello, Santiago, Chile; [(c)]Instituto de Alta Investigación, Universidad de Tarapacá, Arica, Chile; [(d)]Departamento de Física, Universidad Técnica Federico Santa María, Valparaíso, Chile
[147] Department of Physics, University of Washington, Seattle, WA, USA
[148] Department of Physics and Astronomy, University of Sheffield, Sheffield, UK
[149] Department of Physics, Shinshu University, Nagano, Japan
[150] Department Physik, Universität Siegen, Siegen, Germany
[151] Department of Physics, Simon Fraser University, Burnaby, BC, Canada
[152] SLAC National Accelerator Laboratory, Stanford, CA, USA
[153] Physics Department, Royal Institute of Technology, Stockholm, Sweden
[154] Departments of Physics and Astronomy, Stony Brook University, Stony Brook, NY, USA
[155] Department of Physics and Astronomy, University of Sussex, Brighton, UK
[156] School of Physics, University of Sydney, Sydney, Australia
[157] Institute of Physics, Academia Sinica, Taipei, Taiwan
[158] [(a)]E. Andronikashvili Institute of Physics, Iv. Javakhishvili Tbilisi State University, Tbilisi, Georgia; [(b)]High Energy Physics Institute, Tbilisi State University, Tbilisi, Georgia
[159] Department of Physics, Technion, Israel Institute of Technology, Haifa, Israel

[160] Raymond and Beverly Sackler School of Physics and Astronomy, Tel Aviv University, Tel Aviv, Israel
[161] Department of Physics, Aristotle University of Thessaloniki, Thessaloniki, Greece
[162] International Center for Elementary Particle Physics and Department of Physics, University of Tokyo, Tokyo, Japan
[163] Graduate School of Science and Technology, Tokyo Metropolitan University, Tokyo, Japan
[164] Department of Physics, Tokyo Institute of Technology, Tokyo, Japan
[165] Tomsk State University, Tomsk, Russia
[166] Department of Physics, University of Toronto, Toronto, ON, Canada
[167] [(a)]TRIUMF, Vancouver, BC, Canada; [(b)]Department of Physics and Astronomy, York University, Toronto, ON, Canada
[168] Division of Physics and Tomonaga Center for the History of the Universe, Faculty of Pure and Applied Sciences, University of Tsukuba, Tsukuba, Japan
[169] Department of Physics and Astronomy, Tufts University, Medford, MA, USA
[170] Department of Physics and Astronomy, University of California Irvine, Irvine, CA, USA
[171] Department of Physics and Astronomy, University of Uppsala, Uppsala, Sweden
[172] Department of Physics, University of Illinois, Urbana, IL, USA
[173] Instituto de Física Corpuscular (IFIC), Centro Mixto Universidad de Valencia, CSIC, Valencia, Spain
[174] Department of Physics, University of British Columbia, Vancouver, BC, Canada
[175] Department of Physics and Astronomy, University of Victoria, Victoria, BC, Canada
[176] Fakultät für Physik und Astronomie, Julius-Maximilians-Universität Würzburg, Würzburg, Germany
[177] Department of Physics, University of Warwick, Coventry, UK
[178] Waseda University, Tokyo, Japan
[179] Department of Particle Physics, Weizmann Institute of Science, Rehovot, Israel
[180] Department of Physics, University of Wisconsin, Madison, WI, USA
[181] Fakultät für Mathematik und Naturwissenschaften, Fachgruppe Physik, Bergische Universität Wuppertal, Wuppertal, Germany
[182] Department of Physics, Yale University, New Haven, CT, USA

[a] Also at Borough of Manhattan Community College, City University of New York, New York NY, USA
[b] Also at Centro Studi e Ricerche Enrico Fermi, Italy
[c] Also at CERN, Geneva, Switzerland
[d] Also at CPPM, Aix-Marseille Université, CNRS/IN2P3, Marseille, France
[e] Also at Département de Physique Nucléaire et Corpusculaire, Université de Genève, Genève, Switzerland
[f] Also at Departament de Fisica de la Universitat Autonoma de Barcelona, Barcelona, Spain
[g] Also at Department of Financial and Management Engineering, University of the Aegean, Chios, Greece
[h] Also at Department of Physics and Astronomy, Michigan State University, East Lansing MI, USA
[i] Also at Department of Physics and Astronomy, University of Louisville, Louisville, KY, USA
[j] Also at Department of Physics, Ben Gurion University of the Negev, Beer Sheva, Israel
[k] Also at Department of Physics, California State University, East Bay, USA
[l] Also at Department of Physics, California State University, Fresno, USA
[m] Also at Department of Physics, California State University, Sacramento, USA
[n] Also at Department of Physics, King's College London, London, UK
[o] Also at Department of Physics, St. Petersburg State Polytechnical University, St. Petersburg, Russia
[p] Also at Department of Physics, University of Fribourg, Fribourg, Switzerland
[q] Also at Dipartimento di Matematica, Informatica e Fisica, Università di Udine, Udine, Italy
[r] Also at Faculty of Physics, M.V. Lomonosov Moscow State University, Moscow, Russia
[s] Also at Giresun University, Faculty of Engineering, Giresun, Turkey
[t] Also at Graduate School of Science, Osaka University, Osaka, Japan
[u] Also at Hellenic Open University, Patras, Greece
[v] Also at IJCLab, Université Paris-Saclay, CNRS/IN2P3, 91405, Orsay, France
[w] Also at Institucio Catalana de Recerca i Estudis Avancats, ICREA, Barcelona, Spain
[x] Also at Institut für Experimentalphysik, Universität Hamburg, Hamburg, Germany
[y] Also at Institute for Mathematics, Astrophysics and Particle Physics, Radboud University Nijmegen/Nikhef, Nijmegen, The Netherlands

[z] Also at Institute for Nuclear Research and Nuclear Energy (INRNE) of the Bulgarian Academy of Sciences, Sofia, Bulgaria
[aa] Also at Institute for Particle and Nuclear Physics, Wigner Research Centre for Physics, Budapest, Hungary
[ab] Also at Institute of Particle Physics (IPP), Vancouver, Canada
[ac] Also at Institute of Physics, Azerbaijan Academy of Sciences, Baku, Azerbaijan
[ad] Also at Instituto de Fisica Teorica, IFT-UAM/CSIC, Madrid, Spain
[ae] Also at Joint Institute for Nuclear Research, Dubna, Russia
[af] Also at Louisiana Tech University, Ruston LA, USA
[ag] Also at Moscow Institute of Physics and Technology State University, Dolgoprudny, Russia
[ah] Also at National Research Nuclear University MEPhI, Moscow, Russia
[ai] Also at Physics Department, An-Najah National University, Nablus, Palestine
[aj] Also at Physikalisches Institut, Albert-Ludwigs-Universität Freiburg, Freiburg, Germany
[ak] Also at The City College of New York, New York NY, USA
[al] Also at TRIUMF, Vancouver BC, Canada
[am] Also at Universita di Napoli Parthenope, Napoli, Italy
[an] Also at University of Chinese Academy of Sciences (UCAS), Beijing, China
*Deceased